POLYOLEFIN FORMULATIONS FOR IMPROVED FOAMING: EFFECTS OF MOLECULAR STRUCTURE AND MATERIAL PROPERTIES

by

YING ZHANG

A thesis submitted to the Department of Chemical Engineering

In conformity with the requirements for

the degree of Doctor of Philosophy

Queen's University

Kingston, Ontario, Canada

(January, 2013)

Abstract

The morphology and mechanical properties of foams made out of ethylene-α-olefin copolymers (EC) having well-characterized rheological properties were investigated. The polymers differed in the amount of comonomer contained, type of comonomer and molecular weight, resulting in variable thermal properties and different rheological responses under shear and extensional flow. All of the octene-based copolymers with comparable rheological properties had similar foam morphology. However grades with low extensional viscosity and low crystallization points resulted in poor foams. Increasing density resulted in a higher secant modulus of the foamed samples.

To further investigate the effects of material properties, trimethylolpropane trimethacrylate (TMPTMA) and triallyl trimesate (TAM) coagents were used to generate a series of PP derivatives through radical mediated melt state reactive modification. Coagent modification resulted in pronounced effects in the molecular weights and viscosities of the derivatives. However, evidence of long-chain branching (LCB) was only present in TAM modified PPs. Significant increases in the crystallization temperature, heat of fusion and crystallization rate were attributed to the formation of nanoparticles, which resulted in a heterogeneous nucleation effect, both for crystallization and foaming. Generally lower viscosities, coupled by strain hardening, enhanced nucleation and increased crystallization temperatures induced by the nanoparticles resulted in foams with higher expansion ratios and smaller cells, due to higher rates of cell growth, coupled with suppressed coalescence.

Nanocomposites based on isotactic PP and nanosilica (SiO_2) were prepared using a co-rotating twin-screw extruder (TSE) in order to investigate foaming on a larger scale. High shear stress, sufficient residence time, and high fill ratio in the melting section of the screw were the most important factors in achieving good nanosilica dispersion. Well-dispersed surface-modified hydrophobic SiO_2 particles were effective nucleating agents for foaming, when used at loadings below 1 phr.

Co-Authorship

This thesis contains chapters that present results that have been published in the form of original journal articles as well as material that is in preparation for submission. The complete citations for the published papers and the chapters in which they appear are provided below:

Chapter 3:	Zhang, Y., Kontopoulou, M., Ansari, M., Hatzikiriakos, S.G., and Park, C.B. " Effect of molecular structure and rheology on the compression foam molding of ethylene-α-olefin copolymers "Polymer Engineering and Science 2011 (1); 1145-1154
Chapter 6	Lee, S. H., Zhang, Y., Kontopoulou, M., Park, C. B., Wong, A. and Zhai, W. "Optimization of dispersion of nanosilica particles in a PP matrix and their effect on foaming" International Polymer Processing 2011 (26); 388-398

All the papers and manuscripts were co-authored and reviewed prior to publication by Prof. .Kontopoulou and Prof. Park of the Department of Mechanical and Industrial Engineering, University of Toronto. The first paper was co-authored by Dr. Ansari who assisted the author with the extensional viscosity measurements and treatment of the data, under the direction of Dr. Hatzikiriakos of the Department of Chemical and Biological Engineering, University of British Columbia. The second paper was co-authored by a post-doctoral fellow, Dr. Lee. He was responsible for designing the screw configuration, overseeing the compounding operations and directing parts of the characterization. Drs. Wong and Zhai of the Department of Mechanical and Industrial Engineering, University of Toronto assisted in the batch foaming experiments, which were done using equipment available in Prof. Park's laboratory. All of the remaining work and manuscript preparation were performed by the author of this thesis.

Acknowledgements

I would like to thank my supervisor Dr. Marianna Kontopoulou for her continuous encouragement and guidance during my time at Queen's University. In addition to the countless theoretical and technical discussions with me which spent so much of her time, I really appreciate her as a role model of positive attitude and professionalism towards work. I would like to thank Dr. Parent as both a good teacher who taught me critical thinking in a whole new level and an inspiration on my projects. Dr. Park is gratefully acknowledged for his enlightening insight into the topic of foaming from an industrial prospective and the hospitality of towards the author during my many visits to his group. Dr. Hatzikiriakos took out precious time out of his busy schedule to arrange my travel to his group and welcomed me as if a member of his group right before Christmas; for that I am grateful.

Financial support in the form of scholarships from the National Science and Engineering Research Council (NSERC), and Queen's University (Queen's Graduate Award) is gratefully acknowledged. Funding from the Auto 21 Network of Centres of Excellence and the Innovative Plastic Materials and Manufacturing Processes (NIPMMP) NSERC strategic network are greatly appreciated. Materials were supplied by Dow, ExxonMobil, Lyondell Basell and E. I Dupont.

I am grateful to the following people for the technical assistance they provided over the course of this research project: Mr. Charlie Cooney for the SEM apparatus, Dr. Andrea Liskova for her help with the different instruments of polymer characterization. Dr. Mahmoud Ansari for his contribution to Chapter 3, Dr. Sung-Hyo Lee, Dr. Anson Wong and Dr. Wentao Zhai for their contribution to Chapter 6, Kelly Sedore and Steven Hodgson for their help with my experimental work. I thank my labmates Mathieu, Andrew and Karthik for their friendship.

My final gratitude goes to my grandparents and my parents; without their influence in my early years I couldn't possibly start my journey since college. Special thanks goes to my partner, Ms Jingmiao Shi for all the unconditional love and moral support.

Table of Contents

List of Figures

List of Tables

Nomenclature

a	Mark-Houwink constant
A	Area (m^2)
d	Cell diameter (µm)
d_n	Number average diameter (µm)
d_v	Volume average diameter (µm)
E_H	Horizontal activation energy of the flow (kJ/mol)
f	Shape factor
G*	Complex modulus (Pa)
G'	Elastic or Storage modulus (Pa)
G"	Viscous or loss modulus (Pa)
K	Mark-Houwink constant (dL/g)
l	Edge length of geometric feature (µm)
N	Nucleation rate (/(cm^3·s))
n	Shear thinning constant
N_0	Number of cells in a specified area
$N_{unfoamed}$	Cell density of a foam with respect to the unfoamed polymer volume (/cm^3)
$P_{bub,cr}$	Pressure inside a critical cell (Pa)
P_{sys}	System pressure (Pa)
R_{avg}	Average cell radius (µm)
S	Geometric factor
S	Strain hardening coefficient
T	Temperature (°C)
t	Time (s)

T_c	Temperature of crystallization (°C)
T_m	Melting point (°C)
W	Degree of crystallinity (%)

Greek Symbols

ΔH_f	Heat of fusion (J/g)
$[\eta]$	Intrinsic viscosity (dL/g)
$3\eta^+$	Linear viscoelastic envelope in uniaxial extension (Pa.s)
ν	Cell area (μm^2)
β	Half-angle of the geometric feature (°)
γ	Interfacial tension between the polymer and gas (J/m^2)
δ	Phase degree (°)
ΔG_{het}	Activation energy for heterogeneous nucleation (J/g)
ΔG_{hom}	Activation energy for homogeneous nucleation (J/g)
$\dot{\varepsilon}$	Henky strain rate (s^{-1})
η^*	Complex Viscosity (Pa.s)
η_0	Zero shear viscosity (Pa.s)
η_E^+	Tensile stress growth coefficient (Pa.s)
θ_c	Contact angle of the solid-gas-liquid interface (°)
λ	Relaxation time (s)
ν_f	Void fraction
ρ_f	Bulk density of the foam sample (g/cm^3)
ρ_p	Bulk density of the pure polyolefin material (g/cm^3)
ω	Angular frequency (rad/s)

Abbreviations

ASTM	American Society for Testing Materials
AZ	Azodicarbonamide
CG	Constrained Geometry
DCP	Dicumyl Peroxide
DSC	Differential Scanning Calorimetry
EC	Ethylene-α-olefin Copolymer
EVA	Ethylene Vinyl Acetate copolymer
FT-IR	Fourrier-Transformed Infrared
HDPE	High Density Polyethylene
LCB	Long-chain Branching
LCB	Long-chain Branched
LDPE	Low Density Polyethylene
LLDPE	Linear Low Density Polyethylene
L-PP	Linear Polypropylene homopolymer
LVE	Linear Viscoelastic
MA	Maleic Anhydride
MFI	Melt Flow Index
MFR	Melt Flow Rate
mPE	Ethylene-α-olefin copolymer
MW	Molecular Weight
PE	Polyethylene
PETA	Pentaerythritol Triacrylate
phr	Parts per Hundred
PODIC	Peroxydicarbonate

PP	Polypropylene
PP-g-MA	Poly(propylene-graft-maleic anhydride)
PS	Polystyrene
RPM	Revolutions Per Minute
SAOS	Small Amplitude Oscillatory Shear
SCB	Short Chain Branching
SEM	Scanning Electron Microscopy
SiO_2	Silicon dioxide
TAM	Triallyl trimesate
TEM	Transmission Electron Microscopy
TGA	Thermogravimetric Analysis
TMPTMA	Trimethylolpropane trimethacrylate
TPO	Thermoplastic Olefin
TSE	Twin-screw Extruder
VER	Volume Expansion Ratio
PS-b-P2VP	polystyrene-block-poly(2-vinyl pyridine)
PE-g-MA	Poly(ethylene-graft-maleic anhydride)
NA	Nucleating Agent
MSDS	Material Safety Data Sheets
N_2	Nitrogen
CM-PP	Coagent Modified Polypropylene
MWD	Molecular Weight Distribution
TCB	1,2,4-Trichlorobenzene
GPC	Gel Permeation Chromatography
LS	Light Scattering

BHT	Butylated hydroxytoluene
CR-PP	Controlled Rheology Polypropylene
PP-g-TAM	Poly(propylene-graft-triallyl trimesate)
PP-g-TMPTMA	Poly(propylene-graft-trimethylolpropane trimethacrylate)
SSA	Specific Surface Area

Chapter 1

Introduction

Cellular polymers, also known as polymeric foams, consist of a solid porous polymer matrix and a gaseous phase derived from a blowing agent. By varying manufacturing conditions and polymer matrix composition, their properties can be tailored to meet a vast array of applications. Due to their light weight, high strength/weight ratio, and good insulating properties, foams are widely used in many fields including furniture, packaging, recreation, construction, insulation, textiles and automotive applications. According to Industry Canada, the plastic foams sector represented about 6% of the total plastic products industry shipment in Canada in 2010[1].

Polyolefins, including polyethylene (PE), polypropylene (PP) and their derivatives are the largest polymer family by volume of production and consumption and are thus regarded as commodity polymers. They have numerous applications, due to their relatively low cost, and wide range of properties. The good balance of toughness, flexibility and resistance to chemicals and abrasion make them excellent candidates for foams.

Since the first commercial production of PE foams in the early 1940s [2], considerable effort has been devoted to the development of polyolefin foams that possess a morphology characterized by controllable cell size and narrow cell size distribution. Investigations of foaming behavior have included various grades of PE, PP, their blends and composites, as well as branched and cross-linked polyolefins.

In spite of the fact that a vast variety of polyolefins with distinctive chemical compositions have been the subjects of previous investigations using a wide variety of processes, a thorough understanding of the effect of various material properties on foaming is still missing. Lack of control over the polyolefin molecular structure makes it hard to differentiate conclusively the effects of structure on foaming. This situation is further aggravated when cross-linking of the polyolefin is required to provide the melt strength needed to obtain good foams, because it is even harder to track the exact nature of the cross-linked structure.

1.1 Thesis Objectives

The objective of this thesis is to establish rigorous relationships between the structure, thermal and rheological properties of polyolefins and their foaming behaviour, with the ultimate aim of proposing structures and formulations that will provide improved formability compared to commercial polyolefin grades.

To achieve this, a study of the influence of the polymer structure and properties on the foaming characteristics of commercially available polyolefins having well characterized properties has been completed.

To further investigate in detail the effects of polymer structure and thermorheological properties on foaming, reactively modified polypropylenes having well characterized evolving molecular weight, and chain structures were produced using peroxide and coagents. Foaming tests, which included in-situ batch foaming and compression mold foaming were performed to gain an in-depth understanding on how structural characteristics influence the foaming behaviour of polyolefins at different stages.

Finally, the use of nanosilica particles as nucleating agents is investigated as a means to improve the foaming behavior of commercially available polypropylene. In order to make this work more industrially relevant, processing parameters such as screw configuration, screw speed, and compound formulation were studied in detail in order to improve the nanosilica dispersion and improve the foaming behaviour of the composite.

1.2 Thesis Organization

This thesis consists of 7 chapters. Chapter 1 defines the scope of this thesis. Chapter 2 gives a literature review of foaming theory, describes the materials relevant to this work and critically examines the relevant existing studies. In Chapter 3, the effects of molecular structure and rheology on the compression foam moulding of several judiciously chosen commercial ethylene-α-olefin copolymers are studied. Chapter 4 is dedicated to the foaming behaviour of isotactic polypropylene modified by two coagent systems, which generated a series of PP derivatives with different chain structure. Chapter 5 discusses the formation of nano-particles during reactive modification of isotactic polypropylene and investigates their nucleation effect during both isothermal crystallization and batch foaming. In Chapter 6, the dispersion of nanosilica particles in a PP matrix is studied using a melt compounding process and the effect of nanosilica dispersion on extrusion foaming is studied. Chapter 7 serves as a summary of the entire work, where conclusions are drawn and recommendation on future work is made.

Chapter 2

Literature Review

2.1 Polymer Foams

Polymeric foams, consist of a solid porous polymer matrix and a gaseous phase derived from a blowing agent. Thermoplastics and polyurethanes are the most commonly used polymers for foaming. Foaming in general can be carried out by either mechanical, chemical, or physical means. Most commercial polymer foams are produced through an expansion process, which relies on the expansion of a gaseous phase dispersed throughout the polymer melt. Blowing agents are used to generate the gas phase needed for expansion. There are two types of blowing agents: A physical blowing agent is a gas species or a volatile liquid which is dissolved into the polymer melt under pressure. Upon pressure release and/or heating, phase separation occurs and cells (bubbles) are formed within the polymer melt. A chemical blowing agent supplies the gas phase through chemical decomposition. While the gas phase supplied by a physical blowing agent nucleates homogeneously from the polymer melt under ideal conditions, the gas phase supplied by a chemical blowing agent usually nucleates around the decomposition residual. Azodicabonamide (AZ) is a commonly used chemical blowing agent in the industry. The thermal decomposition of AZ results in the evolution of nitrogen, carbon monoxide, carbon dioxide, and ammonia gases.

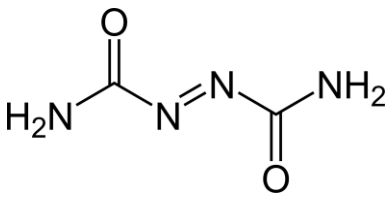

Figure 2.1 Chemical structure of azodicabonamide.

A wide variety of processing methods, ranging from extrusion, injection to compression molding are used to make polyolefin foams. An excellent review of the processes used to produce a large variety of foamed polymers can be found in Park [3]. Regardless of the technique applied, foaming of polyolefins generally occurs in three major steps: nucleation, cell growth, and stabilization. Nucleation involves the formation of expandable bubbles in a polymer melt supersaturated with a blowing agent. After nucleation, the bubbles continue to grow as the blowing agent diffuses into them, until they stabilize or rupture [4].

2.2 Foaming Mechanisms

Starting from a gas-polymer single phase solution, foaming generally occurs in three major steps: nucleation, cell growth, and stabilization (**Figure 2.2**).

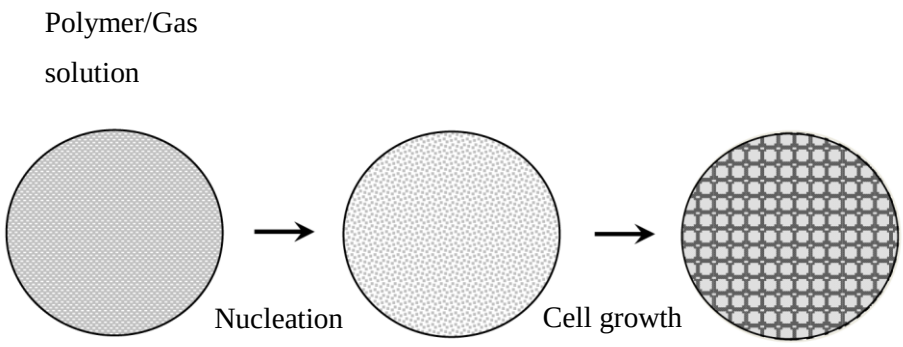

Figure 2.2 Schematic of the three stages of polymer foaming.

Nucleation involves the formation of expandable bubbles in a polymer melt super-saturated with a blowing agent. If a physical blowing agent, such as nitrogen is used, the agent is dissolved into the polymer at higher pressures. Alternatively, if a chemical blowing agent, such as AZ is used, this agent releases gas at a specific decomposition temperature and the gas is then dissolved in the polymer at higher pressures. At lower pressures, a gaseous phase may nucleate right away. After

nucleation, the bubble will continue to grow as the blowing agent diffuses into it until it stabilizes or ruptures [4]. Cell growth is completed when there is no longer any diffusion occurring, and there is force equilibrium between the pressure in the cell, the surrounding pressure, and the surface tension of the polymer, or when the polymer becomes solidified. The major stages involved in foaming are described below:

Nucleation

There are two major types of nucleation in polymer foaming: homogeneous and heterogeneous. Homogenous nucleation refers to the classical nucleation theory used to describe the cell nucleation behaviour in single component or miscible blended systems, in the absence of any impurities. Heterogeneous nucleation typically occurs due to impurities in the sample itself, or in the presence of nucleating agents, such as talc, sodium benzoate or stearic acid. Heterogeneous nucleation may also take place at the phase boundaries between immiscible blends, which have a lower free energy barrier for nucleation [5-7]. Regardless of the nucleation type, conventional nucleation theories assume that the nucleation is a thermodynamic process and the main driving force is degree of supersaturation. The well-known expression for homogeneous or heterogeneous nucleation is:

$$N = Aexp(-B) \tag{2.1}$$

where N is the nucleation rate and A and B are material and system parameters. Different expressions for A and B have been derived through extensive thermodynamics calculations for varying material systems [8-11]. Though is not within the scope of this review to go through these derivations, factors influencing the cell nucleation rate can be identified by observing these equations. Common characteristics exist for these different A and B constants: A normally represents a frequency factor for gas molecules joining the bubble nucleus timed by a

concentration term; *B* represents the energy barrier a particular system has to overcome in order to form nuclei. For homogenous nucleation:

$$A = f_0 C_0 \tag{2.2}$$

$$B = \frac{\Delta G_{hom}}{kT} = \frac{16\pi\gamma^3}{3\Delta P^2} \cdot \frac{1}{kT} \tag{2.3}$$

where f_0 is the frequency factor, C_0 is the concentration of gas molecules in the melt solution, k is Boltzmann's constant, T is the temperature in degrees Kelvin, ΔG_{hom} is generally noted as the activation energy for homogeneous nucleation, γ is the interfacial tension between the polymer and bubble, and ΔP is the difference in pressure between a newly formed bubble and the melt pressure [9]. For heterogeneous nucleation, the concentration term in Eqn. (2.2) is replaced by the concentration of heterogeneous nucleation sites C_1, and ΔG_{hom} is modified with a geometric factor S that takes into account geometrical factors induced by the heterogeneous nucleation sites [10] as follows:

$$\Delta G_{het} = \frac{16\pi\gamma^3}{3\Delta P^2} \cdot S \tag{2.4}$$

From the form of these expressions it is obvious that the concentration of the gas molecules and the number of heterogeneous nucleation sites impose a positive influence on the nucleation process, while the interfacial tension plays a negative role.

Beside the material and system parameters, the state of stress to which the gas/polymer solution is subjected also influence nucleation. Lee [12] studied the nucleation behaviour in the presence of external shear during extrusion foaming of low density polyethylene. It was found that shearing promoted nucleation. A modified cavity model was applied to explain the effect of shear force. It was proposed that the capillary number, specified as the ratio of shear force to surface tension, should be taken into consideration in addition to the degree of supersaturation and the number of nucleators in obtaining desired nucleation during thermoplastic foam extrusion.

Cell Growth and Coalescence

Nucleation is followed by the cell growth stage. For an ideally spherical initial cell, growth is a result of the interaction of the differential pressure, ΔP, between the inside and outside of the cell, the interfacial tension between the polymer and growing cell, and the viscoelastic properties of the melt. At equilibrium, the differential pressure can be expressed by the Young-Laplace equation:

$$\Delta P = \frac{2\gamma}{r} \tag{2.5}$$

where γ is the interfacial tension and r is the radius of the cell at equilibrium. The differential pressure is larger for a smaller cell at a fixed gas-polymer system, where γ can be regarded as constant. Accordingly, smaller cells tend to equalize these pressures by growing faster, breaking the walls separating cells, or by diffusion of the blowing gas from the small cells to larger cells:

$$\Delta P_{1,2} = 2\gamma \left(\frac{1}{r_1} - \frac{1}{r_2}\right) \tag{2.6}$$

where $\Delta P_{1,2}$ is the difference in pressure between cells with radius of r_1 and r_2. The rate of cell growth depends on the viscoelastic nature of the polymer melt, the blowing gas pressure, the external pressure on the foam, the current cell size and the diffusion rate of gas through a polymer phase [13-15].

The tendency for cell coalescence can be explained by considering the free energy change, ΔF, of the foaming system,

$$\Delta F = \gamma A \tag{2.7}$$

where A is the total interfacial area. The system will always tend to minimize its interfacial area to reduce the free energy change for foaming; this is achieved by coalescence [16].

Numerous studies have been done to investigate the factors that govern cell growth and coalescence. Otsuki and Kanai [17] modeled the foaming process using a PP system with carbon

dioxide foaming agent, and found that the strain hardening characteristics of the polymer do not strongly affect the bubble growth rate, while the linear viscoelastic characteristics of the polymer melt are more influential. However, there are a number of other factors which have a larger effect on the bubble growth rate, such as the bubble nucleus population density, surrounding pressure, initial dissolved foaming agent concentration, and the diffusion coefficient. Using a polystyrene/carbon dioxide system, Leung *et al.* [18] modeled the foaming process and found that higher diffusivity of the blowing agent leads to an increase in the cell growth rate; however at longer times, the cells grew large enough that further growth of the bubbles was limited by low gas contents within the surrounding thin shells of polymer melt. Both studies mentioned above found that neither the strain hardening characteristics of the polymer melt, nor the surface tension, had a significant effect on the rate of volume expansion. However, Taki *et al.* [19] examined the relationship between rheological properties and cell coalescence and found that the coalescence time was longer when the strain hardening behaviour was more pronounced.

2.3 Polymer Foam Characterization

The most well recognized classification system for polymer foams is based on cell sizes/cell densities, and bulk foam densities. Foams with large cell sizes of 300 μm and up, with cell densities of the order of 10^6 cells/cm^3 are classified as conventional foams, while small celled foams displaying cell sizes of 10 μm and cell densities of 10^9 cells/cm^3 are classified as microcellular foams. The third category, fine-celled foams, accounts for foams with cell sizes and densities which fall between the conventional and microcellular foams [20]. Other classifications include those based on geometrical or stereometrical schemes. Depending on whether the gas containing cells are isolated or interconnected, foams can be classified as open- or closed-cell. The above classifications are applicable when the relationship between the

morphology and the properties of foamed polymers is to be established and evaluated quantitatively [21]. Bulk foam densities can also be used to classify foams; they are divided into four categories: Foams with an expansion ratio of less than 4 fold are considered high density foams; medium density foams fall between 4 fold and 10 fold; low density foams between 10 fold and 40 fold, and foams with more than 40 fold expansion are labelled as very low density foams. High-density foams are typically used for structural purposes such as wires and cables, while low-density foams are primarily used in cushion packaging [3].

The foam density can be readily measured by utilizing the water displacement method. The volume expansion ratio (VER) is defined as the ratio of the volume of the foamed sample to the volume of the original unfoamed bulk material. In practice, it is calculated as the ratio of bulk density of the pure polyolefin material (ρ_p) to the bulk density of the foam sample (ρ_f):

$$VER = \frac{\rho_p}{\rho_f}. \tag{2.8}$$

With the knowledge of the volume expansion ratio, the cell density of a foam with respect to the unfoamed polymer volume ($N_{unfoamed}$) can be calculated by the following equation [22]

$$N_{unfoamed} = \left(\frac{N_0}{A}\right)^{\frac{3}{2}} VER \tag{2.9}$$

where N_0 is the number of cells in a specified area A, and VER is the volume expansion ratio.

2.4 Polyolefin Foams

2.4.1 Polyethylene Foams

Polyethylene (PE) has been the material of choice for commercial thermoplastic foam production since the early 1940s [2]. PE exhibits excellent mechanical properties, as well as good temperature stability and high chemical resistance. Historically both high density polyethylene (HDPE) and low density polyethylene (LDPE) have been used as foam materials with a later

addition of ethylene-vinyl acetate copolymer (EVA) and metallocene and constrained geometry (CG) catalyzed PE (mPE) to the family.

Due to its high crystallinity, HDPE is able to solidify fast enough to sustain thin cell walls, making it a good candidate for the study of the foam processing mechanisms in the early literature [23,24]. Han and Villamizer [23] determined the cell inflation pressure, which is often referred to as critical pressure, of HDPE blown by a proprietary hydrazide by visual observation of bubble growth and measurement of melt pressure. They found that the critical pressure for bubble growth decreases with increasing melt temperature and increases with increasing blowing agent concentration. A strategy to avoid bubble growth within the die during extrusion foaming was proposed. They also reported a plasticizing effect of the blowing agent. Similar experimental techniques were applied by the same group on injection molding of HDPE to study the effects of processing parameters on the morphology of the resulting foams [24]. It was reported that cell growth and cell uniformity cannot be optimized at the same time. Higher melt temperature, blowing agent concentration and mold temperature resulted in an increase in cell growth and lower cell uniformity. Higher injection pressure, on the other hand, generated more uniform cell size but caused low cell growth.

More recent research has mainly focused on the effect of molecular characteristics on cell morphology as well as the mechanical properties of foams. A comprehensive series of papers by Zhang, Rodrigue and Ait-Kadi is a good representation of such research [25-27]. The molecular weight (MW) of HDPE was identified as a factor influencing both its foaming behaviour and mechanical properties. For the lowest MW HDPE, cell size increased with blowing agent concentration but for HDPE of higher MW values, cell size increased with blowing agent concentration first, then a maximum was reached followed by a decrease. For the highest MW

HDPE, cell size only decreased with blowing agent content because of high viscosity. However, cell density always increased with MW.

LDPE, mPE and EVA are usually used in a cross-linked form in polymeric foams. One of the reasons for cross-linking is to improve melt strength in order to obtain more desirable foaming behaviour, especially to achieve fine cell, high expansion foams. The other reason for cross-linking is to improve the thermal stability, resistance to natural elements, solvents and improved durability. This is particularly important for EVA foams because low heat resistance is their most significant shortcoming [28].

Two main cross-linking procedures are used; physical cross-linking by irradiation (electrons or gamma irradiation [29-31]) and chemical cross-linking by using cross-linking agents such as peroxides [32-36]. Irradiation methods have the advantage of being a clean and continuous process with good control, however they present a thickness limitation due to the penetration limits of the radiation beam [29]. Chemical cross-linking is an economical choice and more flexible in terms of the equipment required.

On a molecular level, both methods modify the chain structure of polyolefins by a free radical reaction. The degree of cross-linking affects the rheological properties of melts and the resulting foam morphology, but the effect is not straightforward. Yamaguchi and Suzuki [33] studied the rheological properties and foam processability of blends of mPE and cross-linked mPE. They found that the addition of a small amount of cross-linked mPE (as low as 1wt.%) enhanced the elongational viscosity and elastic modulus, whereas it had little effect on the steady-state shear viscosity. The foamed blends showed higher expansion ratios and more homogeneous cell size distributions than those made of from pure mPE. However, the increase in gel content caused by cross-linking does not always yield desirable foaming behaviour. Abe and Yamaguchi [34] investigated two dicumyl peroxide cross-linked mPEs for their expansion ratio at different gel

contents. They observed that the elastic modulus and crystallization temperature were related to gel content. The elastic modulus and crystallization temperature in turn determined the expansion ratio of cross-linked PE foams. As the elastic modulus increased, the expansion ratio of the foam decreased. On the other hand, a lowered crystallization temperature due to increasing gel content caused shrinkage of foams, resulting in a lower expansion ratio.

Even though most of the foaming studies on mPEs have been performed on their cross-linked form, uncross-linked mPEs are interesting for foaming studies by their own right. mPEs exhibit controlled molecular structure, including very narrow comonomer composition distribution and narrow MW distribution. Depending on the type of comonomer used during polymerization, there are two types of mPE: Linear mPEs having short chain branches (SCB) and branched mPEs, containing controlled levels of long chain branching (LCB).

It is known that LCB can substantially affect polymer rheology, while SCB has little effect [37]. A polymer with LCB usually exhibits a higher viscosity at low shear rates than that of a corresponding linear polymer, due to the contribution of the LCB to the molecular entanglements. At higher shear rates, the branched polymer has a lower viscosity that the linear polymer, because the contribution of the LCB to the molecular entanglements decreases as a result of branch alignment with increasing shear. LCB is desirable in polymers because it decreases the energy consumption during processing. The literature on the topic of mPE rheology has mainly focused on the comparison of mPEs with traditional PEs and the effect of LCB on their rheological behaviour [38,39]. As summarized by Lai *et al.* [40], incorporation of LCB leads to distinct rheological behaviour for mPE over traditional LLDPE including: 1) greater shear thinning behaviour at higher shear rates; 2) decrease in sharkskin or melt fracture effects at higher shear rates (higher production output); 3) higher melt strength of the polymer. The controllable

branching structure and continuously changing rheological properties within a series of mPE make them ideal candidates for the study of the effect of matrix properties on foaming behaviour.

2.4.2 Polypropylene Foams

Polypropylene (PP) has some properties which make it especially suitable for foaming applications. Its major advantage over the PE family is a relatively higher service temperature. However, foaming of conventional linear PPs is hard compared to the PE family, due to their low melt strength, the high melting/crystallization temperatures and relatively low degradation temperatures, resulting in a very narrow processing window. During foaming, low melt strength causes the cell walls separating the foamed bubbles to become weak and therefore susceptible to coalescence and rupture. Such coalescence problem is reflected on the final product in the form of low expansion ratio and high open cell content, both of which are unsatisfactory for many foam applications. To further improve the foamability of the resins, much research has concentrated on material modification of existing resins or using new types of PPs to increase melt strength.

Chemical modification is commonly practiced to increase the melt strength of PP. By means of reactive melt modification using acrylates [41], silane compounds [42] or peroxide [43], researchers have been able to significantly improve the expansion ratio, cell uniformity and thermoformability of PP foams. Nojiri *et al.* [41] modified PP with triacrylate or trimethacrylate by exposing the extruded sheets to gamma radiation, and produced foams having high elongation, uniform fine cell structure, and a low density of 0.035 g/cm^3. However, excessively modified PP cannot be recycled due to the resulted gels thus much research has been directed away from this method.

Introduction of long chain branched (LCB) PP has been proven to be very satisfactory in the manufacturing of PP foamed products. The mechanism behind this success is the well known

strain hardening of melts caused by long chain branching. Strain hardening of PP melts improves significantly in the presence of even limited long chain branching either from the polymer itself [44] or by adding small amounts of an LCB PP [45]. In foaming tests using AZ as a blowing agent, such favourable extensional viscosity generated a higher expansion ratio, less cell coalescence and more homogenous cell size distribution up to a 50 wt. % of LCB PP [46]. Furthermore Stange and Münstedt reported that different molecular structures lead to comparable foaming behaviour as long as the structures caused similar extensional properties [47]. A synergistic effect in a blend system of linear PP with branched PP foamed with carbon dioxide was found by Spitael and Macosko [48]. Strain hardening was observed for branched PPs and in blends with a concentration of branched PP as low as 10 wt.%. The highest cell density was observed at about 25 wt.% of LCB PP in the blend. It is was shown that the foam morphology was a result of the combined influence of a higher number of nuclei of the linear blend component [49], and the reduction of cell coalescence due to the strain hardening of the LCB component. This method of incorporating small amounts of LCB PP into a dominantly linear PP melt may prove to be the most successful method to produce suitable PP foams for commercial applications.

2.5 Co-agent Modification of Polypropylene

A particularly attractive methodology to increase the melt strength of commercial linear polypropylene (L-PP) is through solvent-free reactive processing, which employs peroxide initiated chain scission and co-agent assisted chain extension/cross-linking. This single stage process involves simultaneous PP fragmentation and cross-linking, the balance of which controls the length, frequency and distribution of branches. A simplified reaction scheme starts with the formation of a PP macro-radical, following the decomposition of a peroxide:

$$ROOR \xrightarrow{\Delta} 2RO\cdot$$

$$PP + RO\cdot \rightarrow RO - PP\cdot$$

In the presence of a multifuctional coagent monomer M, the following three reaction pathways are possible:

$$PP\cdot \rightarrow PP\cdot + PP - CH = CH_2 \quad (\beta - scission)$$

$$2\,PP\cdot + M \rightarrow PP - M - PP \quad (Branching\ /\ Crosslinking)$$

$$RO\cdot + (x+1)M \rightarrow RO - M_x M\cdot \qquad (Oligomerization)$$

A more general and comprehensive scheme of such radical post-modification of PP and a recent review on this topic can be found in the work by Passaglia *et al.* [50].

The melt state rheology of coagent treated PP have been studied under steady shear [51,52], oscillatory shear [53,54] and extensional deformation [53,55]. These studies have shown that a wide range of coagent systems are effective in generating LCB characteristics from a linear PP homopolymer. The efficiency of different systems of coagents to introduce LCB as opposed to cross-linking and degradation of PP homopolymer was compared by Graebling, [56], Borsig et al. [54] and Parent et al. [55]. The sensitivity of the degree of branching to the chemical structure of the coagent is demonstrated by Gotsis and Zeevenhoven [57], who used peroxydicarbonate (PODIC) coagents, with different side groups. The efficiency of the specific PODIC to induce LCB in L-PP depended on the size of the PODIC side groups. Longer and bulkier side groups on the PODIC were found to be more efficient than the equivalent linear ones.

Even though coagent modified PPs have been well-characterized in the literature, their foaming behaviour has not been investigated extensively. The report by Nam et al. [53] found improvements in the foam morphology of a PP treated by trimethylolpropane triacrylate. However the authors focused more on the selection of appropriate processing conditions, rather

than the modification of PP itself. The improved foaming behaviour of modified PP was attributed to the ability to reduce cell coalescence induced by long chain branching. Liao et al. [58] modified a commercial linear PP by addition of peroxide and pentaerythritol triacrylate (PETA). The resulting material was foamed in an autoclave using supercritical carbon dioxide as a physical blowing agent at 130 ℃, which is close to the crystallization temperature of PP. The foaming behavior was correlated with the crystal structure and the rheological properties of polymers. The crystals in PPs acted as heterogeneous nucleation cites for bubbles, but the cell density of LCB PP was much higher than that of linear PP because of its higher spherulite density. The higher viscosity of branched PP further made its cell diameter smaller than that of linear one. However, no explanation was offered on the change in crystallization behaviour of the LCB PP over the original linear PP.

2.6 Nucleating Agents for Foaming and Crystallization of Polypropylene

In PP compounds the polymer morphology and crystallization behaviour can be modified by the incorporation of nucleating agents (NAs). The crystallization temperature, spherulite size, optical properties (e.g. haze, clarity), mechanical properties (eg. elastic and flexural modulus) and cycle time to get the final products are altered in the presence of NAs [59]. Furthermore, during foaming, NA particles provide nucleation sites for gas molecules.

The application of small particle size minerals, such as silica, talc [60], clays, etc., as fillers and as NAs for PP crystallization is common industrial practice. When these minerals are used at loadings under 5 wt. %, they are no longer considered as fillers but as NAs [61].

Certain organic compounds are also used as NAs for crystallization. Sorbitol derivatives form one significant family of NAs applied to PP to induce crystal modification and increase clarity. Addition of about 0.1-0.3 wt. % (1 wt. % at the most) raises the peak crystallization temperature (measured at a cooling rate of 10 °C/min) from ~110 °C for the neat PP to about 125-130 °C for

the PP/NA mixture [62-64]. Other compounds such as sodium benzoate [65] and organic phosphorous [66] have been revealed as effective NA for PP. More recently Blomenhofer et al. [67] have discovered that substituted 1,3,5-benzenetrisamides are extremely efficient NAs for i-PP at exceedingly low concentrations (as low as 0.02 wt %). These compounds are able to increase both the clarity and toughness of i-PP.

2.7 Foaming of Nanocomposites

Nanocomposites usually refer to composites in which at least one phase (the filler phase) possesses ultrafine dimensions (on the order of a few nanometers) [68]. Polymer nanocomposites offer improved mechanical properties (e.g., modulus, strength) and physical properties (e.g., thermal stability, gas barrier properties) over their matrix materials [69,70]. Nanocomposite-based foams have been investigated given the potential of a nano-dispersed phase to act as heterogeneous nucleating agent. To fully utilize the interfacial area between the dispersed phase and polymer matrix for nucleation, much attention must be paid to the interfacial chemistry between the two phases [71-73]. Reduced cell size and increased cell density have been observed as chemical treatment was applied to the nanoparticles to enhance their compatibility with the matrices. Zhu et al. [74] applied a diblock copolymer, polystyreneblock-poly(2-vinyl pyridine) (PS-b-P2VP), to exfoliate an organoclay within a PS matrix. Their experimental results indicated that only exfoliated layered-silicate could inhibit the cell expansion and had high nucleation efficiency during foaming. On the contrary, aggregated layered-silicate in PS did not show any effect on the cell morphology of PS foam produced in a batch foaming process using supercritical CO_2 as a blowing agent. In more industrial oriented practice, coupling agents such as maleic anhydride grafted polyethylene/polypropylene (PE-g-MA/PP-g-MA) have been employed instead of intricate surface chemistry treatments or specialty synthesized polymers [75-77]. It has been

shown that such coupling agents are effective in exfoliating the clay [75] or at least in increasing the layer spacing in the clay structure by polymer molecular chains intercalation with the layer structure of the clay particles [77]. The optimal amounts of clay required to achieve foams with cell densities higher than 10^9 cells/cm^3 was between 0.02 to 0.1 wt. %.

Nanosilica is a low aspect ratio filler, which can potentially act as a nucleating agent. Despite recent research on composites containing nanosilica dispersed in a polyolefin matrix which showed a great potential for significant property improvements [78-81], there are very few studies on the optimization of the compounding conditions for the purpose of foaming in a continuous process.

Chapter 3

Effect of Molecular Structure and Rheology on the Compression Foam Moulding of Ethylene-α-olefin Copolymers*

3.1 Introduction

Metallocene, or single-site catalyst based ethylene-α olefin copolymers (ECs) have found widespread use in the polyolefin industry owing to their narrow molecular weight distribution and uniform comonomer content distribution [82,83], which result in exceptional properties. In recent years, the effects of processing and material properties on the foaming behaviour of ECs and their cross-linked counterparts have been studied extensively [33-36,84]. Mao and Qi reported that the amount of chemical blowing agent and the processing temperature played a significant role on foam density and physical properties [36]. Yamaguchi and Suzuki [33] obtained EC foams with higher expansion ratios and more homogeneous cell size distributions by adding a small amount of cross-linked EC (as low as 1 wt%). This improvement was attributed to the enhancement of the elongational viscosity and elastic modulus in the presence of the cross-linked material. However, the presence of gels caused by cross-linking can cause adverse effects. Abe and Yamaguchi [34] compared the expansion ratio of two dicumyl peroxide cross-linked ECs, containing different gel contents. They found that the changes in elastic modulus and crystallization temperature influenced the expansion ratio of cross-linked PE foams. Specifically, as the elastic modulus increased upon increasing gel content, the expansion ratio of the foams decreased. On the other hand, a lowered crystallization temperature at increasing gel contents caused shrinkage of the

*A version of this chapter has been published. Zhang, Y., Kontopoulou, M., Ansari, M., Hatzikiriakos, S.G., and Park, C.B. Polymer Engineering and Science 2011 (1); 1145-1154

foams, resulting in a lower expansion ratio. The effect of elasticity on the foaming of cross-linked EC was also addressed by Tai [35], who attributed the contraction of the foams to the relaxation process of the highly cross-linked EC matrix. All results found in the existing literature on foaming of cross-linked EC converge to similar conclusions; mainly a good balance between melt viscosity and branching must be maintained in order to obtain good foams [84].

Most work on EC foams has focused on cross-linked EC, because of the perceived industrial importance and flexibility to manipulate the rheological properties. However foaming is a very delicate and involved process and cross-linking introduces further structural complication to the system, making it difficult to gain a fundamental understanding of the effect of various material parameters. Studies on uncross-linked ECs are scarce [85] and not much attention has been paid to the effect of material properties, such as the molecular weight and branch type/branch content on their foaming behaviour. By choosing judiciously EC grades with well-defined structures, it is possible to analyze the effect of molecular structure on the structure and the mechanical properties of the resulting foams. The aim of this chapter is to study a series of well-characterized ECs in an attempt to establish relations among their molecular structure, rheological properties, and foaming behavior.

3.2 Experimental

3.2.1 Materials

Five ethylene-octene copolymers supplied by Dow Chemical (Engage™ grades) and an ethylene-butene copolymer (Exact® grade) supplied by ExxonMobil Chemical were used. All the materials are commercially available. Their properties as reported by the suppliers as well as designation used for this work are presented in **Table 3.1**.

Table 3.1 Material properties and sample designation of the mPE materials.

Material	Supplier	Designation	Comonomer Content (wt.%)	Density (g/cm^3)	Melt Flow Index*
Exact® 4033	ExxonMobil	Bu 0.8/0.880	N/A	0.880	0.8
Engage™ 8842	Dow Chemical	Oct 1.0/0.857	45	0.857	1.0
Engage™ 8100	Dow Chemical	Oct 1.0/0.870	38	0.870	1.0
Engage™ 8003	Dow Chemical	Oct 1.0/0.885	30	0.885	1.0
Engage™ 8450	Dow Chemical	Oct 3.0/0.902	20	0.902	3.0
Engage™ 8480	Dow Chemical	Oct 1.0/0.902	20	0.902	1.0

*190 °C/2.16 kg

The density of the ECs varied from 0.857 to 0.902 kg/m^3 as a result of different amount of copolymer incorporated in the molecule. The melt flow index (MFI) of all the EC samples was around 1.0 g/10 min except for Engage™ 8450, which had a lower molecular weight. Azodicarbonamide (AZ) supplied by Sigma-Aldrich Canada was used as the chemical blowing agent. According to the material data sheet, its decomposition starts at 160°C. However, rheological tests performed on the sample blends showed that it was stable at 180°C for at least 30 min.

3.2.2 Compounding

A constant amount of 0.5 wt% AZ was blended with each sample using a Haake Polylab Rheocord torque rheometer equipped with a mixing chamber and a pair of rotors at 60 rpm. According to the MSDS sheet from the vendor, AZ decomposes at 160°C. The octene-ethylene copolymers were compounded at 120°C and the butene-ethylene copolymer was compounded in

at 140°C. These conditions have been selected to ensure that processing took place at temperatures above the melting points of the materials (shown in **Table 3.2**), but below the decomposition temperature of AZ. The higher temperature for Bu 0.8/0.880 was chosen because of its higher viscosity at shear rates relevant to compounding.

3.2.3 Compression Foam Molding

ECs blended with AZ were charged into a preheated frame mold (197 × 197 × 3 mm^3), having a 3 mm thick copper plate cover, and pressed at 200°C for 15 min under 30 tons of clamping force. Subsequently the clamping force was completely removed, and the pressure was reduced to atmospheric. Foam expansion occurred upon pressure release and the mould assembly was transferred to a press and kept at 50°C to obtain foams with smooth surface.

3.2.4 Rheological Characterization

Shear Oscillatory measurements

Compression molded disks were prepared at 140°C. A controlled stress rheometer, ViscoTech by Reologica, with 20-mm parallel plate fixtures was used in the oscillatory mode at a gap of 1 mm to measure linear viscoelastic properties of as received ECs as a function of angular frequency (ω). The temperature ranged from 150 to 195°C. Stress sweeps were performed to ensure that all measurements were within the linear viscoelasticity regime. The average of three measurements is reported throughout this thesis. The estimated standard deviation is 10%.

Data obtained at 195°C were fitted to the Cross model,

$$\eta(\omega) = \frac{\eta_0}{1+|\lambda\omega|^{(1-n)}} \tag{3.1}$$

where η is the shear viscosity, η_0 is the zero shear viscosity, λ is the relaxation time, n is a constant related to the shear thinning behaviour, and ω is the frequency in rad/s.

Uniaxial Extension

As-received ECs were rheologically characterized in simple uniaxial extension using an SER-2 universal testing platform from Xpansion Instruments hosted on the MCR-501 Anton Paar rheometer [86,87]. Measurements were conducted at 150°C under extension rates ranging from 0.010 and 10 s^{-1} and under a nitrogen atmosphere to limit degradation and the absorption of moisture. Specimens were prepared by compression molding the polymer samples between polyester films to a gage of about 1 mm, using a hydraulic press. Individual polymer specimens were then cut to a width of 6.4–12.7 mm. Typical SER extensional melt rheology specimens ranged from 40 to 150 mg in mass. Linear viscoelastic oscillatory measurements were also obtained at 150°C using the MCR-501 Anton Paar rotational rheometer, in order to calculate the LVE and check the consistency of the extensional measurements.

3.2.5 Mechanical Property Characterization

Test samples conforming to ASTM D412-06a type C were stamped out of foamed EC plates. A crosshead speed of 500 mm/min was applied due to the elastic nature of tested samples at room temperature. Because all studied ECs are not rigid enough to exhibit linear stress-strain behavior during the tensile test, secant moduli values at a strain of 2% were reported rather than the Young's modulus. Five replicates were tested for each sample to ensure reproducibility.

3.2.6 Density Measurements and Foam Characterization

The density of the foams was measured by an electronic densimeter (Mirage MD-200S, Mirage Trading Co., Ltd) based on the water displacement method. It should be noted that the density measurements obtained by this method where in agreement (within 2%) with values obtained using an apparent density measurement, according to ASTM D 1622-98. The volume expansion

ratio (VER) was calculated as the ratio of bulk density of the pure polyolefin material (ρ_p) to the bulk density of the foam sample (ρ_f):

$$\mathrm{VER} = \frac{\rho_p}{\rho_f}. \tag{3.2}$$

The void fraction (v_f), which is the ratio of the volume of the gas phase contained in a foam sample to the total volume of the foam, was calculated by

$$v_f = 1 - \frac{1}{VER}. \tag{3.3}$$

3.2.7 Differential Scanning Calorimetry

Differential scanning calorimetry (DSC) was conducted on all ECs to determine their crystallization temperature using a TA Instrument DSC Q 100. Weighted samples were sealed in aluminum hermetic pans and heated up to 170°C at a rate of 5°C/min. They were then held isothermally at 170°C for 1 min before cooling at 5°C/min to −60°C to measure the crystallization temperature (T_c). After maintaining the temperature for 2 min at −60°C, a second heating cycle was conducted at 5°C/min to 170°C in order to determine the melting point (T_m) and heat of fusion. The crystallinity (W) of the samples was calculated by dividing the heat of fusion using the heat of fusion of 100% crystalline PE (293 J/g).

3.2.8 Scanning Electron Microscopy and Cell Size Determination

EC foam samples were cryogenically fractured under liquid nitrogen and sputtered with gold. A JEOL JSM-840 scanning electron microscope was used to characterize the cell morphology of the foams. The image analysis software, SigmaScan Pro, was utilized to estimate the cell diameters, according to $d = \sqrt{\frac{4A}{\pi}}$. The number average, d_n and volume average, d_v, diameters were calculated from the resulting data. Generally since the plane of observation does not always cut

the particles through their equator, the Schwartz-Saltikov correction [88] is commonly employed to provide a corrected diameter. However for a nearly monodisperse distribution, where $d_v/d_n \cong 1$, the diameter correction is given by a constant equal to $4/\pi = 1.27$ and commonly neglected when employed for comparison purposes [89]. In the case of the foams under consideration in this chapter, $d_v/d_n \cong 1.2$.

The cell density of the foams with respect to the unfoamed polymer volume (*N*) was calculated by the following equation [22]:

$$\mathrm{N} = \left(\frac{\mathrm{N_0}}{\mathrm{A}}\right)^{\frac{3}{2}} \mathrm{VER} \tag{3.4}$$

where N_0 is the number of cells in a specified area *A*, and *VER* is the volume expansion ratio.

3.3 Results and Discussion

3.3.1 Small Amplitude Oscillatory Shear Rheology

The storage moduli and complex viscosity of all EC samples as a function of the angular frequency (ω) at 195°C are presented in **Figure 3.1 (a)** and **(b)**, respectively. As expected all the octene-ethylene copolymers with an MFI value of 1 (g/10 min) have very similar viscoelastic behavior in terms of complex viscosity and storage modulus. In the low frequency range (<1 rad/s), the storage modulus of ethylene-octene copolymers with an MFI of 1.0 showed a slight increase with decreasing comonomer content (increasing density). However, this difference was subtle and disappeared as the frequency increased.

Sample Oct 3.0/0.902 exhibited lower storage modulus and complex viscosity over the entire frequency range due to its lower molecular weight as indicated in **Figure 3.1**. The response of Bu

0.8/0.880 is highly differentiated from the others, since it is the least elastic and least shear thinning sample, due to the presence of short chain branching, as opposed to the long chain branching of the octene-based materials. These findings are also reflected by the Cross model parameters (**Table 3.2**) in terms of the zero shear viscosity and the characteristic relaxation time, the inverse of which indicates the characteristic frequency for the onset of shear thinning.

Table 3.2 Cross model parameters at 195°C obtained by fitting of the dynamic oscillatory curves shown in **Figure 3.1 (b)**, and thermal properties measured by DSC.

Sample Name	**η_0 (Pa.s)**	**λ (s)**	**T_m (°C)**	**T_c (°C)**	**W (%)**
Bu 0.8/0.880	8980	0.03	62.1	49.4	15.6
Oct 1.0/0.857	9558	0.18	39.2	11.6	7.1
Oct 1.0/0.870	9765	0.17	59.2	44.9	12.6
Oct 1.0/0.885	11326	0.38	81.6	59.9	18.9
Oct 3.0/0.902	3234	0.05	100.5	79.7	28.8
Oct 1.0/0.902	17328	1.82	100.2	81.9	28.9

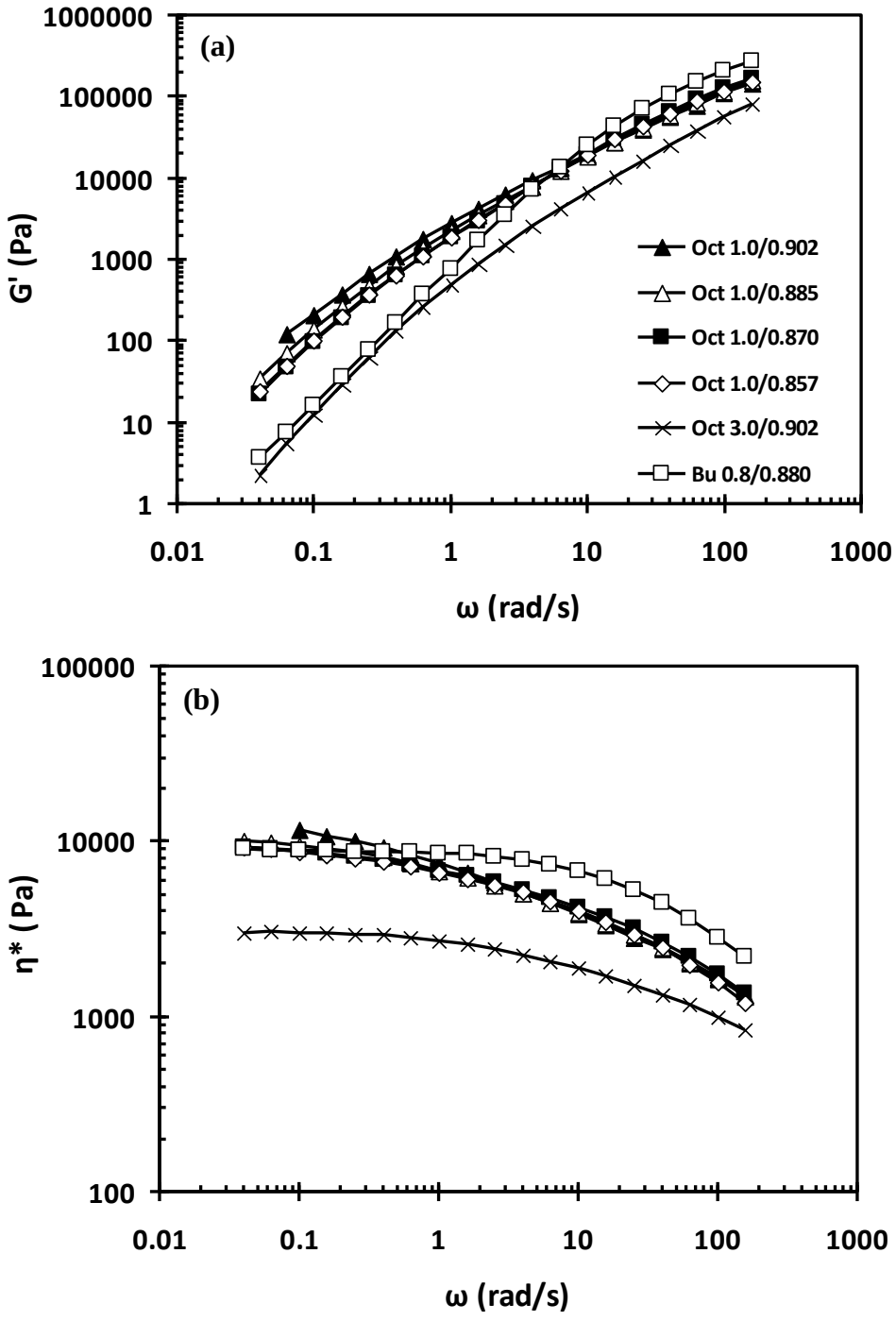

Figure 3.1 Shear oscillatory data of ECs as a function of frequency at 195°C; **(a)** storage modulus; **(b)** complex viscosity.

Van Gurp-Palmen plots can be used to further differentiate the polymers with similar MFI, since they provide an effective phenomenological approach to detect the presence of long chain branching (LCB) in linear polyolefins [39,90,91]. As seen in **Figure 3.2**, the loss angle values were lower as sample density increased for octene-ethylene copolymers. From the Van Gurp-Palmen plots it can be inferred that sample Oct 1.0/0.902 has the highest LCB level among all materials tested and Bu 0.8/0.880 contains small amounts of short chain branching (SCB). On the other hand Oct 1.0/0.902 has a lower M_w than Oct 1.0/0.870 and Oct 1.0/0.885 [90] but exhibited highest G', η_0 and degree of shear thinning, which is a result of its LCB structure [39]. It was also noted that the degree of superposition of Van Gurp-Palmen plots measured at different temperatures varies. Perfect superposition was observed in plots of Bu 0.8/0.880, while Oct 1.0/0.902 did not superimpose well (see **Figure 3.3**). Lack of superposition indicates temperature dependence of the flow activation energy, and is usually observed in LCB containing polyethylene [39,92,93]. The activation energies for the octene-based LCB polyethylenes, as determined through time-temperature superposition ranged between 44 and 46 kJ/mole, whereas that for the butene based material was much less, at 35 kJ/mole.

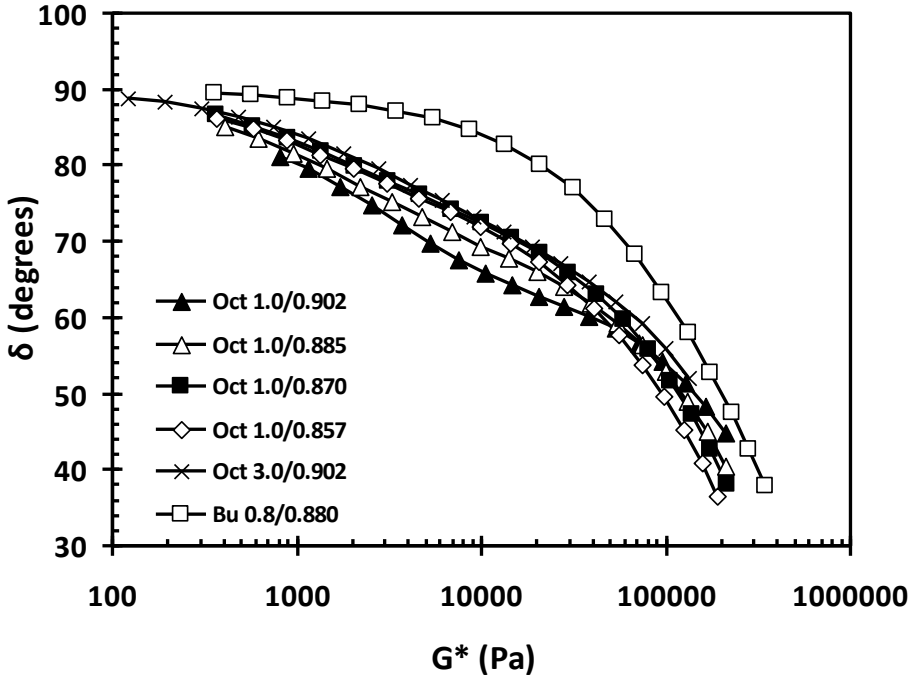

Figure 3.2 Van Gurp plots showing phase angle as a function of complex modulus at 195 °C.

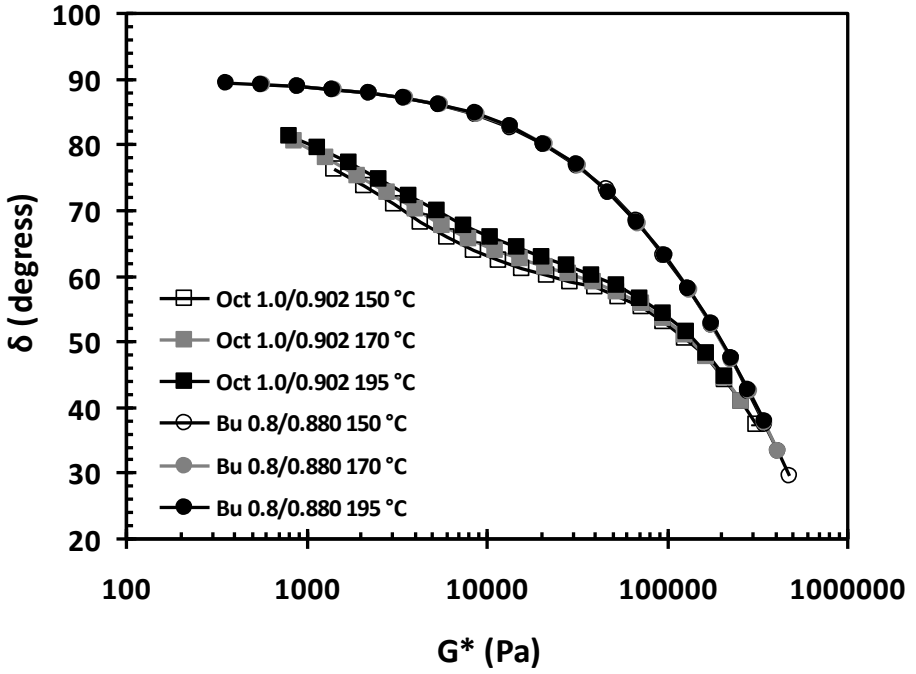

Figure 3.3 Van Gurp plots showing phase angle as a function of complex viscosity for Oct 1.0/0.902 and Bu 0.8/0.880 at three temperatures.

3.3.2 Extensional Rheology

Measurements of the tensile stress growth coefficient of all ECs are shown in **Figure 3.4** at several Hencky strain rates. The individual curves have been multiplied by an arbitrary factor (listed in the figure) for the sake of clarity. The initial parts of the extensional response for all cases followed the theoretical LVE stress growth curves. However, at larger times all tested samples exhibited a negative deviation (strain softening) up to an inflection point, beyond which strain hardening was observed. This negative deviation of the tensile stress growth coefficient from the LVE has never been reported before.

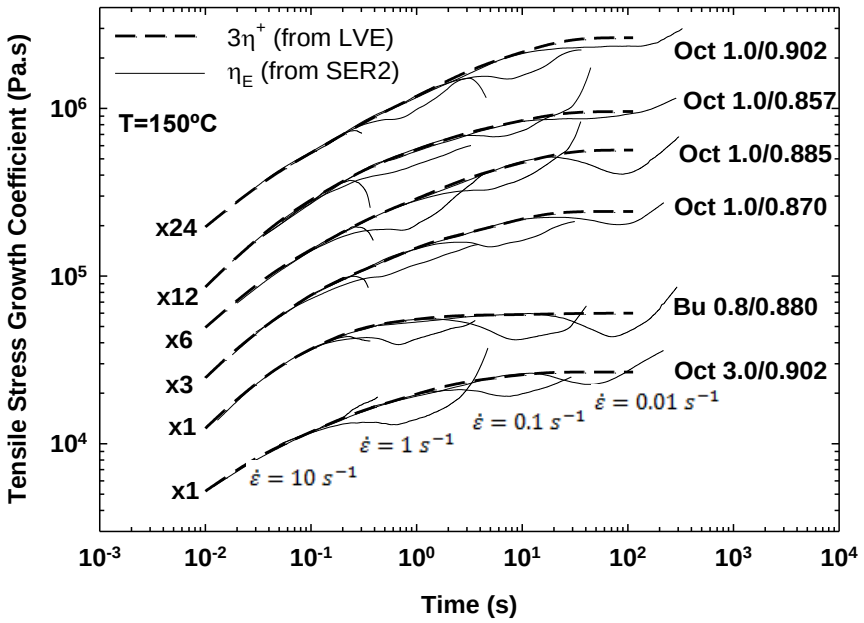

Figure 3.4 Tensile stress growth coefficient of all EC samples at different strain rates at T=150 °C.

Further extensional tests performed at lower temperatures of 80, 100, and 120 °C, accompanied with visual observations excluded the possibility that such downward deflection of the curves (initial strain softening) was caused by sagging of the samples. **Figure 3.5** plots the stress growth

coefficient for sample Oct 1.0/0.870 at several Hencky strain rates and temperatures as low as 80°C. The initial strain softening and subsequent strain hardening is observed at all temperatures and Hencky strain rates, except at 10 s^{-1} where the significant stretching causes failure of the sample before the occurrence of hardening. The response is due to some initial yielding of the sample (similar to that observed in the extension of solid PE samples) that is followed by a subsequent hardening and finally a brittle catastrophic failure.

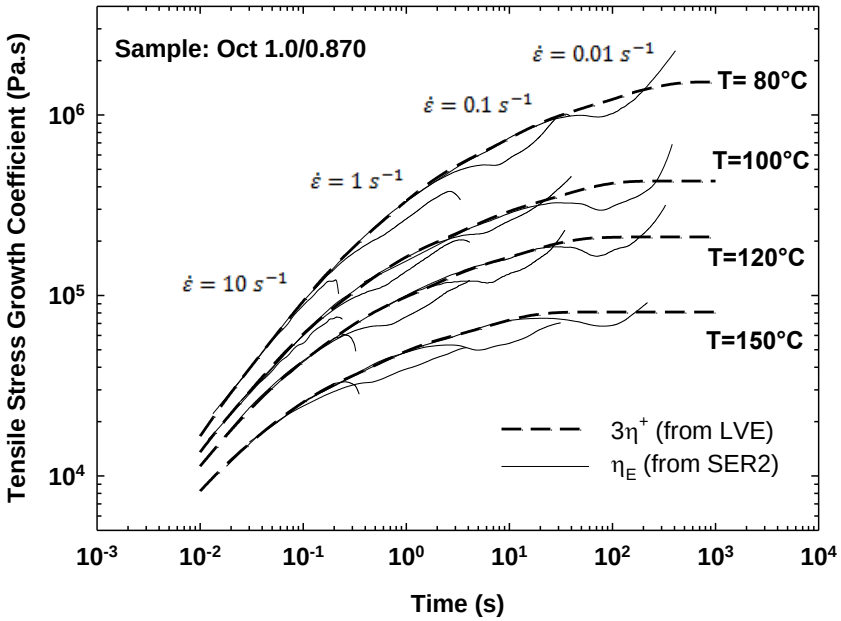

Figure 3.5 Tensile stress growth coefficient of Oct 1.0/0.870 at different strain rates and temperatures. The initial strain softening appears at temperatures as low as 80°C (only slightly above the melting point).

Figure 3.6 and **7** further demonstrate that the initial strain softening is not due to sagging of the material. **Figure 3.6** plots the tensile stress growth coefficient of sample Oct 1.0/0.870 at the Hencky strain rate of 0.1 s^{-1} at the temperature of 80°C. Corresponding images of the tested sample at the numbered locations along the curve appear in **Figure 3.7**.

Clearly sagging is excluded and it is evident that the material undergoes some initial yielding that leads to strain softening, followed by strain hardening. Previous results on the tensile stress growth coefficients of other linear polyethylenes would lead to ductile failure of the material. On the contrary, the present materials after yielding (ductile response) recover to exhibit strain hardening, which subsequently leads to brittle catastrophic failure (note the sudden drop of the coefficient at point 7).

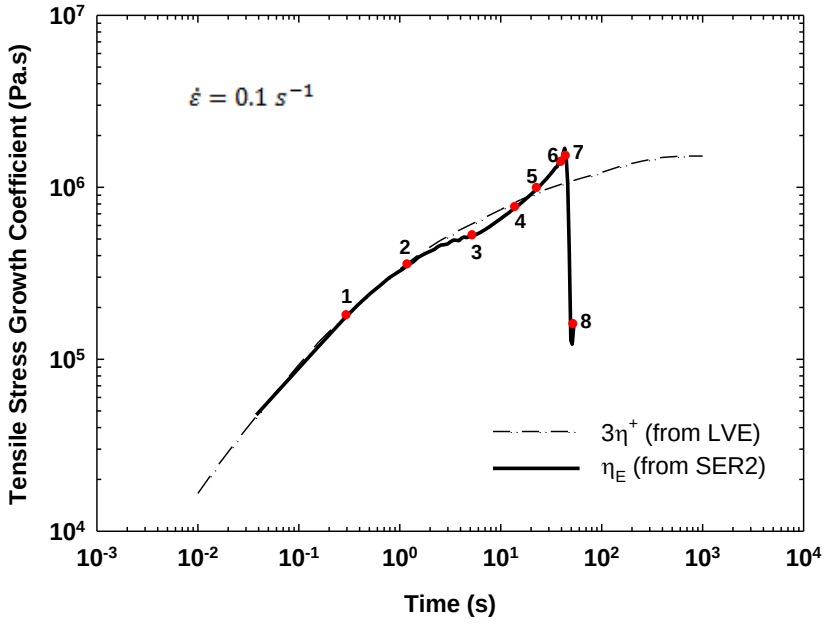

Figure 3.6 Tensile stress growth coefficient of Oct 1.0/0.870 at a Hencky strain rate of $0.1s^{-1}$ at T=80°C. Images of the condition of the samples at numbered locations appear in **Figure 3.7**.

Furthermore the trends observed for the various samples were different, depending on the material structure (octene versus butene based). This is better seen in **Figure 3.8 (a)** and **(b)**, which summarize the curves at the lowest and highest Henky strain rates, respectively. At a strain rate of 0.01 s^{-1} the tensile stress growth coefficient of Bu 0.8/0.880 was lower than that of the

octene-ethylene copolymers with an MFI of 1.0. On the contrary, the stress growth coefficient was highest for the butene-based material at all times at the highest strain rate.

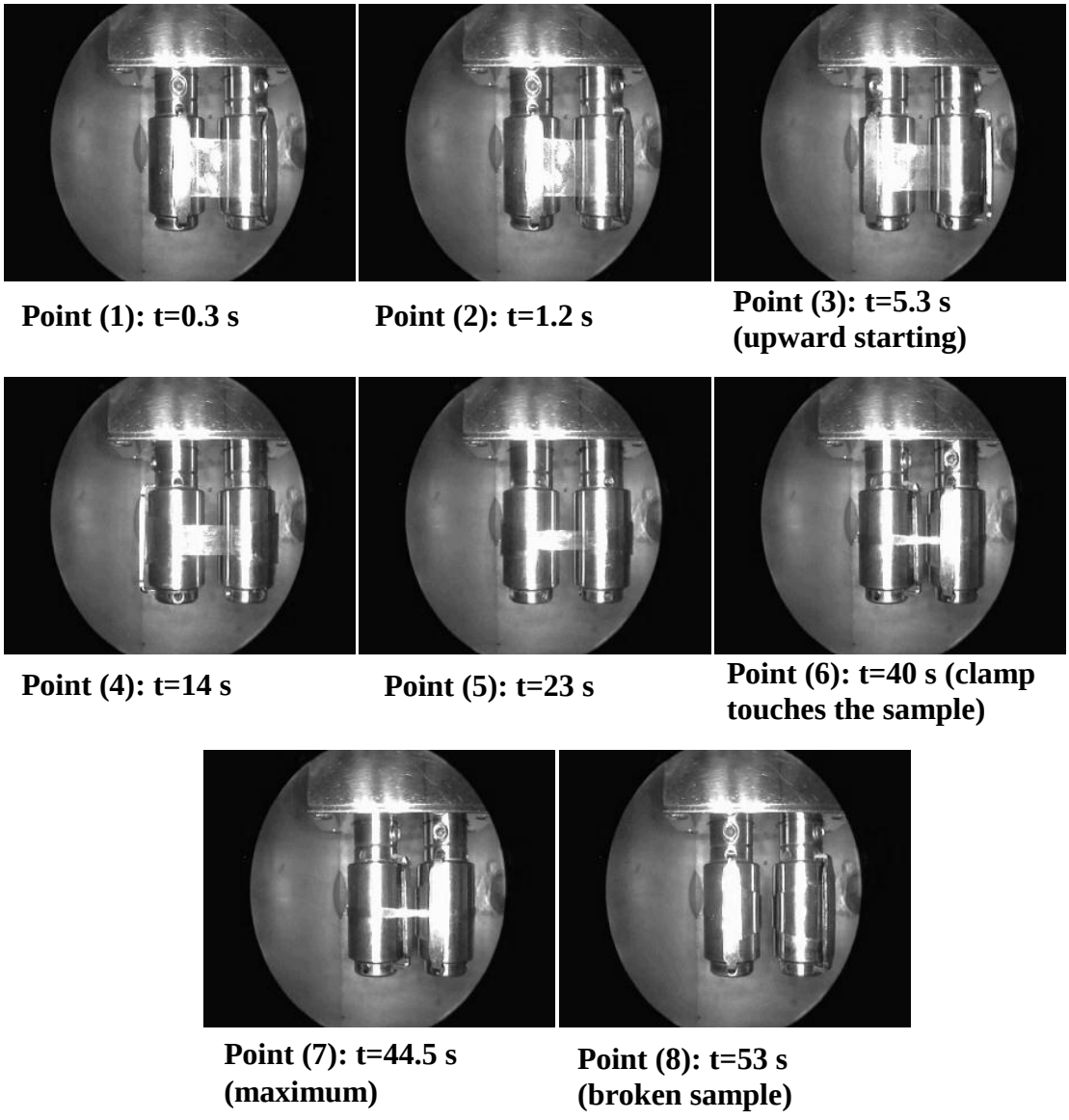

Figure 3.7 Slide show showing the extensional test of sample Oct 1.0/0.870 at a Hencky strain rate of $0.1s^{-1}$ at T=80°C. Images have been taken at times corresponding to the points numbered in **Figure 3.6**.

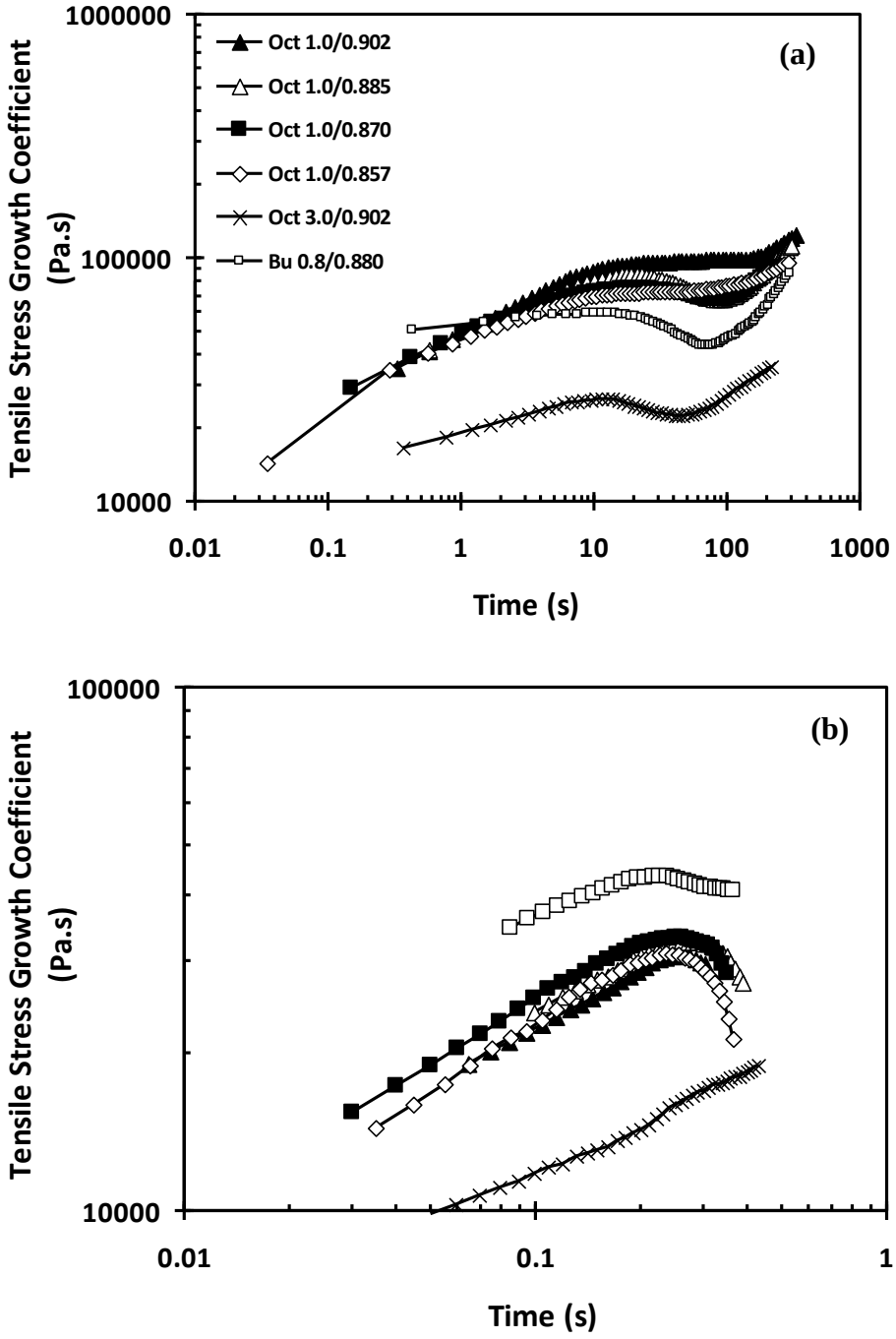

Figure 3.8 The tensile stress growth coefficient of EC samples at 150°C; **(a)** 0.01 s^{-1} strain rate, **(b)** 10 s^{-1} strain rate.

3.3.3 Cellular Morphology

Foams exhibited a typical skin-core structure, which is a characteristic result from compression molding. However, an observation of the well-developed core part of the foams revealed that the cell diameter of Oct 1.0/0.857 and Bu 0.8/0.880 was significantly larger than the rest of the ECs, which featured similar cell morphology, with uniform, spherical cells (**Figure 3.9** and **Figure 3.10**).

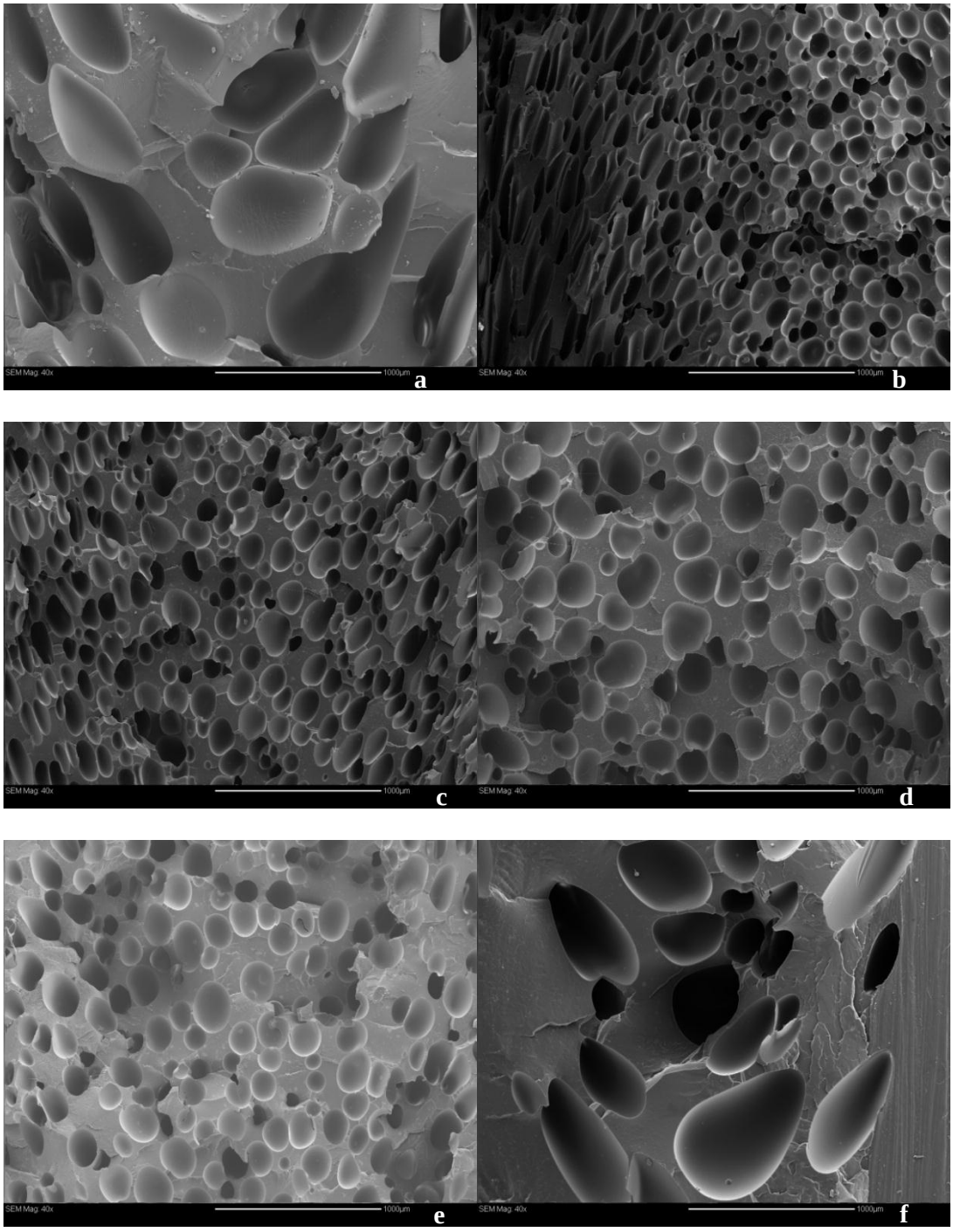

Figure 3.9 SEM images taken from the cross-section of EC foams: **(a)** Oct 1.0/0.857, **(b)** Oct 1.0/0.870, **(c)** Oct 1.0/0.885, **(d)** Oct 1.0/0.902, **(e)** Oct 3.0/0.902, **(f)** Bu 0.8/0.880. The scale bar represents 1000 μm.

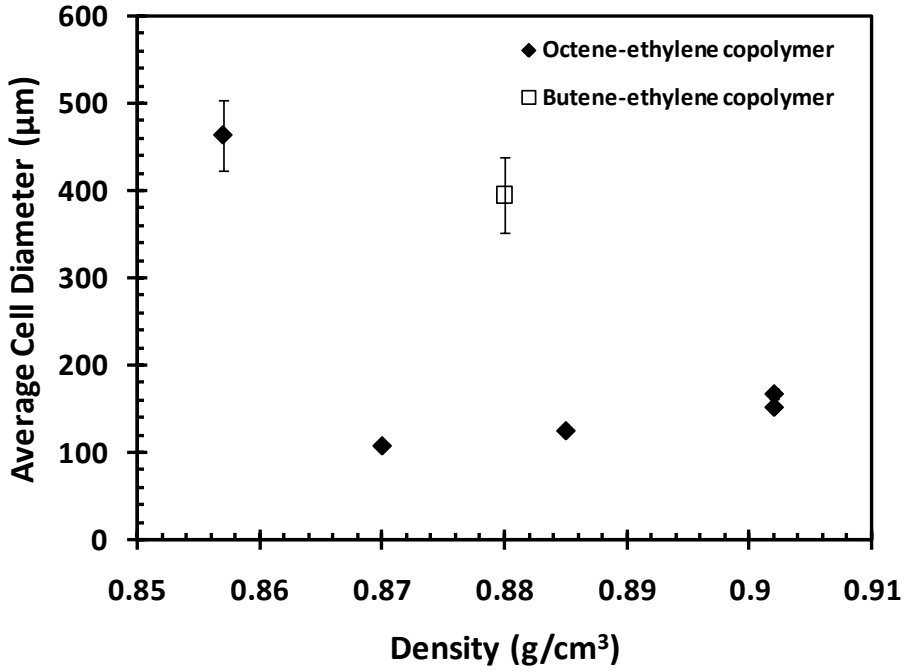

Figure 3.10 Average cell diameter of foamed ECs as a function of polymer density. Error bars represent the standard deviation.

The void fraction of all foams, obtained based on ***Enq.*3.3**, follows a linear trend when plotted as a function of cell density [94] as shown in **Figure 3.11**. This plot shows clearly a discrepancy for the Oct 1.0/0.857 sample, as it deviates from the otherwise linear trend. For this sample the high void volume arises from a small number of large, distorted cells, as can be seen from **Figure 3.9 (a)**, but otherwise the cell density defined as the number of cells per unit volume of the unfoamed polymer [95] is low. From **Figure 3.11** it becomes clear that the cell density was significantly lower for Oct 1.0/0.857 and Bu 0.8/0.880 compared with the rest of the octene-based materials.

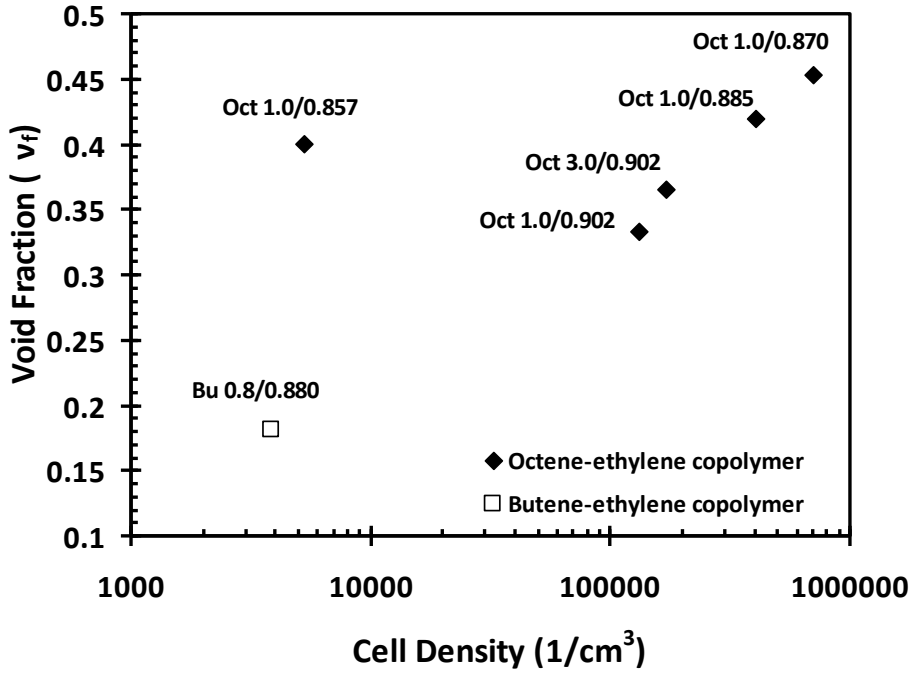

Figure 3.11 Void fraction of the foamed ECs as a function of cell density.

From these results it is obvious that the foaming behavior of Oct 1.0/0.857 and Bu 0.8/0.880 was distinct. The low cell number density of Oct 1.0/0.857 and Bu 0.8/0.880 foams, characterized by large, distorted cells, may be attributed to severe coalescence of cells during expansion. Upon simple inspection of **Figure 3.1-5** it is obvious that the rheological properties of Oct 1.0/0.857 are similar with the rest of the octene-based materials. Therefore differences in rheology cannot be the reason for its different foamability. However, as shown in **Figure 3.12**, this material has no distinct crystallization peak compared to the other ECs, which is an indication of a highly amorphous material. For clarity in **Figure 3.12** the crystallization exotherms of only three materials are shown, whereas all the crystallization points are summarized in **Table 3.2**. A weak and very wide peak is located around 12°C, which means that during cooling of the compression molded foams, which was done by maintaining the press to 50°C, the material remained in a softened state for much longer time than the rest of the polymers. This should result in

significantly higher gas diffusivity within Oct 1.0/0.857, causing more severe coalescence and/or gas escaping from the foamed sample. The combined final result was the observed large cell morphology. This indicates that proper control of cooling conditions is required for producing a desirable foam structure.

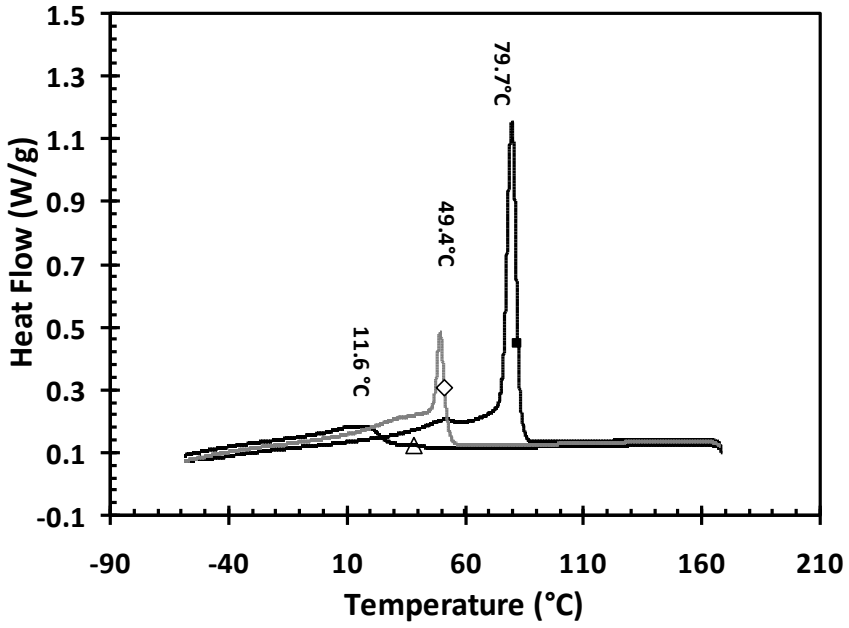

Figure 3.12 DSC exotherms of selected ECs recorded during cooling at 5 °C/min. Crystallization temperatures are shown over the respective peaks; ■ Oct 3.0/0.902, ◊ Bu 0.8/0.880, Δ Oct 1.0/0.857.

On the other hand, Bu 0.8/0.880 displays differences in its extensional properties, having a higher value of extensional viscosity than the rest of the materials at high strain rates, and lower values at a low strain rate. Given that the coalescence stage during foaming most likely is associated with low strain rates [96], the low extensional viscosity of this material might be the cause for its higher propensity toward cell coalescence. It should be noted that Oct 3.0/0.902 also has a low extensional viscosity. This might be counteracted by its higher crystallization temperature (see

Figure 3.12), which results in faster solidification of the foam, thus reducing the probability of cell coalescence. Surprisingly in spite of its substantially lower molecular weight, this material showed a very similar foaming behavior as its higher molecular weight Oct 1.0/0.902 counterpart. The complex interplay between viscosity, elasticity and melt strength on one hand, and thermal properties on the other, which affect both the rate of cell growth and cell coarsening may be responsible for this observation. More in-depth studies are needed to clarify these phenomena.

In addition to the above reasons, a few other factors must be considered as well: First, Oct 1.0/0.857 and Bu 0.8/0.880 could have nucleated a smaller number of cells. The initial amount of blowing agent was the same in all the samples, and thereby the initial number of nuclei may be considered to be the same [97]. However, the solubility of gas in the materials would be different because of the varying amount and type of branching of the EC materials, resulting in different free volume and different swelling behavior [98,99]. Therefore, the extent of thermodynamic instability during decompression may be different, even with the same amount of dissolved blowing agent. Additionally, proprietary additive packages, added to each material may also have an effect on heterogeneous cell nucleation. Since the homogeneous cell-nucleation rates are very low, most cell nucleation would be heterogeneous, occurring at the surface of additives and impurities compounded in the polymer matrix [100,101]. The effect of such additives on the cell nucleation density is generally very difficult to predict, unless they are well-known cell-nucleating agents with low activation energy such as talc or silica [60]. It should be noted however that TGA analysis of examined samples showed that they contained a very small (less than 0.1 wt%) inorganic solids content.

3.3.4 Mechanical Properties

As expected, the foams have a decreased secant modulus and elongation at break compared to the unfoamed samples, because of the density reduction (**Figure 3.13** and **14**). The classic rule of dependence of material strength on its density was obeyed by all samples. Oct 1.0/0.902 has a slightly higher modulus value compared to Oct 3.0/0.902 due to its higher molecular weight. The effect of type of branching was found to be insignificant in agreement with Sehanobish et al.'s work [102]. This implies that the worse cell foam structure of the butene-based copolymer actually did not affect the mechanical properties of the foam. In fact the secant modulus of the Bu 0.8/0.880 foam exhibited a positive deviation from the linear modulus/density dependence trend.

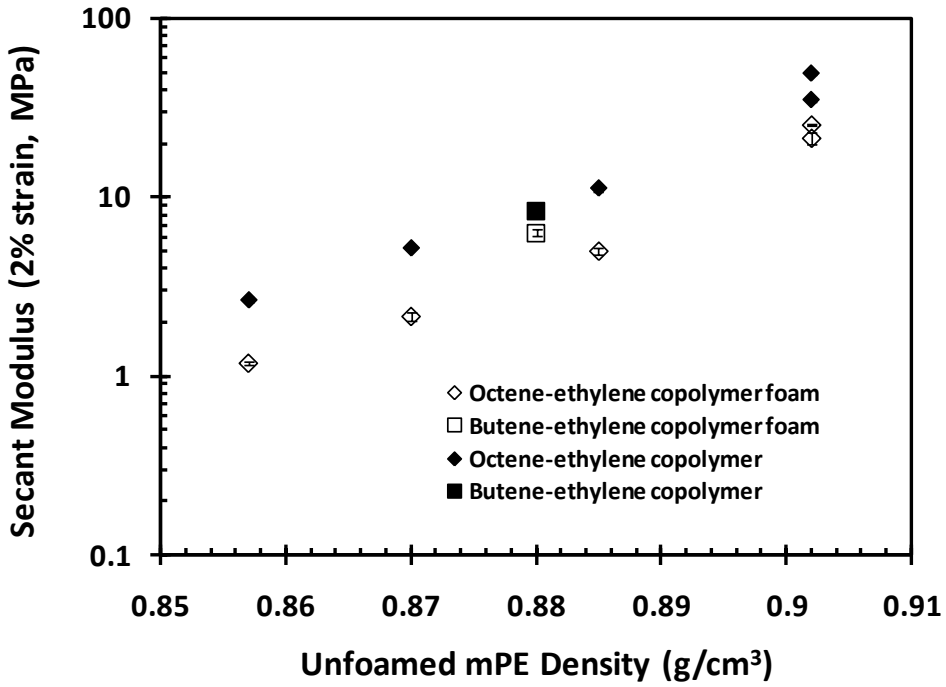

Figure 3.13 Secant modulus values of unfoamed and foamed EC as a function of unfoamed mPE density. Error bars represent one standard deviation.

The elongation at break values of pure EC samples did not vary significantly for any of the materials tested as shown in **Figure 3.14**. For the unfoamed samples all values were around 1400% with the exception of Oct 1.0/0.857, which exhibited a value of 947%. The foamed samples followed the same trend. It should be noted though that foams based on Oct 1.0/0.857 behaved uniquely, having the highest elongation than all other samples, with most specimens not breaking during the test.

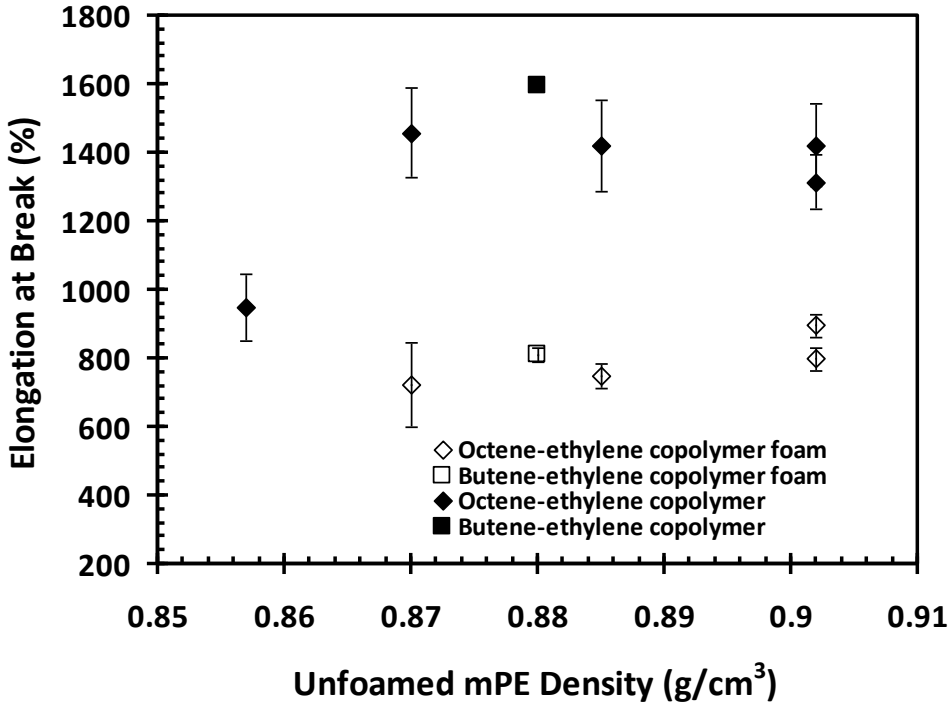

Figure 3.14 Elongation at break values of unfoamed and foamed EC as a function of unfoamed EC density. Error bars represent one standard deviation.

3.4 Conclusions

Ethylene-α-olefin copolymers of the same melt flow index displayed similar rheological properties irrespective of their density. A peculiar behavior was demonstrated during extensional

growth experiments, where all samples exhibited yielding followed by strain hardening, before brittle failure. This response was not associated to sagging of the samples.

The cell morphology of compression molded foams made out of ethylene-α-olefin copolymers was similar for all the octene-based grades having similar rheological properties. The butene-based sample had significantly lower extensional viscosity at low strain rates, which might have led to increased propensity for cell coalescence, leading to a coarser morphology. Coarser morphology was also noted for the octene-based copolymer sample with the lowest density, which did not have a well-defined crystallization point. This presumably led to increased chance of cell coalescence during cooling of the foam.

The mechanical properties of all foams were lower than those of the unfoamed samples, but kept the same trends; the highest density material had increased secant modulus, whereas the elongation at break was essentially unaffected by density.

This preliminary study on commercial polyolefins has highlighted the importance of extensional properties, as well as crystallization temperature on the foam quality. Based on the results, polymers with higher amounts of LCB are less prone to coalescence. However increasing the amount of LCB might lead to lower densities and to a suppression of the crystallization temperature, with detrimental effects. This study suggests that a molecular structure with small amounts of LCB to suppress coalescence, while maintaining a high crystallization temperature, to stabilize the foam structure during cooling, would provide the most desirable outcome. Such a fine tuning of structure is not possible by using commercially available polyolefins, therefore in the next chapter chemical modification approaches are suggested to obtain well-controlled structures having different molecular weights and levels of branching, as needed for a systematic

study. Polypropylene is employed, because of its commercial interest, and because it is easily amenable to well-known chemical modification methods.

Chapter 4

Structure, Rheology and Foaming Behaviour of Coagent Modified Polypropylene

4.1 Introduction

Although linear polypropylene (L-PP) has many desirable attributes, it is challenging to process on a commercial scale in processes involving extensional flow, such as thermoforming, cast and blown film extrusion, as well as foaming. This has been attributed to its low melt strength at processing temperatures [103]. Modification of PP to introduce long chain branching (LCB) is commonly practiced to provide increased melt strength and strain hardening, thus improving its processability in processing operations that involve extensional deformation [57]. In extrusion foam processing it has been shown that branched polypropylene (B-PP) offers a higher expansion ratio, alleviates cell coalescence and provides a more homogeneous cell structure compared to L-PP [49,60,104-106].

Among the methods available to increase the melt strength of commercial L-PP, solvent-free reactive processing, which employs peroxide initiated chain scission and coagent assisted cross-linking is a particularly attractive methodology [55]. This single-stage process involves simultaneous PP fragmentation and cross-linking, the balance of which controls the length, frequency and distribution of branches. A general scheme of such radical post-modification of PP and a recent review on this topic can be found in Passaglia et al. [50]. A wide range of coagent systems have been proven effective in generating long-chain branching (LCB) characteristics from a linear PP homopolymer. The efficiency of different systems of coagents to introduce LCB was compared by Borsig et al. [54], Graebling [56] and Parent et al. [55].

It is well known that reactive modification of PPs in the presence of peroxide and coagents results in substantial changes of their rheological and thermal properties, including viscosity decrease due to degradation, as well as increased melt elasticity and strain hardening attributed to the introduction of LCB. The melt state rheology of coagent treated PP has been studied under steady [51,52] and oscillatroy shear deformation [53,54] as well as extensional deformation [53,55,57,107]. Tian et al. [108] showed that increasing the pentaerythritol triacrylate (PETA) content in reactively modified samples resulted in a shift of the transition from the Newtonian plateau to the shear thinning regime indicative of the presence of LCB. Their Cole-Cole plots were also sensitive to the different LCB amounts. Similar trends in the complex viscosity curves, accompanied with the appearance of longer relaxation modes were also reported by Parent et al. [55] for triallyl and triacrylic systems.

Even though coagent modified PPs have been well-characterized in the literature, their foaming behaviour has not been investigated extensively. Nam et. al. found that introduction of LCB through reactive modification using trimethylolpropane triacrylate resulted in foams with higher expansion ratios [53], whereas Li et al. found that the melt strength as well as foamability of PP were improved as a result of LCB achieved through chain extension using an amine-glycidyl reaction [109]. It is generally accepted that these changes are due to the increased melt strength of LCB PPs, resulting in reduced coalescence and a more stable foam structure. However, as demonstrated by Gotsis and Zeevenhoven [57] in extrusion foaming of peroxydicarbonate (PODIC) modified L-PP, very high degrees of branching are not necessary to achieve improvements in foam processing properties. An optimum of 3 mmol/100 g PP PODIC concentration was identified as the composition that produced the most narrowly distributed small cell sizes. Possible reasons for the presence of an optimal LCB amount were that the increase in melt strength was counteracted by a reduction of the strain at break of the melt and that very high

amounts of LCB are accompanied by the presence of gel, which might compromise processability.

In spite of the vast literature pertaining to foaming, a clear understanding of the effect of polyolefin structure and rheological properties on the various foaming stages, such as nucleation, cell growth and coalescence is still lacking, due to the complexity of the process. This makes it difficult to understand how the modifications in the chain architecture of coagent modified PPs influence their foaming behaviour. This chapter employs chemical modification techniques, through the use of peroxides and coagents, to obtain well-controlled chain architectures starting from the same L-PP precursor. Modified PPs with well characterized evolving molecular weight, and chain structures make it possible to study separately the effects of polymer structure and thermorheological properties on the different stages of foaming.

4.2 Experimental

4.2.1 Materials

Triallyl trimesate (TAM, 98%, Monomer Polymer Inc.), trimethylolpropane thrimethacrylate (TMPTMA, 98%, Sigma-Aldrich) and dicumyl peroxide (DCP, 98%, Sigma-Aldrich) were used as received. ESCORENE™ PP 1042, an isotactic linear polypropylene homopolymer (L-PP) manufactured by ExxonMobil (MFR = 1.9 g/10 min,) was used as the starting material. N_2 and azodicarbonamide (AZ, Sigma-Aldrich Canada) was used as the physical and chemical blowing agent, respectively.

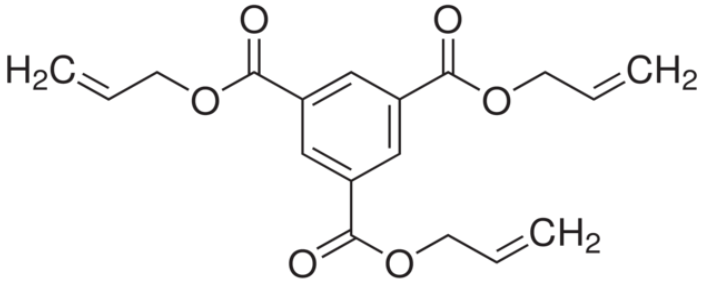

(a)

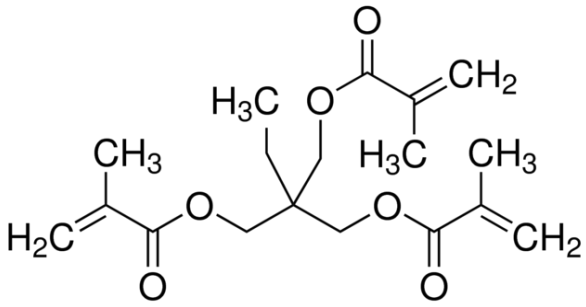

(b)

Figure 4.1 Chemical structures of **(a)** triallyl trimesate, and **(b)** trimethylolpropane thrimethacrylate.

4.2.2 Compounding

All blends were prepared using a Haake Polylab Rheocord torque rheometer equipped with a mixing chamber with a pair of rotors at 180 °C, 60 rpm. L-PP was also processed under identical conditions, to ensure consistent thermal history.The formulations and sample designations are listed in **Table 4.1**. PP powder was coated with DCP and coagent using acetone as a solvent. After the acetone was evaporated, the PP powder was charged into the mixing chamber and compounded for 10 min to ensure complete decomposition of DCP and reaction of the coagent. To prepare blends for compression molding, 1 phr AZ was charged into the chamber at the beginning of the eighth minute and mixed for 3 more minutes. A steady state torque reading was obtained for each formulation.

Table 4.1 Formulations and molecular weights of linear PP and its derivatives.

Sample Designation	DCP (phr*)	TAM (phr)	TMPTMA (phr)	M_n (kg/mol)	M_w (kg/mol)	M_w/M_n
L-PP	0	0	0	96.2	458	4.76
0.1 DCP	0.1	0	0	60.9	211	3.46
0.2 DCP	0.2	0	0	63.1	159	2.51
0.3 DCP	0.3	0	0	51.6	126	2.44
0.2 DCP 3 TAM	0.2	3	0	106.7	305	2.86
0.2 DCP 6 TAM	0.2	6	0	79.8	235	2.95
0.3 DCP 3 TAM	0.3	3	0	104	330	3.17
0.3 DCP 6 TAM	0.3	6	0	95.2	266	2.80
0.2 DCP 3 TMPTMA	0.2	0	3	67.1	210	3.13
0.2 DCP 6 TMPTMA	0.2	0	6	77.5	209	2.70
0.3 DCP 3 TMPTMA	0.3	0	3	83.0	212	2.55
0.3 DCP 6 TMPTMA	0.3	0	6	69.1	183	2.59

*part per hundred resin

The resulting coagent modified PPs (CM-PPs), PP-g-TAM and PP-g-TMPTMA were subjected to solvent extraction using boiling xylenes for 6 hrs in 120 mesh stainless steel pockets, according to test method ASTM D 2765. 0.3 g of each sample was placed in a pouch and sealed. The extracted pouches were dried in a vacuum oven at 150 °C for 12 hr. Multiple runs were performed for each sample.

4.2.3 Gel Permeation Chromatography (GPC)

Average molecular weights and molecular weight distributions (MWDs) were measured using triple detector GPC (GPCIR made by PolymerChar) at 145 °C. 1,2,4-Trichlorobenzene (TCB) was used as the mobile phase. Polymer samples were dissolved in TCB at a concentration of 1 mg mL^{-1} and held at 150 °C for 60 min. Samples with an injection volume of 200 µL were eluted through three linear Polymer Laboratories columns which were calibrated with polystyrene standards and operated with a flow rate of 1 ml min^{-1}. The light scattering (LS) detector at 15° from the incident beam was used for MW determinations.

4.2.4 Extraction of Insoluble Particles

Isolation of particles from CM-PP was accomplished by hot xylenes extraction of the polymer from Soxhlet cellulose thimbles. Solvent was replaced every 3 hours, and after 12 hours no residual polymer could be recovered by precipitation from acetone. The thimble was cut into pieces, soaked in acetone and sonicated. The resulting dispersion was deposited onto glass slides, and coated with gold after solvent evaporation. A JEOL JSM-840 Scanning Electron Microscope (SEM) instrument was used to determine the size of isolated particles, using SigmaScan Pro® 5.0 (SPSS Inc.) for image analysis.

4.2.5 Rheological Characterization

Compression moulded discs of 20 mm in diameter at 180 °C were used for rheological characterization. A controlled stress rheometer, ViscoTech by Reologica, with parallel plate fixtures was used in the oscillatory mode at a gap of 1 mm to measure linear viscoelastic properties of prepared PP samples as a function of angular frequency (ω) at 170, 180 and 200 °C, using nitrogen purge to limit degradation and absorption of moisture. Stress sweeps were

performed to ensure that all measurements were within the linear viscoelasticity regime. Data were fitted to the Cross model:

$$\eta\,(\omega) = \frac{\eta_0}{1+|\lambda\omega|^{(1-n)}} \tag{4.1}$$

where η is the shear viscosity, η_0 is the zero shear viscosity, λ is the relaxation time, n is a constant related to the shear thinning behaviour, and ω is the frequency in rad/s.

Time-temperature superposition was performed based on the unified framework proposed by Mavridis and Shroff [110] to study the temperature dependence of rheological data and calculate activation energies. Small amplitude oscillatory shear rheology (SAOS) data obtained at different temperatures were shifted to a temperature of 170 °C. A horizontal shift was adequate for all samples and resulted in the estimation of the horizontal activation energy of the flow (E_H).

PP samples were also characterized in simple uniaxial extension using an SER-2 universal testing platform from Xpansion Instruments hosted on the MCR-501 Anton Paar rheometer [86,87]. Measurements were conducted at 170 °C at extension rates ranging from 0.010 and 10 s^{-1} and under a nitrogen atmosphere. Specimens were prepared by compression molding the polymer samples between polyester films to a gauge of about 1 mm, using a hydraulic press. Individual polymer specimens were then cut to a width of 6.8 mm. Linear viscoelastic oscillatory measurements obtained at 170 °C were used to calculate the LVE stress growth curve and check the consistency of the extensional measurements. For a more quantitative estimation of the strain hardening phenomenon, the strain hardening coefficient S was calculated according to

$$S = \frac{\eta_E^+(t,\dot{\varepsilon}_0)}{3\cdot\eta^+(t)} \tag{4.2}$$

where $3\eta^+$ represents the linear viscoelastic (LVE) envelope in uniaxial extension.

4.2.6 Thermal Analysis

Differential scanning calorimetry (DSC) was conducted on PPs that were purified by xylene extraction to determine their crystallization temperature (T_c), heat of fusion (ΔH_f) and melt temperature (T_m) using a TA Instruments DSC Q 100. Weighed samples were sealed in aluminum hermetic pans and analyzed between -30 and 210 °C at a heating/cooling rate of 5 °C/min. After the first heating, each sample was held isothermally at 210 °C for 3 minutes before cooling, followed by a second heating step.

4.2.7 Foaming Visualization and Analysis

Foaming visualization experiments were conducted using a batch foaming simulation system, consisting of a pressurized chamber equipped with a sapphire glass window, and a high speed camera/image grabbing system [111]. An ADAC board and a high speed CMOS camera was used to record the pressure drop data and video images of the foaming processes, respectively. Disks having dimensions 7 mm in diameter and 200 μm in thickness were prepared by compression molding using a Carver hydraulic press heated at 180ºC. The disks were then placed into the chamber, which was set to 180ºC at a N_2 pressure of 2000 psi (202.6 MPa) and saturated for 30 minutes. The temperature and pressure in the simulation chamber were regulated using a thermostat and a syringe pump, respectively. A program based on Labview was used to open the solenoid valve and record the pressure decay, while simultaneously, the high speed camera recorded the cell growth and collapse phenomena. For each sample, at least three separate experiments were run, and the images were extracted using the Sigma Scan Pro Plus 6.0 image analysis software. The cell density was calculated by counting the number of cells observed from the images taken at a given moment in time. The cell densities with respect to the unfoamed volume ($N_{unfoamed}$) were then calculated using **Eqns. (4.3-4.5)** [112]:

$$N_{unfoamed}(t) = \left(\frac{N(t)}{A_C}\right)^{\frac{3}{2}} \times VER(t) \quad (4.3)$$

where N(t) is the number of bubbles observed in an analysis area of A_c.

The volume expansion ratio (VER) was calculated as the ratio of bulk density of the pure polyolefin material (ρ_p) to the bulk density of the foam sample (ρ_f):

$$VER(t) = \frac{\rho_p}{\rho_f(t)} \quad (4.4)$$

In the case of the batch foaming experiments, the observations are made only for the initial growth stage, and therefore the VER is approximately equal to 1. Hence, the expression for $N_{unfoamed}$ can be reduced to:

$$N_{unfoamed}(t) = \left(\frac{N(t)}{A_C}\right)^{\frac{3}{2}} \quad (4.5)$$

4.2.8 Compression Foam Molding

A Carver® manual hydraulic press was used to produce PP foams by compression moulding. The polymer melt was compression moulded inside a frame mold between two copper plates at 205 °C under 3000 psi for 3 minutes, followed by the release of pressure, upon which expansion of the foam took place. The foams were kept on the hot copper plate for 30s on each side before they were removed to a cool aluminum block.

Compression foam molded samples were characterized based on their expansion ratio and cell morphology. The density of the foams was measured by an electronic densimeter (Mirage MD-200S, Mirage Trading Co., Ltd) based on the water displacement method. The VER values were calculated through **Eqn. 4.4**.

Foams were subjected to cryogenic fracture for SEM imaging. A JEOL JSM-840 SEM was used to characterize the cell morphology of foams. SigmaScan Pro® 5.0 (SPSS Inc.) was utilized to measure the average cell size of each sample.

The shape factor *f* was evaluated as follows:

$$f = \frac{4\pi v}{l^2} \tag{4.6}$$

where *v* is the cell area in the planar profile of a 3D cell and *l* is total edge length in the planar profile of a 3D cell. Values of *f* closer to 1 indicate a more spherical sample.

4.3 Results and Discussion

4.3.1 Structure, Rheology and Thermal Properties of PP Derivatives

Coagent modification of PP involves the use of peroxides, which affect significantly the molecular weight and viscosity of the PPs, through β-scission of the tertiary carbons of linear PP caused by the initiator radicals [113]. The decrease in molecular weight and narrowing of the molecular weight distribution, which are characteristic of controlled rheology PPs (CR-PPs), are evident in **Table 4.1**.

The decrease in molecular weight caused by the macroradical mediated chain scission results in a dramatic decrease in the complex viscosity of CR-PPs as shown in **Figure 4.2 (a)**. The presence of a slope of 2 in the G′ vs ω graph (**Figure 4.2 (b)**) as well as the appearance of a plateau value of 90° at low values of G*, as shown by the Van Gurp plots of **Figure 4.2 (c)** indicate that the CR-PPs reach terminal flow in the frequency range investigated.

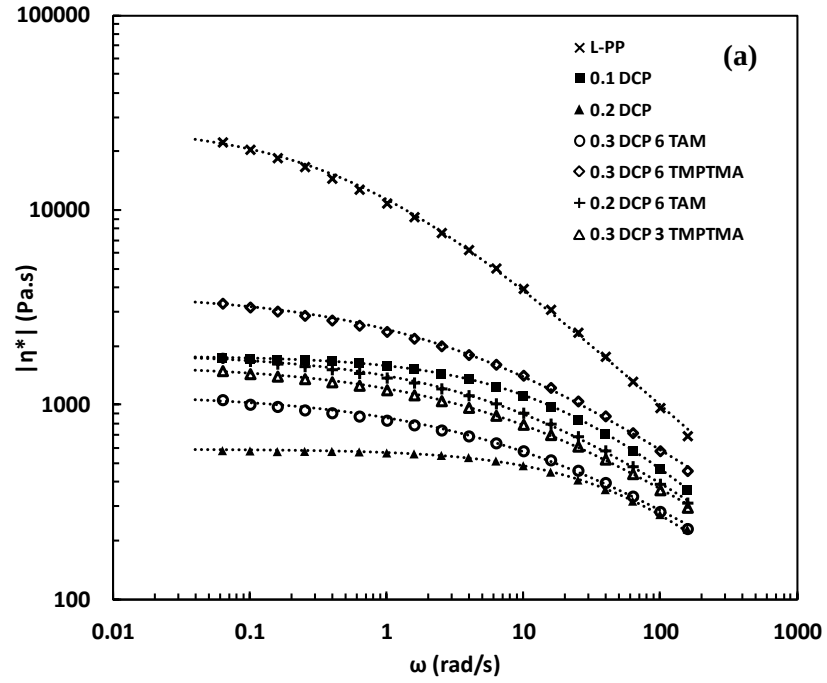
(a)
L-PP
0.1 DCP
0.2 DCP
0.3 DCP 6 TAM
0.3 DCP 6 TMPTMA
0.2 DCP 6 TAM
0.3 DCP 3 TMPTMA
|η*| (Pa.s)
ω (rad/s)
100000
10000
1000
100
0.01
0.1
1
10
100
1000

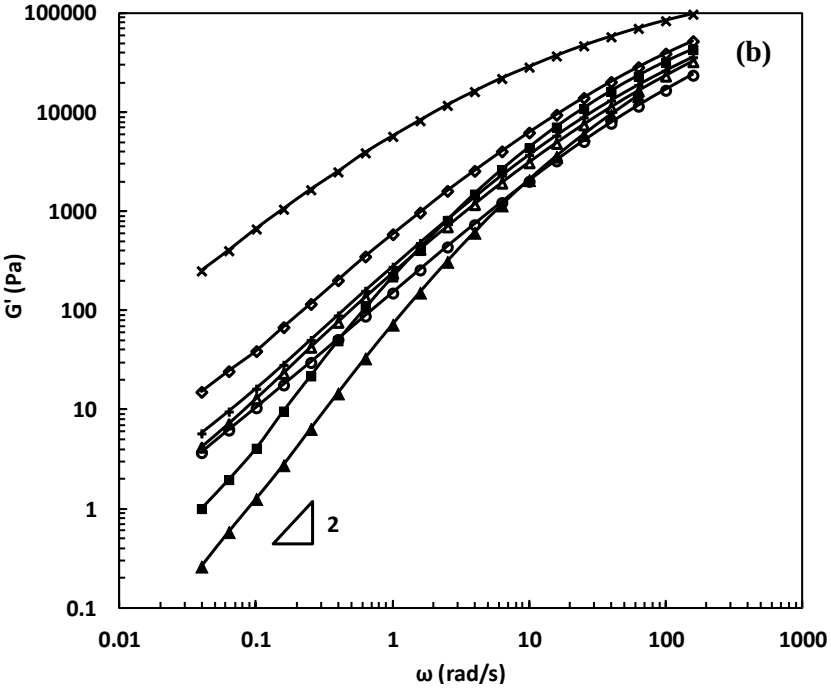
(b)
G' (Pa)
ω (rad/s)
2
100000
10000
1000
100
10
1
0.1
0.01
0.1
1
10
100
1000

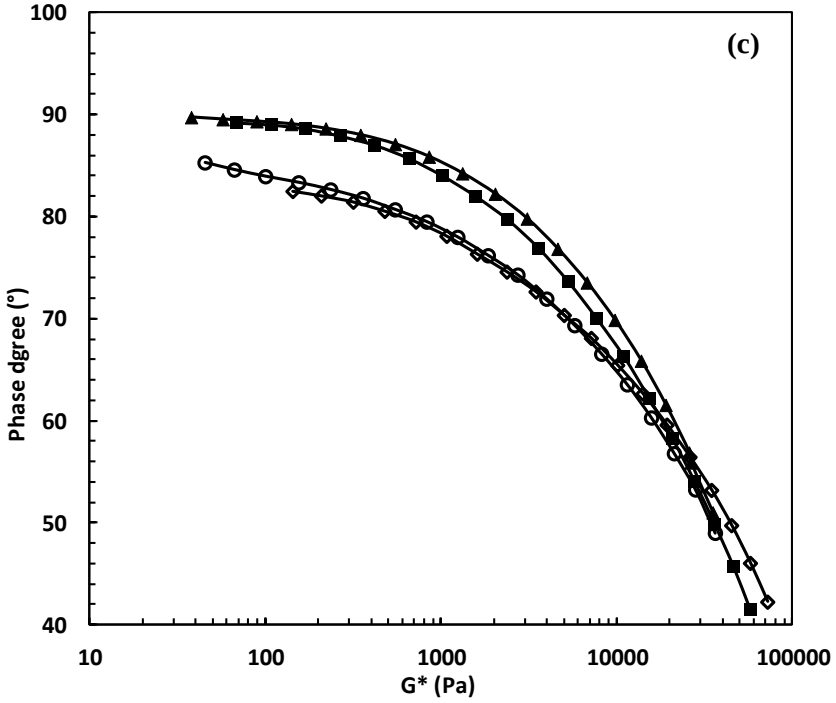

Figure 4.2 (a) Complex viscosities and **(b)** storage modulus as a function of angular frequency; **(c)** phase angle of TAM modified L-PP as a function of complex modulus for selected samples Dotted lines in **(a)** represent the respective Cross model fits to each sample at 180 °C.

When coagents are added, some of the macroradicals are converted to more stable secondary radicals through attacks on the moiety of the coagent. Depending on the chemical nature and reaction conditions, these secondary macroradicals may result in extension, branching or even cross-linking of the PP chains [114]. In the present work, the possibility of PP cross-linking is low, because of the relatively low molecular weights and the absence of detectable amount of gel. GPC revealed that the molecular weight of PP-g-TAM and PP-g-TMPTMA derivatives was higher compared to their degraded counterparts obtained using the same amount of DCP (see **Table 4.1**). However, the derivatives still have lower molecular weights than the original linear PP, which means that scission dominates all other reaction pathways (**Table 4.1**).

The light scattering intensities of selected samples are plotted as a function of retention volume in **Figure 4.3**, which shows that PP-g-TAM samples have a bi-modal molecular distribution

consisting of a high MW fraction. On the contrary, TMPTMA modified samples exhibit only a single peak, with a shift of the peak center towards the low retention volume, signaling increased MW compared to the CR-PP modified at the same DCP level. The presence of a secondary peak at a lower retention volume is indicative of a hyper-branched fraction [115].

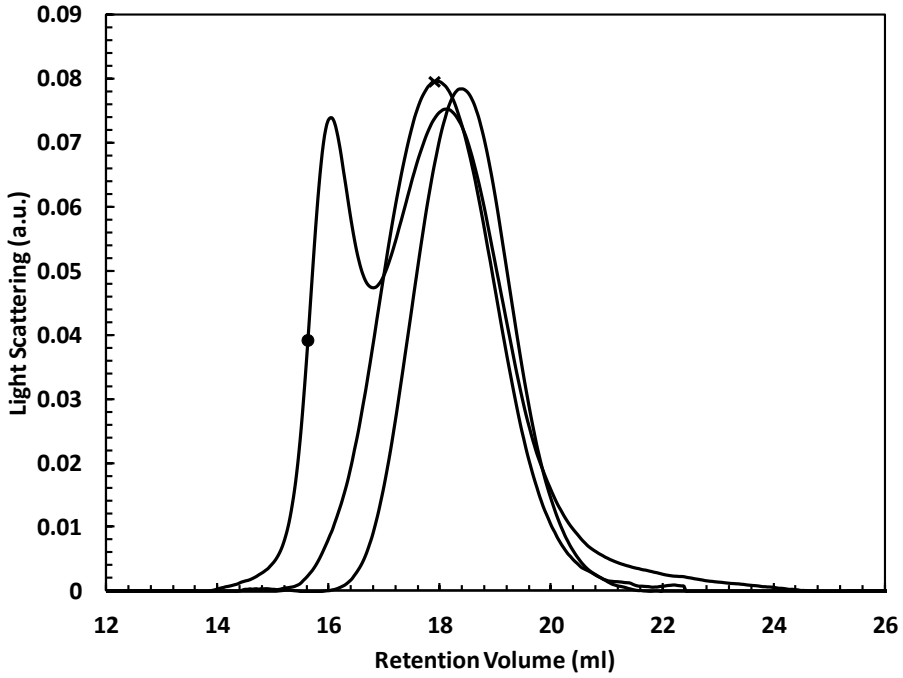

Figure 4.3 Light scattering intensity and absolute molar mass obtained through the LS detector of - 0.3 DCP (M_w=126 kg/mol), **x** 0.3 DCP 6 TMPTMA (M_w=183 kg/mol) and ● 0.3 DCP 6 TAM (M_w=266 kg/mol) as a function of retention volume.

Given that the derivatives containing coagents have higher molecular weights than their CR-PP counterparts modified with 0.3 DCP, in the following their properties will be compared with those of a CR-PP containing 0.1 DCP, which generated comparable molecular weights and rheological properties.

Further evidence of a branched architecture in the PP-g-TAM derivatives is provided by the Mark-Houwink plots, presented in **Figure 4.4**. As expected for linear polymers, the CR-PPs follow the Mark-Houwink relation, which is represented by the solid line. For PP-g-TAM samples, the curve deviates negatively from the $[\eta] = KM^a$ relation and a pronounced drop in intrinsic viscosity is present at the high molecular weight range, as expected for branched polyolefins. PP-g-TMPTMA samples do not exhibit a significant deviation from linearity, even at the highest DCP and TMPTMA contents.

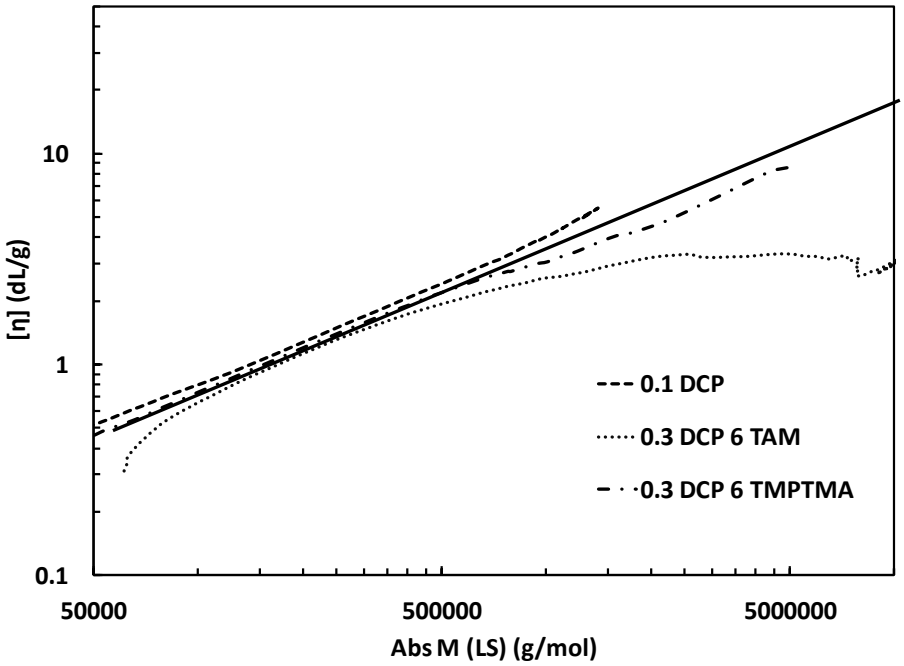

Figure 4.4 Intrinsic viscosity as a function of the absolute molecular weight of the GPC elution, obtained from the light scattering detector for 0.1 DCP, 0.3 DCP 6 TAM and 0.3 DCP 6 TMPTMA samples.

The linear viscoelastic properties are very sensitive to the structural change of materials and thus have been used to verify the existence of LCB on the linear PP backbone [107,116,117]. Overall, coagent modification resulted in higher zero shear viscosities, more shear thinning and longer

relaxation times than their counterparts with similar DCP concentration (**Table 4.2** and **Figure 4.2**). An increase in activation energy can also be seen in **Table 4.2**.

Table 4.2 Shear viscosity, relaxation times estimated based on the Cross model (at 180 °C) and strain hardening coefficients (at Hencky strains of 1 s^{-1} and 170 °C).

Sample	η_0 (Pa.s)	λ (s)	n	E_H (kJ/mol)	S (at 1s^{-1})
L-PP	27138	1.72	0.36	52.0	1.04
0.1 DCP	1770	0.05	0.32	47.4	N/A*
0.2 DCP	587	0.01	0.26	41.9	N/A*
0.3 DCP	292	0.005	0.23	40.8	N/A*
0.2 DCP 3 TAM	1280	0.06	0.43	43.0	1.65
0.2 DCP 6 TAM	1828	0.1	0.46	46.3	2.06
0.3 DCP 3 TAM	644	0.04	0.51	48.6	N/A*
0.3 DCP 6 TAM	1126	0.10	0.52	47.3	2.20
0.2 DCP 3 TMPTMA	3766	0.21	0.44	50.1	0.90
0.2 DCP 6 TMPTMA	6687	0.38	0.45	47.7	1.00
0.3 DCP 3 TMPTMA	1602	0.11	0.49	46.6	0.96
0.3 DCP 6 TMPTMA	3704	0.27	0.50	47.4	1.05

*The strain hardening coefficient cannot be determined due to sagging.

As shown in **Figure 4.2 (b)**, the slopes of G' for the modified PPs are lower than 2, indicating longer relaxation times, which possibly arise from the presence of LCB. The van Gurp plots of the phase degree δ against the complex shear modulus provide further evidence of a modified chain architecture (**Figure 4.2(c)**). Contrary to the degraded samples, which show a plateau value

of 90 °, coagent addition caused a significant deviation in the low range of the complex modulus. Such observations are typically interpreted as proof of the presence of LCB. However, in the samples of this work, the GPC data provide evidence of branching only in the PP-g-TAM samples (see **Figure 4.4**).

Furthermore, tensile stress growth coefficients obtained in uniaxial extension, shown in **Figure 4.5**, reveal strain hardening only in the PP-g-TAM samples, whereas the linear PPs and PP-g-TMPTMA do not show any evidence of strain hardening, pointing once again to the absence of significant amounts of LCB. Data corresponding to the CR-PPs are not included in **Figure 4.5**, due to excessive sagging.

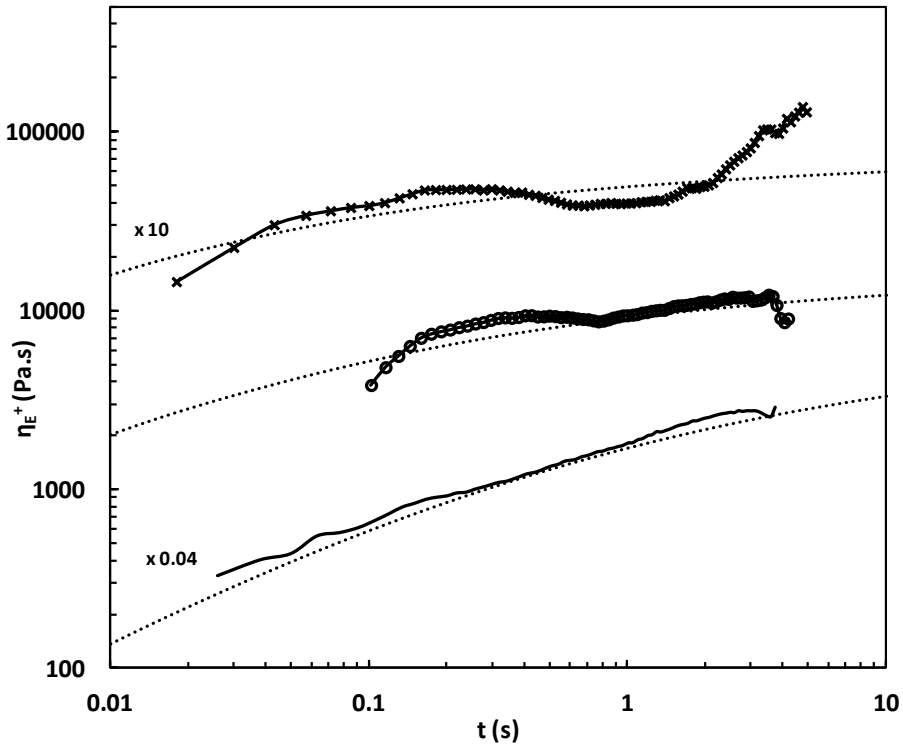

Figure 4.5 The tensile stress growth coefficient (η_E^+) of ━L-PP, × 0.3 DCP 6 TAM and ○ 0.3

DCP 6 TMPTMA samples as a function of strain rate and time at a strain rate of $1s^{-1}$. Curves are shifted by an arbitrary factor for the sake of clarity. Dotted lines represent the LVE envelop for each respective sample.

These results suggest that evidence based on SAOS measurements alone, such as increases in elasticity and activation energy, should be viewed with caution, as they may be attributed to other reasons, such as chain extension, or formation of small amounts of gel/particles, without necessarily involving LCB. Thus SAOS measurements should always be applied in conjuction with other methods when diagnosing unknown polymer chain architecture.

Formation of Nanoparticles

In addition to the modification in the polymer chain architecture, small amounts of nanoparticles, were isolated from the coagent modified PPs. These particles are most likely attributed to a side oligomerization reaction of the coagent [115] and have been isolated through xylene extraction from both the PP-g-TMPTMA and PP-g-TAM samples. SEM images, obtained from the extracted samples (**Figure 4.6 (a)** and **(b)**) suggest that the particle yield is higher for PP-g-TMPTMA (**Figure 4.6 (b)**) and that the particles were coated with insoluble polymer that could not be removed from their surface. This indicates that PP-g-TMPTMA contained a small amount of gel, as well as a significant population of cross-linked particles. For PP-g-TAM, the particles appear mostly separated, with an average diameter in the order of 1 μm.

The effect of these particles on the thermal properties of the PP derivatives is profound, including an increase in crystallization temperatures of the order of 10-12°C and crystallinity (**Table 4.3**). These particles may act as nucleating agents, providing heterogeneous nucleation sites thus enhancing crystallization rates. This will be discussed further in Chapter 5.A possible effect on the rheological properties cannot be excluded either. Decreased slope of G', as well as an

moderately increased melt viscosity, have been reported in slightly filled composite systems [118,119]. The effect of particles on the rheological properties of the CM-PPs should be the subject of a separate investigation.

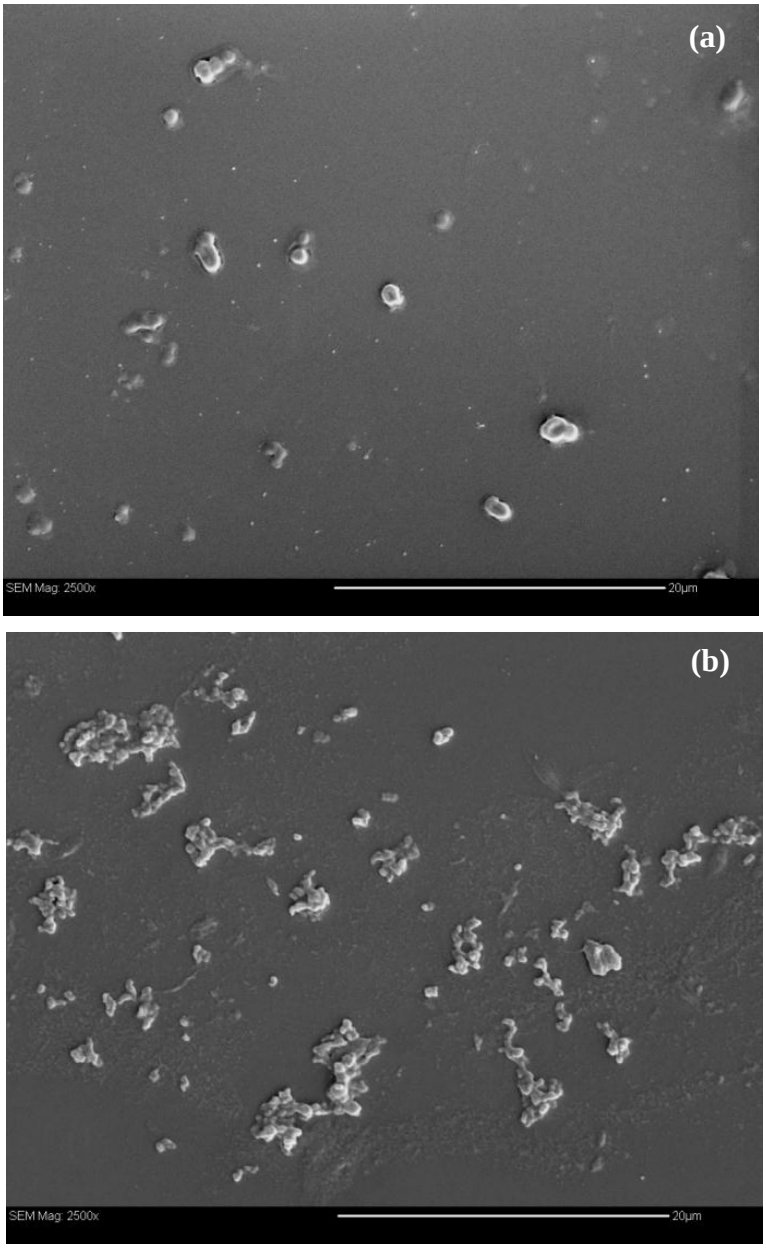

Figure 4.6 SEM images of particles isolated from **(a)** 0.3 DCP 6 TAM and **(b)** 0.3 DCP 6 TMPTMA samples. The scale bar represents 20 micrometers.

Table 4.3 Melting points (T_m), crystallization points (T_c) and heat of fusion (H_f) of PP derivatives

Sample	T_m (°C)	T_c (°C)	H_f (J/g)
L-PP	163	118	99
0.1 DCP	158/164	113	89
0.2 DCP	155/163	113	90
0.3 DCP	154/163	113	89
0.2 DCP 3 TAM	163	127	108
0.2 DCP 6 TAM	163	128	104
0.3 DCP 3 TAM	162	127	103
0.3 DCP 6 TAM	163	130	95
0.2 DCP 3 TMPTMA	163	129	95
0.2 DCP 6 TMPTMA	164	129	101
0.3 DCP 3 TMPTMA	163	129	94
0.3 DCP 6 TMPTMA	164	130	95

4.3.2 Foaming of PP Derivatives

Effect of Viscosity

Given that coagent modification results in substantial decreases in molecular weight and viscosity due to chain scission in the presence of peroxides (**Figure 4.2** and **Table 4.1**), the effect of viscosity on the foaming behaviour of the controlled rheology PPs will be investigated first.

Figure 4.7 (a) and **(b)** show a pronounced effect of the viscosity of the linear samples on the VER (defined in **Eqn. (6)**) and the average cell diameter of the foams. **Figure 4.7 (a)** suggests that cell growth is facilitated when the viscosity is lower, whereas higher viscosity poses increased resistance to cell growth. **Figure 4.7 (b)** and the corresponding SEM images of **Figure**

4.8 show that the cell sizes are smaller when viscosity is higher. This is more evident from the SEM images of **Figure 4.8**, which showed that, while the cells of compression foamed L-PP appeared to be very irregular with a wide spread in cell size, 0.1 DCP and 0.2 DCP foams feature cells that are larger, mostly spherical and more uniform in size, as reflected by the increased shape factor from 0.76 for L-PP foams to 0.81 for 0.2 DCP foams.

.

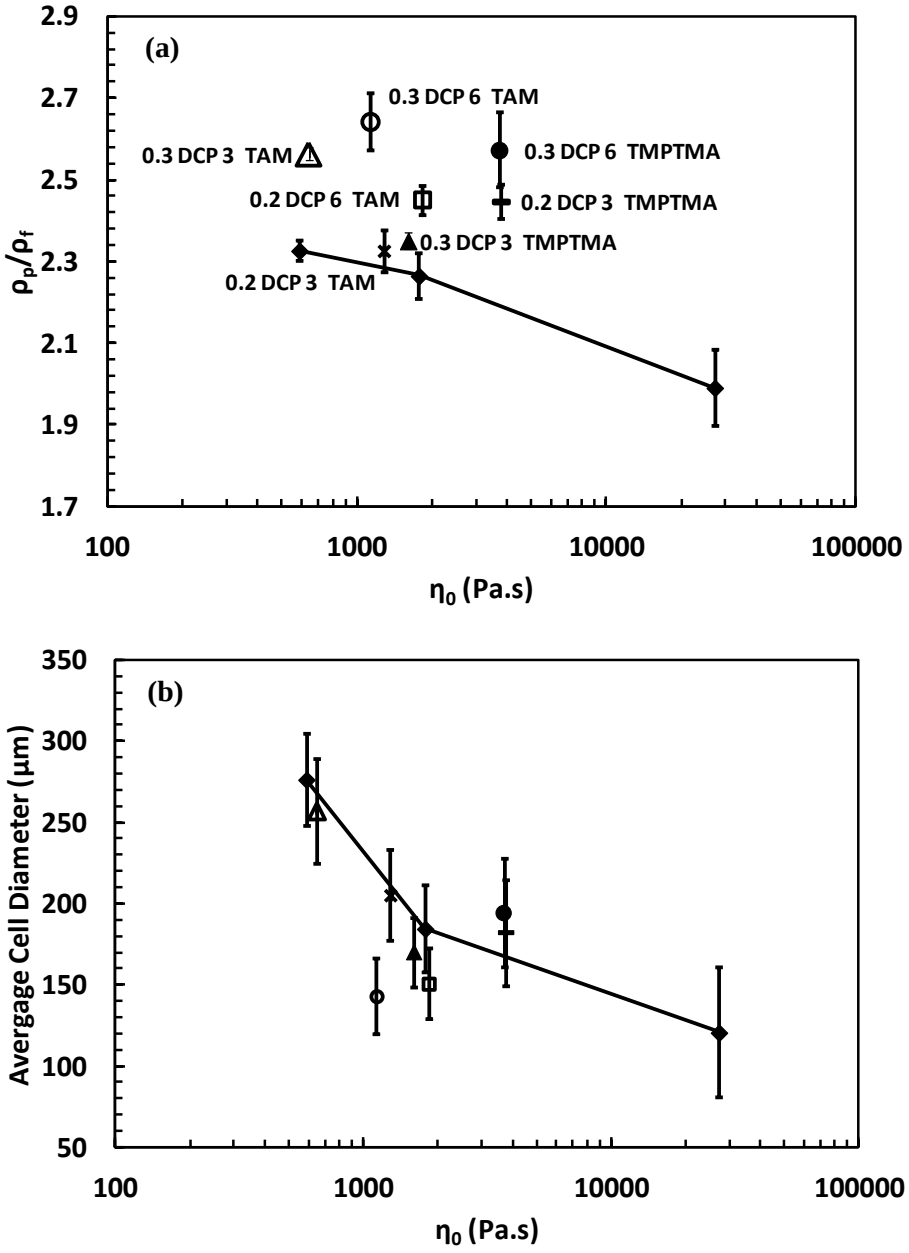

Figure 4.7 (a) Volume expansion ratio, **(b)** Average cell diameter and as a function of zero shear viscosity values. Samples connected by solid lines (intended to guide the eye) correspond to the linear PP derivatives. The error bars represent one standard deviation.

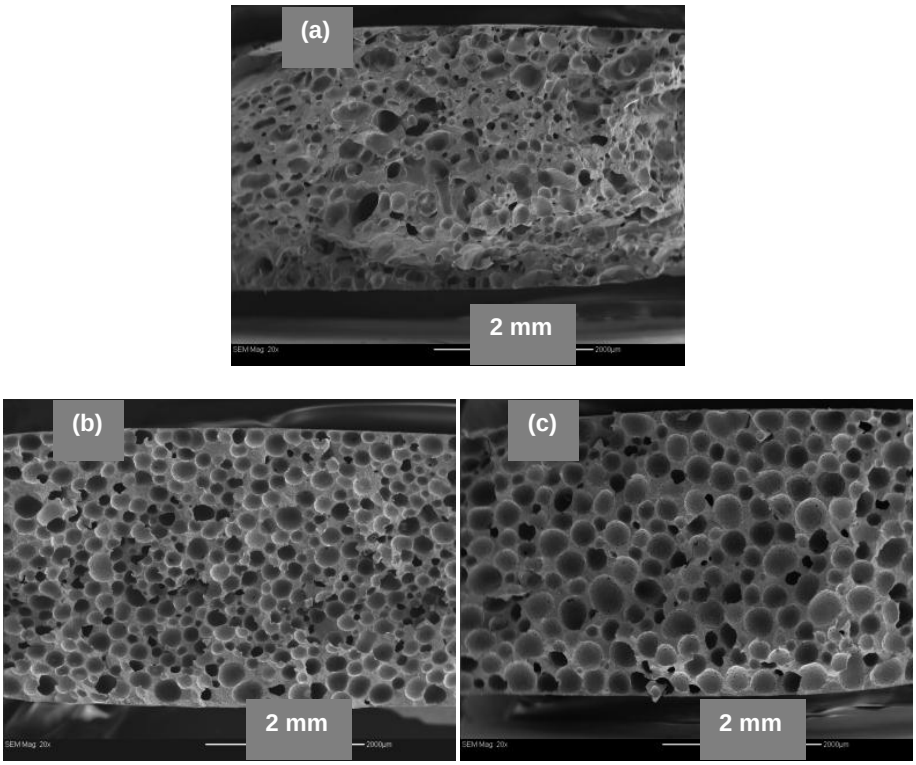

Figure 4.8 SEM images of the fracture surface of PP samples**: (a)** L-PP (η_0=27138 Pa.s); **(b)** 0.1 DCP(η_0=1770 Pa.s); **(c)** 0.2 DCP (η_0=587 Pa.s).

The effect of viscosity can also be seen in results obtained through in-situ batch foaming experiments, using nitrogen as a physical blowing agent. **Figure 4.9** shows a comparison of the cell density versus time for selected samples; these curves exhibit an initial growth in cell density and then a relatively stable plateau, followed by a drop in cell density after ~0.37 s, which correspond to the cell nucleation, growth and coalescence stages of foaming.

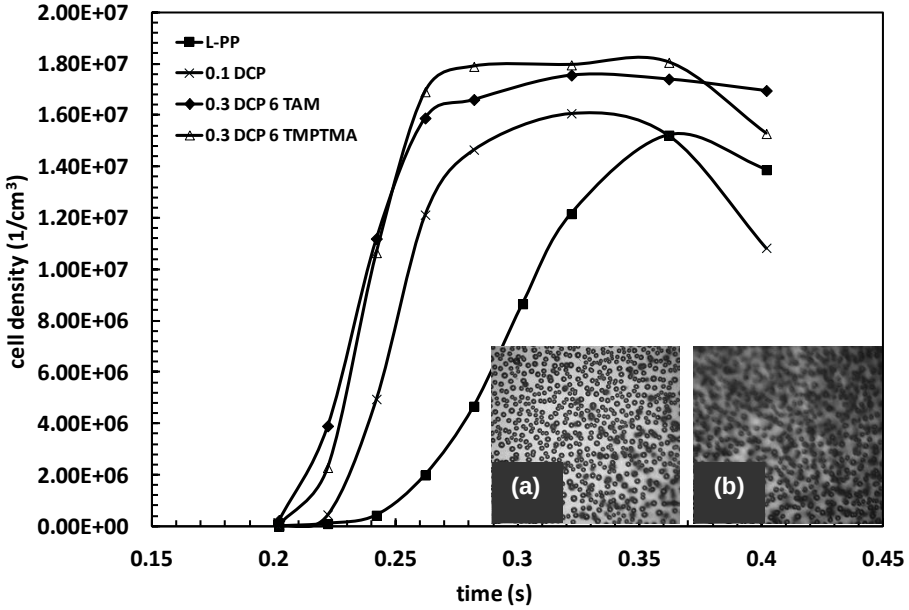

Figure 4.9 Cell density as a function of time in the batch foaming process for L-PP, 0.1 DCP, 0.3 DCP 6 TAM and 0.3 DCP 6 TMPTMA samples. The inserts are cell structures at 0.4 s during batch foaming for **(a)** 0.3 DCP 6 TAM (left) and **(b)** 0.3 DCP 6 TMPTMA (right) to demonstrate difference in cell coalescence.

First of all, the rate of cell density growth is higher in 0.1 DCP compared to the L-PP, suggesting that lower viscosity poses less resistance to cell density growth. Furthermore, an effect of molecular weight on the nucleation time can be seen, as evidenced by the delayed onset of cell growth in the L-PP sample. This is presumably because of higher surface tension, due to its higher molecular weight, resulting in a stronger energy barrier for cell nucleation, thus delaying the onset of nucleation [120].

The results presented above suggest a strong effect of the melt viscosity on the foaming characteristics, with lower viscosities favouring cell growth and generating foams with larger VER and cell density.

Effect of Coagent Modification

The CM-PPs prepared by compression foam molding have consistently higher VER values than the envelope defined by the CR-PPs (**Figure 4.7 (a)**). The effect of coagent addition on the foaming behaviour can be specifically demonstrated by comparing samples with similar complex viscosity and molecular weight (0.1 DCP, 0.3 DCP/ 3 TMPTMA and 0.2 DCP/ 6 TAM). The highest VERs were recorded upon the addition of higher amounts of DCP and coagent, while no obvious correlation with viscosity exists.

Differences in the cell nucleation and coalescence stages during compression mold foaming are a possible reason for this observation. An examination of the batch foaming curves (**Figure 4.9)** reveals that the cell density growth rate of coagent modified PPs is higher than the linear PPs, with an earlier onset of nucleation, and higher plateau cell densities. This behavior points out to an enhanced heterogeneous nucleation mechanism, which is most likely caused due to the presence of nucleation sites provided by the nanoparticles contained within the CM-PPs. This enhanced nucleation effect is most likely the cause for the high VERs observed in the CM-PPs. Larger amounts of coagent are expected to generate larger amounts of nanoparticles, due to the oligomerization side reaction, therefore producing a more enhanced nucleation effect and higher VERs for the TMPTMA modified PPs.

In **Figure 4.9** it is also noteworthy that linear PP and PP-g-TMPTMA samples show a downturn at longer times, which is due to cell coalescence, resulting in a coarsening of the structure (see optical image **(a)** in the inset). This result is expected since these samples do not display any strain hardening (see **Figure 4.5**), which would suppress cell coalescence.

On the contrary PP-g-TAM samples display ample evidence of strain hardening, which, based on the results from the the LS data and Mark-Houwink plots provide evidence of the presence of

LCB. Increased strain hardening results in a suppression of coalescence, as suggested by the sustained plateau observed in cell density.

As shown in **Figure 4.7 (b)** the structure stabilization afforded in the presence of LCB results in a finer structure, as evidenced by the smaller average cell diameter in the two PP-g-TAM materials modified with the highest amount of coagent, which also have the highest strain hardening coefficient (**Table 4.2**). On the contrary the rest of the samples follow the trends established by the linear PPs. Overall, the PP-g-TAM sample modified by 0.3 DCP/ 6 TAM, which has a low viscosity, coupled by the highest strain hardening coefficient, exhibited the higher cell density growth rate, finest cell size and highest VER and cell density. This is further demonstrated in **Figure 4.10**, which clearly shows that the 0.3 DCP/ 6 TAM material has a finer cell structure. A noteworthy feature of foam morphology of those modified with TMPTMA is a scattered populace of larger cells (**Figure 4.10)**. Such localized un-uniformity of cell size suggests localized coalescence, which is very likely given that TMPTMA modified samples generated more initial cells (**Figure 4.9**) as a result of more efficient nucleating particles (**Figure 4.6**) but subsequently coalesced locally due to lack of strain hardening (**Figure 4.5**). The resulting foams have high VER, but less uniform cell structure.

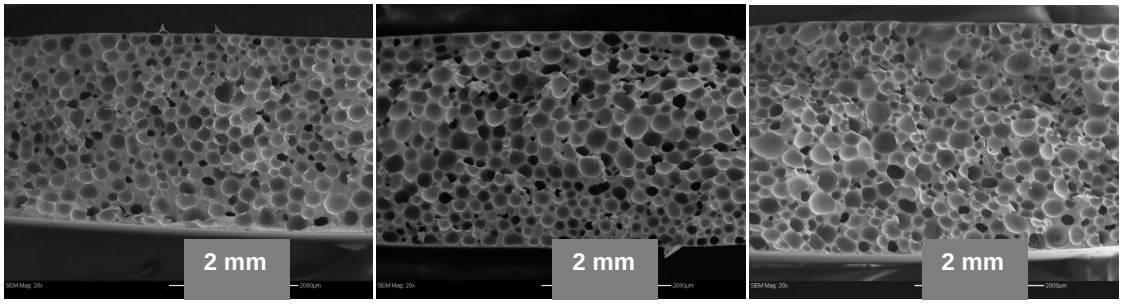

Figure 4.10 SEM images of the fracture surface of PP samples: (from left to right) 0.1 DCP (R_{avg} = 185±27 µm), 0.3 DCP 6 TAM (R_{avg} = 143±23 µm) and 0.3 DCP 6 TMPTMA (R_{avg} = 194±33 µm).

In addition to the foam nucleation, and rheological effects, it must be noted that compression foam molding involves solidification of the melt after the pressure is released. The higher crystallization temperature of the coagent modified PPs (**Table 4.3**) means that crystal domains appears sooner in the cooling melt, slowing down the diffusion of gas from/between the cells, and resulting in higher VER. Early crystalline domain formation during cooling also helps to stabilize the cell structure [121].

These results suggest a synergy between the presence of nanoparticles, which enhance the nucleation behaviour, low viscosity, which facilitates cell growth, strain hardening, which stabilizes the growing cells and enhanced crystallization rates, which result in cell structure stabilization during the cooling process.

4.4 Conclusions

Reactive modification of linear PP by radical mediated grafting in the melt state was employed as a means of obtaining well controlled structures and elucidating the effects of molecular structure on the various stages of foaming.

A series of controlled rheology linear PPs were produced through reaction with dicumyl peroxide as the free radical initiator, to investigate the effect of molecular weight and viscosity on foaming. Foaming experiments, both by compression molding using a chemical blowing agent and by batch foaming using a physical blowing agent revealed that lower viscosity favours higher expansion ratios and larger cells, due to reduced resistance to cell growth.

Furthermore modification of the linear PP structure through the introduction of LCB using a triallyl trimesate (TAM) coagent, resulted in increased melt strength, with beneficial effects on the volume expansion ratio, and cell stabilization.

The detection of nanoparticles, formed presumably from the coagent oligomerization side reaction is a significant finding of this chapter. The thermal properties of the coagent modified PPs are altered significantly in their presence, including a drastic increase in the crystallization temperature, and increases in the crystallinity of the final samples.

The effects of these nanoparticles on the foaming behavior of coagent modified PPs is more evident by examining foams produced from the PP-g-TMPTMA derivatives, which did not demonstrate evidence of branching. In spite of the lack of branching, these derivatives had high volume expansion ratios, and enhanced nucleation and cell density growth rate, presumably due

to the nucleation effect of the nanoparticles. However in the absence of strain hardening, these samples were still prone to cell coalescence.

Overall the PP-g-TAM derivatives with the highest amount of TAM coagent generated foams with the highest expansion ratios and finer cell structure, due to the favourable balance of low viscosity and high strain hardening coefficient imparted by the introduction of LCB, and the high crystallization temperature due to the presence of nanoparticles.

The research concluded in this chapter has identified a one-pot approach for creating LCB, while at the same time synthesizing in situ a sub-micron scale nucleation agent. The following chapter focuses on the formation of these coagent-rich nanoparticles and elucidates their nucleating effects on the isothermal crystallization and foaming processes.

Chapter 5

Crystallization and Foaming of Coagent-Modified Polypropylene: Nucleation Effects of Cross-linked Nanoparticles

5.1 Introduction

As discussed in Chapter 4, the chemical modification of linear, isotactic PP (L-PP) by peroxide-initiated grafting of coagents can provide long-chain branched derivatives with improved melt elasticity and extensional viscosity [55]. These solvent-free processes involve simultaneous chain scission and cross-linking, the balance of which controls the product's molecular weight and branching distributions [50]. In general, products derived from coagents bearing multiple acrylate, allylic or styrenic groups are comprised of a linear chain population of relatively low molecular weight, and a high molecular weight chain population containing a disproportionate amount of long chain branching.

The effect of these microstructure changes on melt-state rheological properties are well documented, with several groups reporting losses in complex viscosity as well as enhanced elasticity and strain hardening characteristics [51-54]. However, only recently has the generation of cross-linked particles within coagent modified atactic PP (CM-PP) been identified [115]. These nanoparticles are produced by a precipitation polymerization mechanism wherein coagent oligomerization yields adducts that are insoluble in the polymer melt, leading to the separation of a coagent-rich phase that cross-links to a very high extent [122]. As a result, CM-PP samples prepared by this chemistry can contain small, rigid particles that are well-dispersed throughout the polymer matrix. The work presented in Chapter 4 has demonstrated the appearance of these particles in CM-PP samples derived from isotactic PP.

A prime motivation for preparing CM-PP is to develop the extensional strain hardening characteristics needed to suppress cell coalescence during melt foaming processes. When compared to L-PP materials, CM-PP derivatives provide higher volume expansion ratios and more uniform cell sizes [53,123]. These improvements to foam properties have, to date, been attributed to the melt state rheology, while the potential of coagent-rich nano-particles to affect the foaming of CM-PP has been overlooked. Similarly, significant differences in the crystallization behavior of linear and coagent-modified PP samples have been observed [53,124,125]. Whereas branching in homogeneous polyethylenes is usually associated with lower crystalization rates and crystallinities [126,127], CM-PP materials are reported to crystallize at higher temperatures. Similar observations were reported in Chapter 4, where the changes in thermal properties were attributed to the presence of sub-micron particles that are formed during the melt grafting process and are finely dispersed within the melt.

This chapter aims at further investigating the formation of nanoparticles in coagent modified PPs, and clarifying their effects on crystallization and foaming. This is accomplished by comparing a linear isotactic PP (L-PP) with two of its derivatives: peroxide degraded PP (DCP-PP), and TMPTMA-modified PP (CM-PP). These materials are subjected to standard characterization techniques including molecular weight distribution as well as oscillatory shear and extensional rheometry. CM-PP is subjected to further analysis by FT-IR to confirm TMPTMA graft content, as well as SEM studies of the sub-micron particles dispersed throughout the sample. Controlled studies of polymer crystallization and foaming are presented, with the objective of discerning the effect of coagent-rich nano-particles on phase nucleation phenomena.

5.2 Experimental

5.2.1 Materials and Reactive Modification

Trimethylolpropane trimethacrylate (TMPTMA, 98%) and dicumyl peroxide (DCP, 98%) were used as received from Sigma-Aldrich. ESCORENE™ PP 1042, an isotactic linear polypropylene homopolymer (L-PP) (MFR = 1.9 g/10 min), with a number average molecular weight (M_n) of 96 kg/mol and a weight average molecular weight (M_w), of 460 kg/mol, as determined by triple detector gel permeation chromatography (GPC), was obtained from ExxonMobil.

Peroxide-degraded PP (DCP-PP) was prepared by coating ground L-PP powder (40 g) with an acetone solution containing DCP (0.08 g, 296 μmole) and allowing the solvent to evaporate. The resulting mixture was charged to a Haake Polylab R600 internal batch mixer at 180°C at 60 rpm for 10 min, yielding DCP-PP with a M_n = 63.1 kg/mol and a M_w= 159 kg/mol.

Coagent-modified PP (CM-PP) was synthesized as described for DCP-PP from a mixture of L-PP (40 g), DCP (0.08 g, 296 μmole) and TMPTMA (2.4 g, 7.1 mmole). The product had a M_n = 77.5 kg/mol and a M_w= 209 kg/mol.

Gel content analysis was conducted by extraction into boiling xylenes from a 120 mesh stainless steel sieve for 6 hours, according to ASTM D 2765. Residual polymer was dried to constant weight, with gel contents reported as a weight percentage of unextracted material.

Isolation of particles from CM-PP was accomplished by hot xylenes extraction of the polymer from Soxhlet cellulose thimbles. Solvent was replaced every 3 hours, and after 12 hours no residual polymer could be recovered by precipitation from acetone. The thimble was cut into pieces, soaked in acetone and sonicated. The resulting dispersion was deposited onto glass slides, and coated with gold after solvent evaporation. A JEOL JSM-840 Scanning Electron Microscope (SEM) instrument was used to determine the size of isolated particles, using SigmaScan Pro® 5.0 (SPSS Inc.) for image analysis.

5.2.2 Characterization

Molecular weight distributions were measured using a triple detector GPC (GPCIR by PolymerChar) at 145°C, employing 1,2,4-trichlorobenzene (TCB) as the mobile phase. Polymer samples were dissolved in TCB at a concentration of 1 mg mL^{-1} and held at 150 °C for 60 min. Samples with an injection volume of 200 µL were eluted through three linear Polymer Laboratories columns which were operated at a flow rate of 1 ml/min. The light scattering (LS) detector at 15° from the incident beam was used for molecular weight determinations.

FT-IR measurements were carried out in transmittance mode with an Avatar 360 FT-IR ESP spectrometer. Samples were purified by dissolving in boiling xylene and precipitating from acetone prior to drying under vacuum and melt pressing into thin films.

A controlled stress rheometer (ViscoTech by Reologica) with parallel plate fixtures was used in the oscillatory mode at 180 °C with a gap of 1 mm under a nitrogen purge to limit potential air oxidation and moisture absorption. Stress sweeps were used to ensure that measurements were made within the linear viscoelasticity region. Samples were further characterized in uniaxial extension using an SER-2 universal testing platform from Xpansion Instruments hosted on the MCR-501 Anton Paar rheometer [86,87]. Measurements were conducted at 170 °C at extension rates ranging from 0.010 to 10 s^{-1} under nitrogen purge.

Differential scanning calorimetry (DSC) was conducted to determine the melting and crystallization temperatures (T_m and T_c respectively), and heat of fusion (ΔH_f) using a DSC Q 100 by TA Instruments. Samples were sealed in aluminum hermetic pans and scanned between -30 and 210 °C at a heating/cooling rate of 5 °C/min. After the first heating, each sample was held isothermally at 210 °C for 3 min before cooling, followed by a second heating step.

Isothermal crystallization experiments were performed using a Linkam CSS 450 hot stage mounted on an Olympus BX51 optical microscope. Thin films were first heated to 200 °C at a rate of 20 °C /min and held for 10 minutes to eliminate their heat history. The melt was then cooled to 140 °C at 20 °C/min and the temperature was kept constant for 1 hour. The crystallization process was recorded using a Sony ExwaveHAD 3 CCD digital recorder.

5.2.3 Foaming Visualization

Foaming visualization experiments were conducted using a batch foaming simulation system, consisting of a pressurized chamber equipped with a sapphire glass window, and a high speed camera/imaging system [111]. Disks (7 mm diameter x 200 μm thickness) were heated to 180ºC at 203 MPa of N_2. The temperature and pressure in the simulation chamber were regulated using a thermostat and a syringe pump, respectively. N_2 was used as the blowing agent. A program based on Labview® was used to open the solenoid valve and record the pressure decay after the pressure within the chamber had been maintained for 30 minutes of saturation, while simultaneously, a high speed camera recorded the cell growth and collapse phenomena at 500 hundred frames per second. For each sample, at least three separate experiments were run, and the images were extracted using the Sigma Scan Pro Plus 6.0® image analysis software.

5.3 Results and Discussion

5.3.1 Material Characterization

Three materials have been investigated, unmodified linear PP (L-PP) and two of its chemically modified derivatives, peroxide-degraded PP (DCP-PP), and coagent-modified PP (CM-PP). The parent material, L-PP, had a unimodal molecular weight distribution with M_w = 460 kg/mole and a polydispersity of 4.8 (**Figure 5.1**). Its melt state rheological properties were typical of an unbranched polymer of relatively high molecular weight. Oscillatory shear rheometry

demonstrated conventional shear thinning behavior (**Figure 5.2**), while no evidence of strain hardening was observed when the sample was subjected to an extensional deformation (**Figure 5.3**).

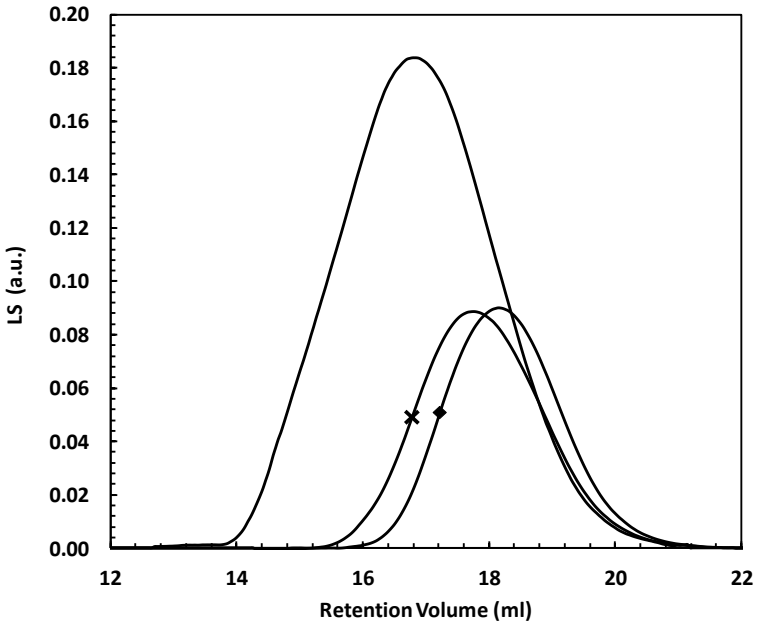

Figure 5.1 Light scattering intensity as a function of retention volume for: – L-PP, ◆ DCP-PP and ✕ CM-PP.

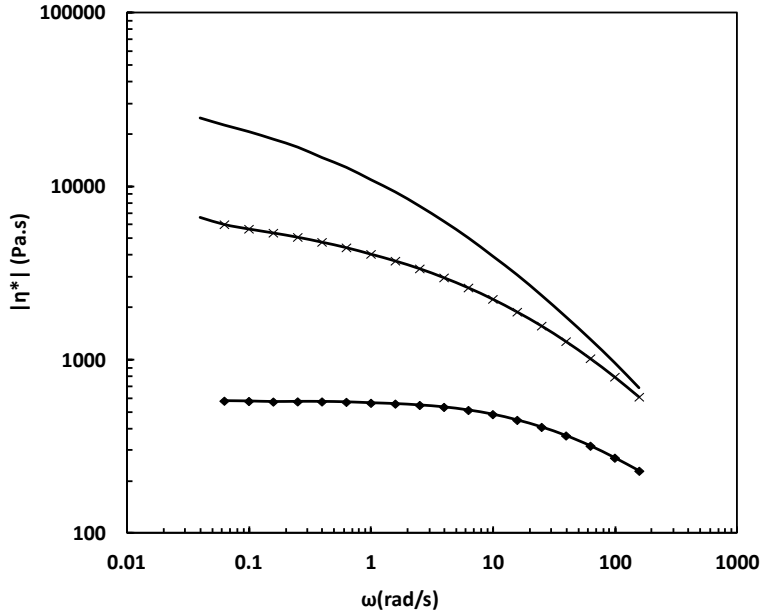

Figure 5.2 Complex viscosity as a function of angular frequency for: – L-PP, ◆ DCP-PP and ✕ CM-PP.

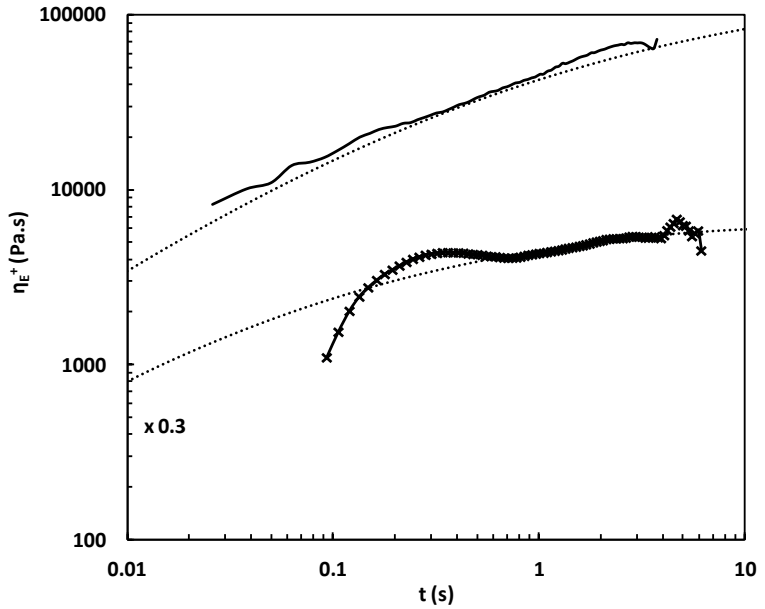

Figure 5.3 Tensile stress growth coefficient at $1s^{-1}$ (η_E^+) as a function of time. The dotted lines indicate the LVE envelope. – L-PP; ◆ DCP-PP; ✕ CM-PP.

Although extraction of CM-PP from the wire mesh did not isolate insoluble material, extraction from a Soxhlet thimble was capable of separating particles from most of the polymer matrix. An SEM image of the nanoparticles separated by this technique is provided in **Figure 5.4**. Note that these particles are similar in dimension to those observed previously for atactic-PP modified by DCP and triallyl trimesate, with average diameters on the order of 500 nm [115]. However, unlike this previous work, particles were coated with insoluble material that could not be removed from their surface. It can be concluded that CM-PP contained a small amount of gel as well as a significant population of cross-linked particles. Based on the measured difference in the thimble weight, the amount of these nanoparticles is estimated to be in the order of 1 wt %.

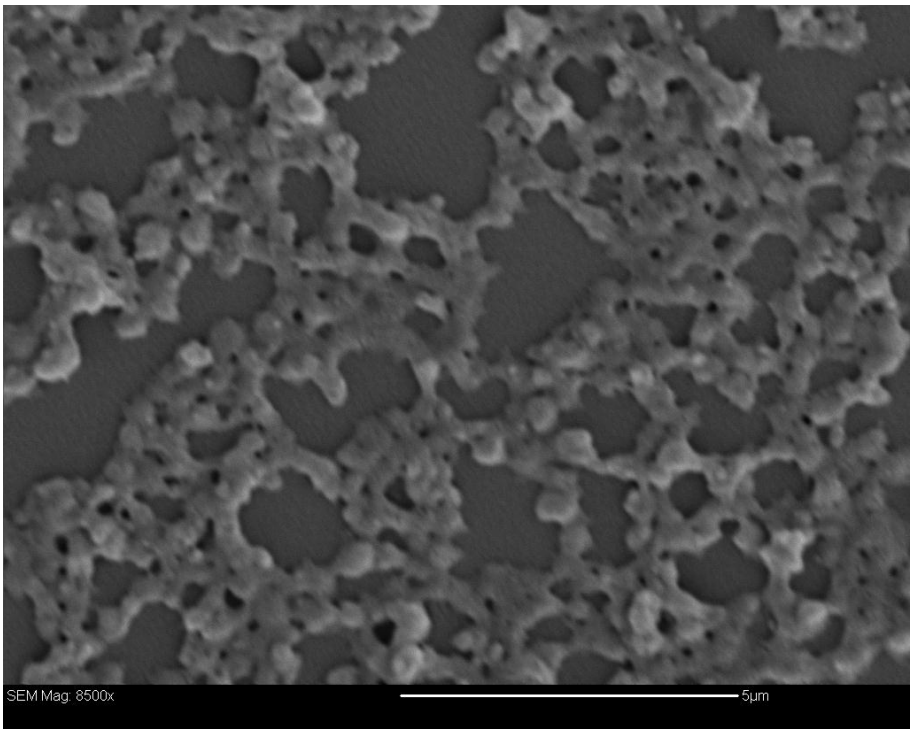

Figure 5.4 SEM image of nanoparticles extracted from CM-PP.

5.3.2 Crystallization Behaviour

The potential for the dispersed solid phase within CM-PP to affect crystallization was examined through DSC studies and optical microscopy analysis. The crystallization exotherms illustrated in **Figure 5.5** show the peak of DCP-PP crystallization was 113°C, whereas CM-PP crystallization peaked at 129 °C - fully 16 °C higher. Higher crystallization temperatures are not unique to the present CM-PP material, as this finding is consistent with reports of other coagent-modified PP formulations [53,124,125]. A commonly offered explanation in the literature for the appearance of higher crystallization temperature in coagent modified PPs is that the LCB served as nucleating sites. This explanation would be in apparent contradiction with the tendency of LCB to disrupt chain packing, thus reduce crystallinity. In this chapter, a CM-PP containing no significant amount of LCB was observed with this crystallization behaviour. Thus the role of particles in polymer crystallization has been identified.

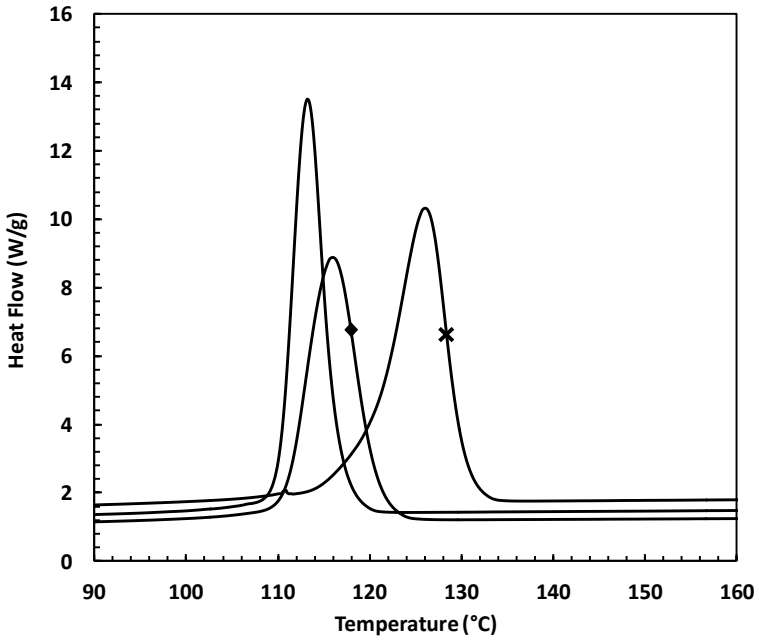

Figure 5.5 Crystallization exotherms for: – DCP-PP, ◆ L-PP and ✕ CM-PP.

Further evidence of heterogeneous nucleation in CM-PP was gained by optical microscopy studies of isothermal crystallization. The images presented in **Figure 5.6** show the advanced rate of spherulite formation in CM-PP relative to L-PP and DCP-PP, leading to significantly smaller spherulites in the coagent-modified sample. Solidified thin films of CM-PP where opaque, compared to the L-PP and DCP-PP films which were transparent, presumably due to the different size of the spherulites.

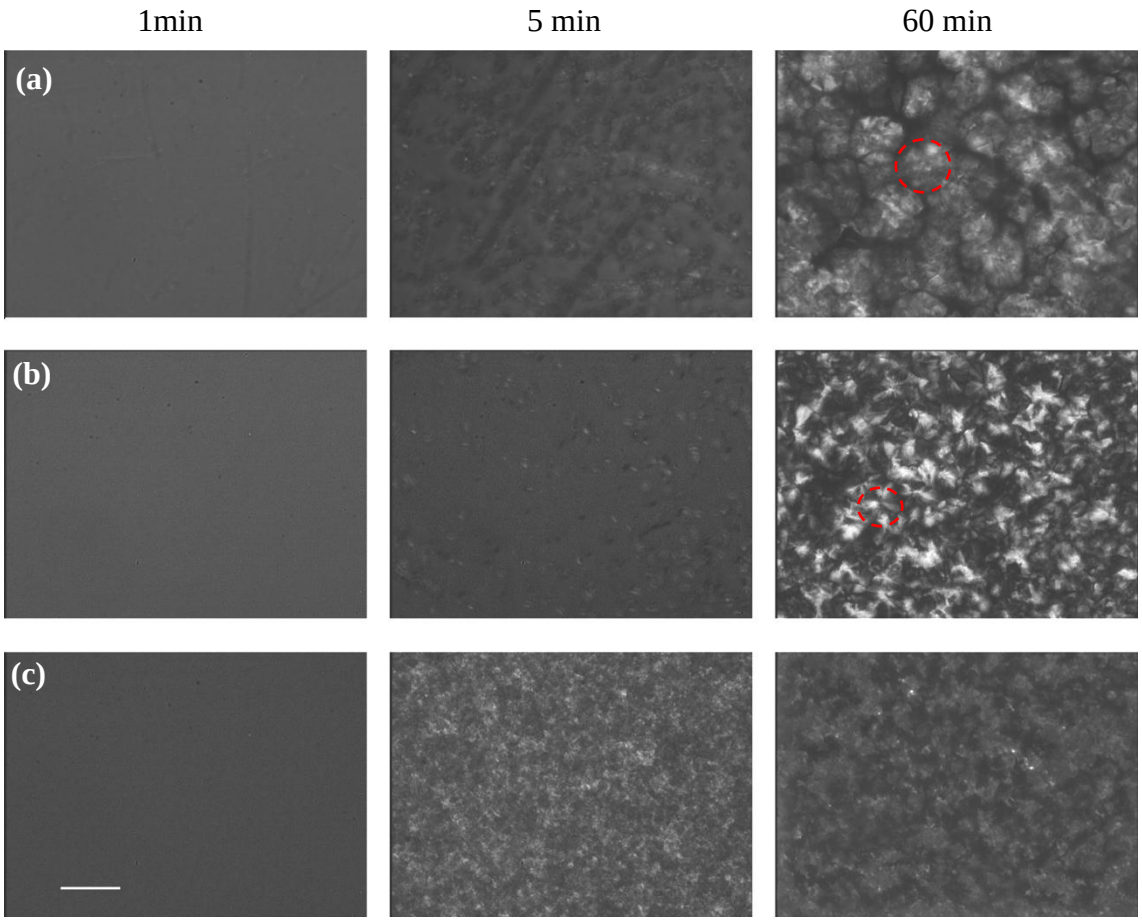

Figure 5.6 Optical microscope images of **(a)** L-PP; (b) DCP-PP and **(c)** CM-PP during isothermal crystallization at 140 °C. The scale bar represents 60μm. Representative spherulites are marked with the dashed circle.

It is noted that increases in T_c, crystallinity and crystallization rate are commonly observed in formulations containing small amounts (0.1-0.3 wt %) of organic nucleating agents such as carboxylate salts [67] and sorbitol-based clarifiers [128]. Talc and other inorganic fillers provide similar effects, albeit at higher solids loading due to their lower nucleating efficiency [129,130]. In the present context, the solid phase present in the CM-PP material has dimensions that are consistent with common nucleating agents, and a defined interface between the melt-state and the cross-linked particle [65,130]. The notion that nanoparticles formed during the coagent modification of PP affect crystallite nucleation has significant implications for material processing operations such as injection molding.

5.3.3 Foaming Behaviour

In addition to polymer crystallization, the dispersed nano-particle phase within CM-PP affect the formation of an incipient gas phase during conventional polymer foaming. Given the importance of nucleation on foaming dynamics and final properties [60], the performance of CM-PP relative to L-PP and DCP-PP was investigated in a simple batch foaming process. The sequence of images shown in **Figure 5.7** reveals clear evidence of improved nucleation rates and cell densities in the coagent-modified material. Consistent with the enhanced nucleation effect reported in crystallization, it is suggested that nanoparticles provide sites for heterogeneous nucleation in foaming, resulting in more efficient initial nucleation, as well as sustained cell nucleation throughout the foaming process, thereby providing foams of higher cell density.

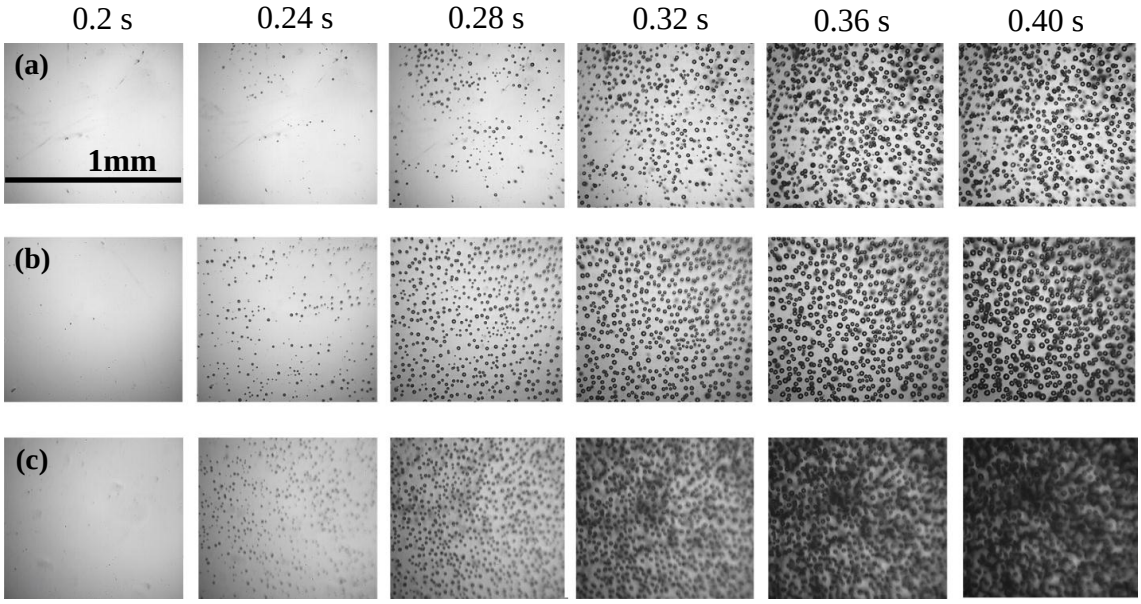

Figure 5.7 Images of cell nucleation sequence of **(a)** L-PP, **(b)** DCP-PP and **(c)** CM-PP.

5.4 Conclusions

Cross-linked nanoparticles generated *in situ* during coagent-modification of PP can serve as heterogeneous nucleation sites for crystallization from the melt, and gas phase formation during batch foaming.

Chapters 4 and 5 have demonstrated that the performance of these materials is dictated not only by the rheological properties brought about by chemical modification, but also through the enhanced nucleation generated by the dispersed solid phase.

Chapter 6 will focus on the heterogeneous nucleation effects on PP. In the interest of generating more industrially relevant materials on a larger scale, that would be also suitable for a continuous extrusion foaming process, Chapter 6 will investigate the potential of nanosilica as a nucleating agent for foaming.

Chapter 6

Optimization of Dispersion of Nanosilica Particles in a PP Matrix and Their Effect on Foaming*

6.1 Introduction

Chapters 4 and 5 reported the presence of a nanoparticle phase within coagent modified PP and studied the effect of these particles on nucleation during foaming. Being formed in-situ during melt state reactive modification, these nanoparticles are expected to disperse reasonably well in the PP matrix. In this chapter nanosilica was chosen as the dispersed phase in L-PP in order to confirm the benefits of heterogeneous nucleating agents for foaming under a more industrial oriented setting.

Nanofillers, such as nanoclays have been reported to have a beneficial effect as nucleating agents in foaming [75,131-133]. In spite of its previously reported beneficial properties in PP-based nanocomposites [79,81], nanosilica has not seen widespread use as a nucleating agent in polyolefins.

Most major challenges associated with the processing of nanocomposites are related to the choice of a compatibilization strategy, including appropriate filler treatment and/or matrix functionalization techniques, to ensure good matrix-filler interaction. In order to reach the full potential of nanocomposites, a homogeneous dispersion of the nano-particles in the polymer matrix is a prerequisite. Achieving good dispersion therefore is a key consideration when designing an efficient compounding process. In particular, the reduction of the size of filler aggregates and agglomerates is related to the intensity of the applied hydrodynamic stress and

* A version of this chapter has been published. Lee, S. H., Zhang, Y., Kontopoulou, M., Park, C. B., Wong, A. and Zhai, W. International Polymer Processing 2011 (26); 388-398

residence time in mixing devices such as extruders. The mechanisms involved in the intercalation/exfoliation of fillers such as nanoclays and in the breakup of nanosilica aggregates are quite complex and sensitive to the compounding conditions. Several studies have been published on the effect of twin-screw compounding conditions on the morphology of organoclay/polymer nanocomposites [134].

Although fine dispersion of the nanosilica has been identified as a key factor to obtain optimum properties [78,79,135-140]., there are very few studies on the optimization of the compounding conditions for the preparation of these composites [80]. This chapter also presents a systematic study of the effect of the screw configuration and operating conditions of a closely intermeshing co-rotating twin-screw extruder on the morphology of PP/nanosilica composites. The optimized processing conditions were used to obtain finely dispersed composites, which were subsequently used in foaming experiments performed in a batch foaming simulation setup and in extrusion foaming.

6.2 Experimental

6.2.1 Materials

Polypropylene, Escorene PP 1042, MFR 1.9 g/10 min at 230°C, was supplied by ExxonMobil Chemical. Maleated PP (PP-g-MA), Fusabond® PM 613, MFR 49 g/10 min at 190°C containing 0.55 wt% of succinic anhydride grafts, was supplied by E.I. DuPont Canada. The weight average molecular weight of this material is 9100 g/mol. Two fumed nanosilica grades with a mean particle size of 12 nm, were supplied by Evonik Industries (formerly Degussa Corp.): Aerosil® R200 with specific surface area (SSA) of 200±25 m^2/g, which does not contain any surface modification and Aerosil® R805, with a specific surface of 150±25 m^2/g, modified with octylsilane. The density of fumed silica is 2200 kg/m^3 and the tamped densities reported by the

supplier are 50 g/l and 60 g/l for R200 and R805 respectively. Throughout this work the Aerosil® R805 silica is used, unless otherwise specified.

6.2.2 Twin-Screw Extruder Configuration

Nanosilica was compounded into PP using a Werner Pfleiderer ZSK-30 (L/D=40, D=30.7mm) co-rotating twin screw extruder. Four different configurations, selected to provide different combinations of dispersive and distributive mixing, are shown in **Figure 6.1**. For each screw configuration, the shear mixing intensity and residence time depended on the kneading zone design.

The basic configuration incorporated three kneading block sections. The first set of kneading discs is normally used to enhance the melting of the polymer inside the extruder to facilitate vigorous rapid dispersive mixing of ingredients further downstream. The kneading disc block section in the middle consisted of disks with different widths. Staggered 45° kneading elements were used to generate higher shear intensity, thus achieving better dispersive mixing than the neutral kneading elements [141]. The configurations shown in **Figure 6.1 (a)** and **(b)** have small staggered angle discs, which lead to shorter residence time and better dispersive mixing. On the contrary, the greater stagger angles of the configurations shown in **Figure 6.1 (c)** and **(d)** provide longer residence time and better distributive mixing.

In addition, the residence time of a given element of polymer within the kneading block, and thus the extruder, was varied by including a reverse or neutral kneading element in the kneading block section[142,143]. The inclusion of a reverse or neutral kneading element in the kneading block section causes an element of polymer to spend more time in the kneading block and increases the distributive mixing intensity of the screw configuration. Therefore, the residence time for the screw configurations shown in **Figure 6.1** should increase in the order of B < C < A < D. The residence time is higher in screw D compared to screw A, because the neutral kneading elements

provide longer residence time [142,143]. Introduction of the additional reverse screw element in the first two kneading zones, corresponding to melting and initial dispersion, is expected to generate more efficient distributive mixing, resulting in better degree of filler dispersion in the polymer matrix.

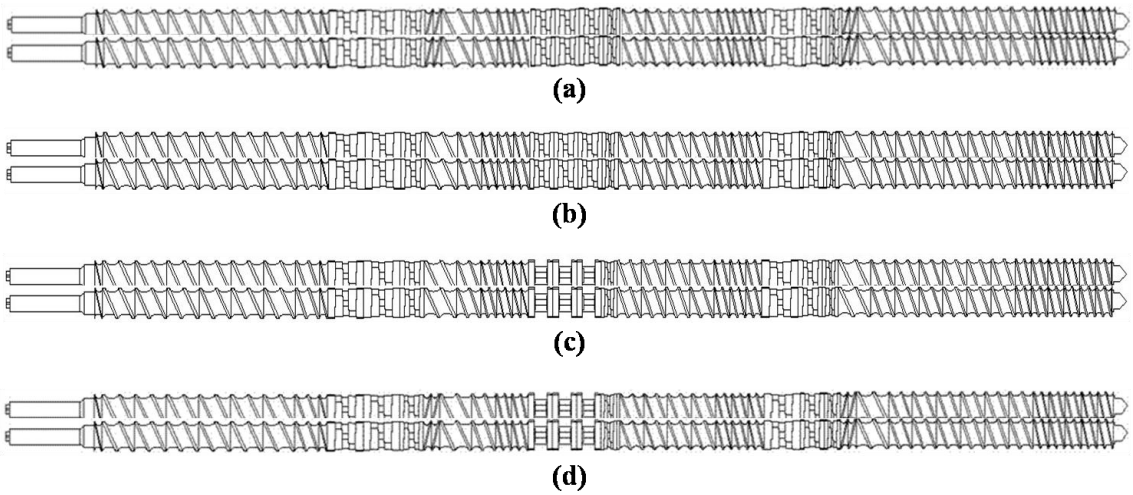

Figure 6.1 Four screw configurations providing good dispersive mixing **(a)** and **(b)**; and distributive mixing **(c)** and **(d)**.

6.2.3 Compounding Procedure and Characterization

All composites were prepared based on the compounding conditions shown in **Table 6.1**. The extrusion rate was 2.5 kg/h. The temperature profile in the extruder barrel from the feeding zone to the die was kept to 190-200-210-210-220-220-200°C. The state of dispersion of the filler in the polymer blends was assessed by using TEM imaging on a Hitachi 7000 instrument operated at 75 kV. The samples were embedded in between two pieces of polystyrene plate, and cut in 70 nm thickness with an ultramicrotome.

The TEM images were analyzed by using the Image Pro image analysis software to estimate the area of the dispersed nanosilica aggregates. Given the irregularity of the particles, the Feret diameter, defined as the distance between two tangents on opposite sides of the particle profile that are parallel to a fixed direction, was evaluated. A mean Feret diameter was calculated by averaging the chord lengths between parallel tangents obtained at different angles, as shown in **Figure 6.2**.

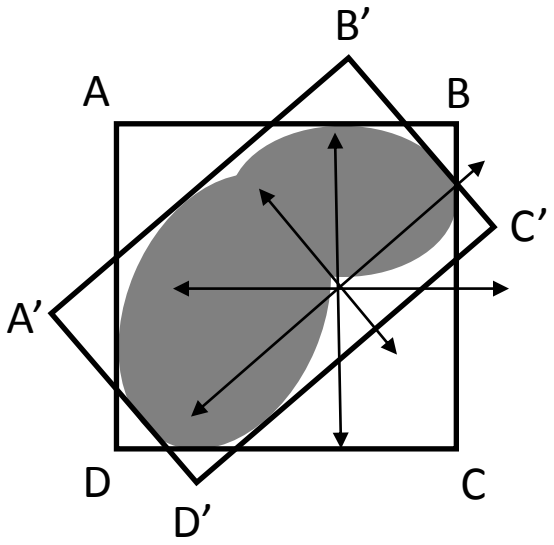

Figure 6.2 Schematic showing the evaluation of the mean Feret diameter. Feret diameters AB, AD, A'B' and A'D' are generated by rotating the caliper frame. An average of these lengths obtained at different angles is calculated by the software as the mean Feret diameter of the particle shown.

Rheological characterization was carried out using a Reologica ViscoTech oscillatory rheometer using 20 mm parallel plate fixtures, with a gap of 1 mm at 190 °C, under nitrogen blanket. The rheometer was operated in the dynamic oscillatory mode in the linear viscoelasticity region. Steady-shear viscosity measurements were done using a Rosand RH2000 Dual Bore Capillary rheometer.

Table 6.1 Blending conditions and compositions of PP/nanosilica composites

	SiO_2 (phr[a])	PP-g-MA (phr)	Screw RPM	Screw Configuration
Series I	1	5	150	A B C D
Series II	1	5	100 150 200	A
Series III	0 0.3 0.5 1 2 3	5	200	A
Series IV	2	0 0.5 1 5 7 10	200	A

[a] parts per hundred resin

6.2.4 Foaming Visualization and Analysis

Foaming visualization experiments were conducted using a batch foaming simulation system, which has been described in detail previously [18,111]. The temperature and pressure in the simulation chamber were regulated using a thermostat and a syringe pump, respectively. An ADAC board and a high speed CMOS camera was used to record the pressure drop data and video images of the foaming processes, respectively.

The foaming experiments were performed using composites containing 0-3 phr SiO_2 prepared at the optimum compounding conditions, as described below, using the twin-screw extruder. Disks having dimensions 7 mm in diameter and 200 μm in thickness were prepared by compression molding using a Carver hydraulic press heated at 200ºC. The disks were then placed into the

chamber, which was set to 180ºC at a pressure of 2000 psi (202.6 MPa). The maximum pressure drop rate for all experiments was 38 MPa/s. Both N_2 and CO_2 blowing agents were used, however only the results obtained with N_2 are reported here, because distinct cells were obtained, making it possible to conduct reliable image analysis. A program based on Labview was used to open the solenoid valve and record the pressure decay, while simultaneously, the high speed camera recorded the cell growth and collapse phenomena. For each condition, three separate experiments were run, and the images were analyzed using the Sigma Scan Pro 5.0 image analysis software. The cell density was calculated by counting the number of cells observed from the images taken at a given moment in time, *t*. The average cell diameter was obtained by taking the averages of the diameter of 10 randomly selected cells. The cell densities with respect to the unfoamed volume ($N_{unfoamed}$) were then calculated using **Eqns (6.1-6.3)**:

$$N_{unfoamed}(t) = \left(\frac{N(t)}{A_C}\right)^{\frac{3}{2}} \times VER(t) \tag{6.1}$$

where N(t) is the number of bubbles observed in an analysis area of A_c.

The volume expansion ratio (VER) was calculated as the ratio of bulk density of the pure polyolefin material (ρ_p) to the bulk density of the foam sample (ρ_f):

$$VER(t) = \frac{\rho_p}{\rho_f(t)} \tag{6.2}$$

In the case of the batch foaming experiments, the observations are made only for the initial growth stage, and therefore the VER is approximately equal to 1. Hence, the expression for $N_{unfoamed}$ can be reduced to:

$$N_{unfoamed}(t) = \left(\frac{N(t)}{A_C}\right)^{\frac{3}{2}} \tag{6.3}$$

6.2.5 Extrusion Foaming

The single extrusion foaming system used has been previously described by Park and Cheung [49]. A filamentary die with L/D 0.413”/0.051” was used for the foaming experiments. The blowing agent was CO_2, and its content was fixed to 5 wt% throughout the experiment. CO_2 was injected into the barrel, and regulated by controlling both the gas flow rate from the syringe pump and the material flow rate that passed through the die. When the polymer/gas solution entered the filament die, it experienced a rapid pressure drop which caused a sudden decrease in gas solubility in the polymer; hence a large number of bubbles were nucleated in the polymer matrix, resulting in foaming. The extruder had 4 heating zones; the temperatures of the first 3 zones were 150, 200, and 190 °C respectively. The 4th zone temperature was set equal to the die temperature, which ranged from 132 to 170°C. The die pressure ranged from about 1000 psi (101.3 MPa) at 170°C, to a maximum of 5000 psi (506.5 MPa) at the lowest die temperature of 132°C. The foamed samples at different die temperatures were collected for cell morphology observation and density measurements. The cell densities of foams were obtained based on **Eqns. (6.1-6.2)** and the VER was calculated in accordance with **Eqn. (6.2)**:

$$VER = \frac{\rho_p}{\rho_f} \tag{6.4}$$

where ρ_p and ρ_f are the mass densities of samples before and after foaming, respectively, which were measured via the water displacement method in accordance with ASTM D792.

6.3 Results and Discussion

6.3.1 Effect of Composition and Operating Parameters on the Degree of Dispersion of the Nanosilica

Effect of Screw Configuration

In order to investigate the effect of screw configuration on the degree of nanosilica dispersion, composites containing 1 phr of nanosilica were prepared using the configurations shown in **Figure 6.1**. The results of the image analysis obtained based on the TEM images are summarized in **Figure 6.3**.

Comparison of the configurations containing narrow staggered kneading disks to provide better dispersive mixing (A and B) to the configurations designed for better distributive mixing (C and D) clearly shows that the higher shear intensity provided by the former is necessary to provide good dispersion of low aspect ratio fillers such as nanosilica. In both the dispersive (A and B) and distributive (C and D) groups, the presence of reverse screw elements proved to be beneficial, since it increased the residence time inside the screw.

Overall screw configuration A, which has narrow staggered kneading disks and additional reverse screw elements, generated the best dispersion. This is because the narrow staggered kneading disc and reverse pumping element generate higher shear stress and longer residence time inside the screw. The reverse screw elements also functioned to increase the pressure and thus caused the development of fully filled regions. Given that screw configuration A generated the best outcome, it was the configuration of choice for the subsequent series of experiments, which explored the effect of processing conditions and composition.

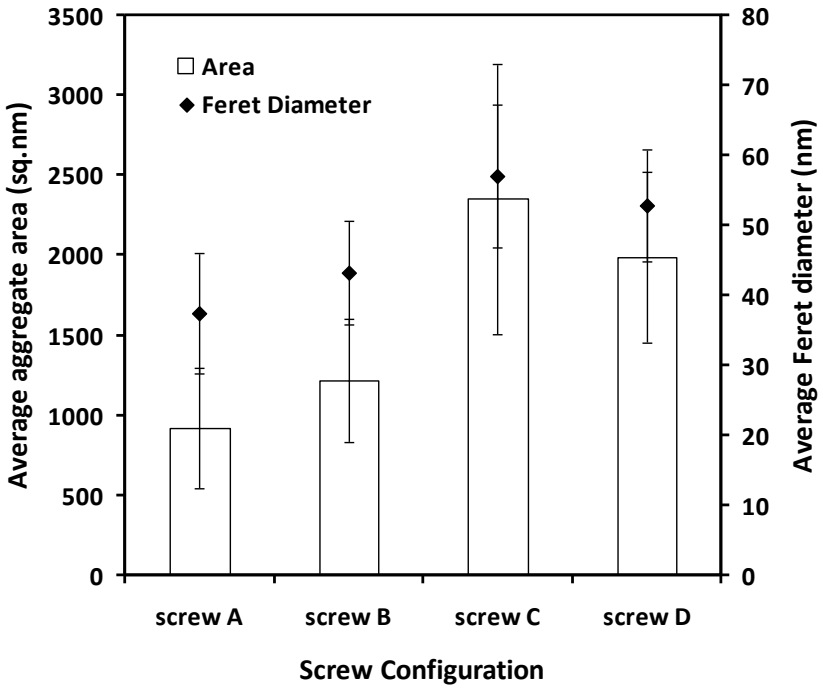

Figure 6.3 Effect of screw configuration on the average silica aggregate Feret diameter and area for 1 phr PP/silica composites, at a screw speed of 150 rpm. The error bars represent 95% confidence intervals.

Effect of Screw Speed

Figure 6.4 summarizes the effect of screw speed, using screw configuration A, as identified above. It is obvious from the results that increasing the speed from 100 to 150 rpm improves the dispersion, while beyond this, there is no statistically significant effect. This implies that high shear stresses, generated by a high extrusion rate are required in order to obtain good filler dispersion. 200 rpm was chosen as the screw rotation speed for the subsequent series of experiments because of the more uniform aggregate size generated.

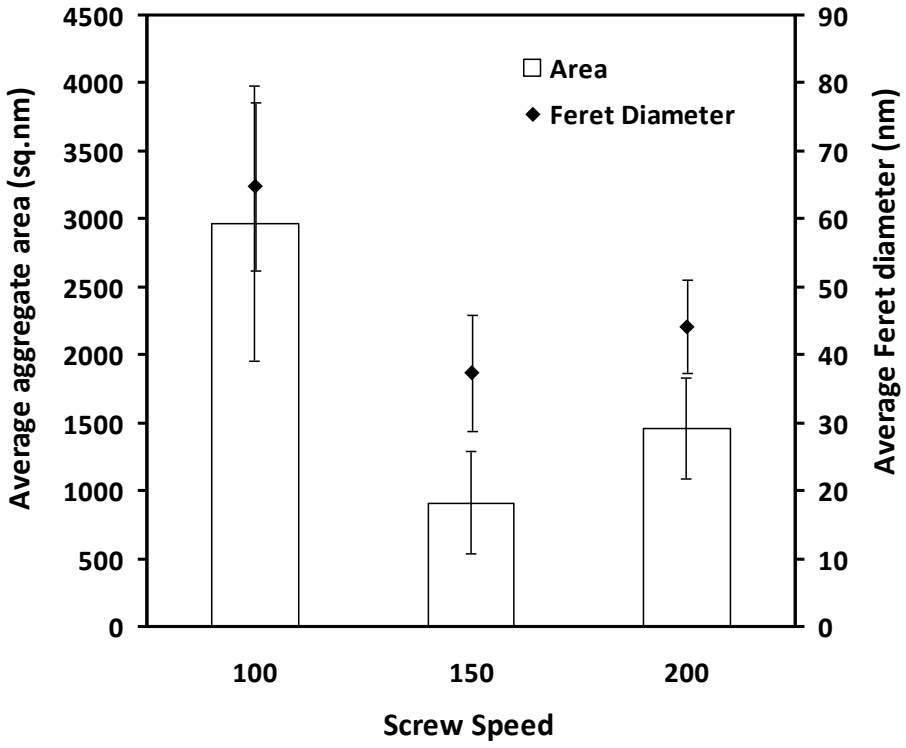

Figure 6.4 The average silica aggregate Feret diameter and area for 1 phr silica composites at different screw speeds using screw configuration A. The error bars represent 95% confidence intervals.

Effect of Nanosilica Content

The effect of silica content on the morphology of the extruded nanocomposites using the optimized configuration and screw rotation speed is shown in **Figure 6.5** and **6.6**. The size of the silica aggregates depended strongly on the filler content; larger and more irregular aggregates formed as the amount of SiO_2 increased (**Figure 6.5**). These results are in good agreement with the findings of Bikiaris et al. [78], who reported that increasing the content of SiO_2 led to larger aggregates, and a wider particle size distribution. The surface hydroxyl groups of the fumed silica have a high tendency to create hydrogen bonds, causing the formation of aggregates, which

cannot be broken down even in the presence of the high shear forces generated during the compounding process.

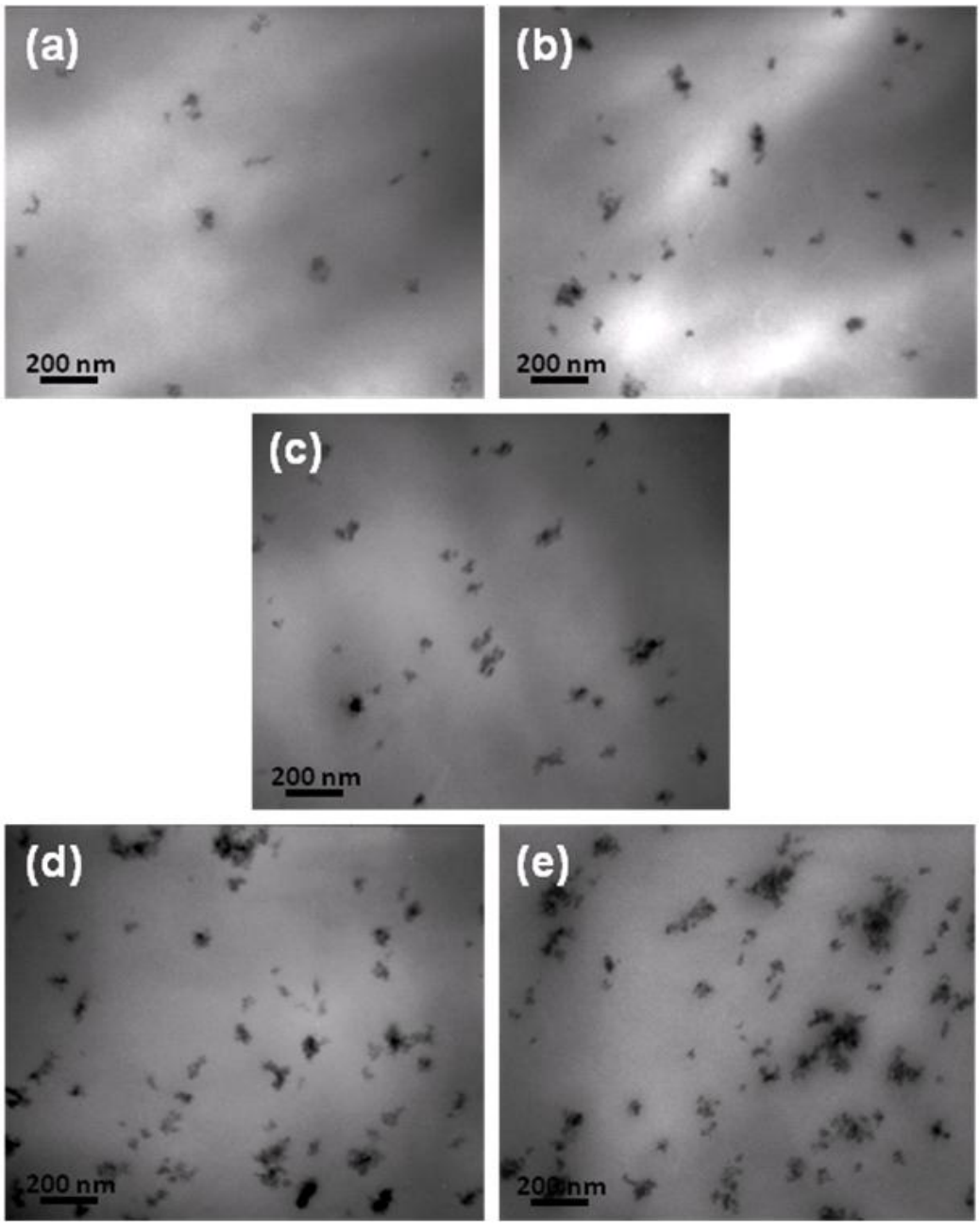

Figure 6.5 Transmission electron photomicrographs for nanocomposites prepared at different nanosilica loading. **(a)** 0.3 phr SiO_2; **(b**) 0.5 phr SiO_2; **(c)** 1 phr SiO_2; **(d)** 2 phr SiO_2; **(e)** 3 phr SiO_2. (Magnification x50,000)

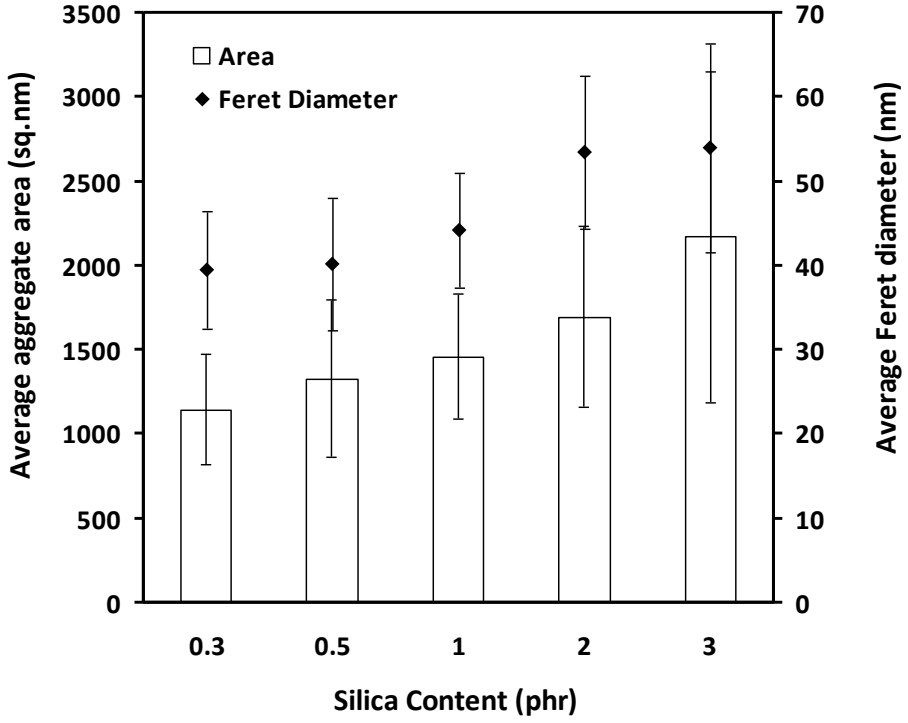

Figure 6.6 Average silica Feret diameter and area for PP/SiO_2 nanocomposites prepared at different nanosilica loading. The error bars represent 95% confidence intervals.

Effect of Compatibilizer Content

In order to take full advantage of the potential of nanoparticles to act as reinforcing agents in polyolefins, good interfacial adhesion between the non-polar matrix and the polar filler must exist. In the present study PP-g-MA was used as a compatibilizer, since it has been shown to be effective in PP/nanosilica composites [78,79]. As shown in the previous section higher amounts of silica led to increased propensity toward aggregation. Given that the appearance of aggregates was more pronounced at loadings of 2 phr and higher, the effect of PP-g-MA content on the size of silica aggregates, at a constant loading of 2 phr, was examined. According to **Figure 6.7** addition of PP-g-MA reduces the number of large aggregates and increases the number of

particles with moderate or small size. The interaction of the silica surface hydroxyl groups with the succinic anhydride groups of PP-g-MA resulted in more efficient stress transfer and break-up of the aggregates. A PP-g-MA content of 5 phr was sufficient to obtain finely dispersed nanosilica particles when using the optimized screw configurations and extruder operating conditions. However above 7 phr, the silica particles started to re-agglomerate in the PP matrix. It is speculated that when higher amounts of the PP-g-MA compatibilizer, which has very low viscosity (MFR 49 g/10 min at 190°C) were used, the viscosity of the polymer decreased significantly, thus leading to less efficient stress transfer. Additionally, it might be difficult to mix higher amounts of PP-g-MA efficiently in the PP matrix. As a result, the PP-g-MA may form a separate phase that is more polar than the PP matrix phase [144], into which the fillers will tend to migrate. Based on the results of this study, 5 phr PP-g-MA was used for the subsequent rheological and foaming investigations.

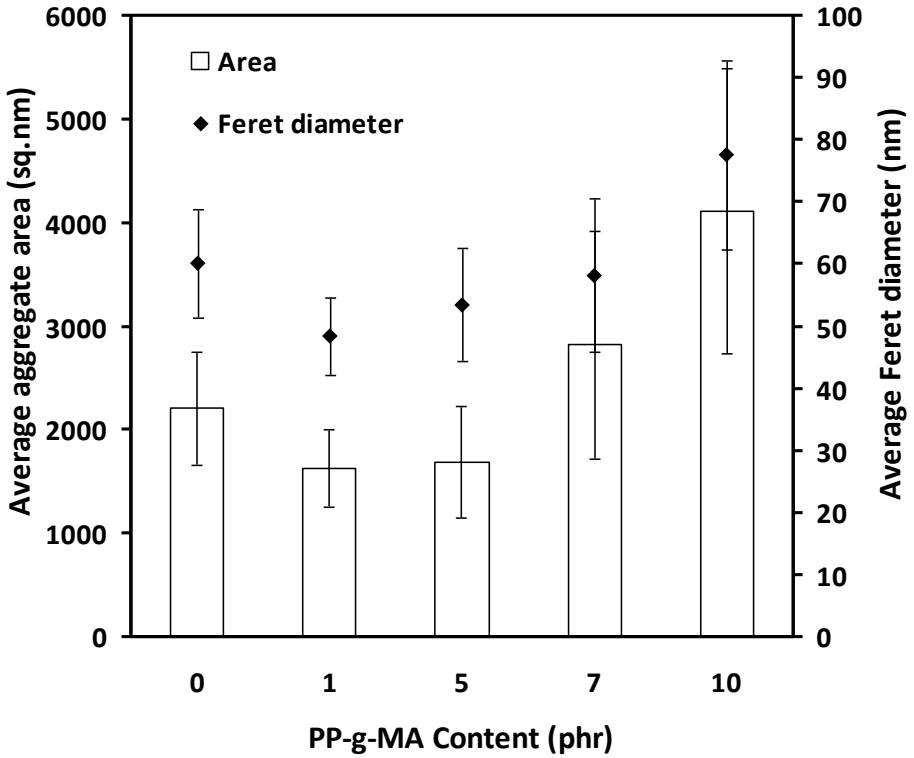

Figure 6.7 Effect of PP-g-MA content on the average silica Feret diameter and area for composites containing 2 phr silica. The error bars represent 95% confidence intervals.

6.3.2 Effect of Nanosilica on Rheological Properties

Given that the amount of nanosilica contained in the composites in this work is extremely low, below 0.9 vol%, it did not affect substantially the magnitude of the complex viscosity of the polymer, as evidenced in **Figure 6.8**. Actually the nanocomposites containing low amounts of silica show non-Einstein behaviour, given that the rheological properties appear the same, or even slightly reduced in the presence of low amounts of the nanosilica particles, as better seen in the inset of **Figure 6.8**. It has been shown before that very small and well-dispersed nanoparticles do not affect the rheological properties of the matrix at very low filler loadings [145]. A reduction in viscosity has been noted in polystyrene matrices containing highly cross-linked polystyrene

particles, and has been attributed to a confinement effect of the linear chain, when the interparticle separation between nanoparticles is smaller than the radius of gyration of the linear polymer coil [146]. However this is clearly not the case in the PP/nanosilica composites presented here, given that the size of the nanosilica aggregates is in the 30-70 nm range. It has been suggested that in highly concentrated suspensions air entrained by the particles during processing affects the microstructure of the suspensions and hence their rheological behaviour [147,148]. However such an effect has not been reported for very dilute suspensions. An increase in free volume in the presence of nanodispersed particles, which leads to a plasticizing effect is another plausible explanation [149]. A plasticizing effect has been reported by Lakdawala and Salovey [150] in carbon black filled PS, and Hatzikiriakos et al.[151] upon addition of very low amounts of organically modified nanoclays to polyethylene, which has led to speculation that at low loadings nanofillers may act as processing aids. Clearly further research is needed to further explain these findings.

At high shear rates, relevant to extrusion foam processing, there was essentially no effect of SiO_2 loading on the rheological properties as evidenced through experiments performed in a capillary rheometer (results not shown here). Therefore it is anticipated that rheological effects do not influence the extrusion foaming conditions in this work, or the cell growth and coalescence behaviour.

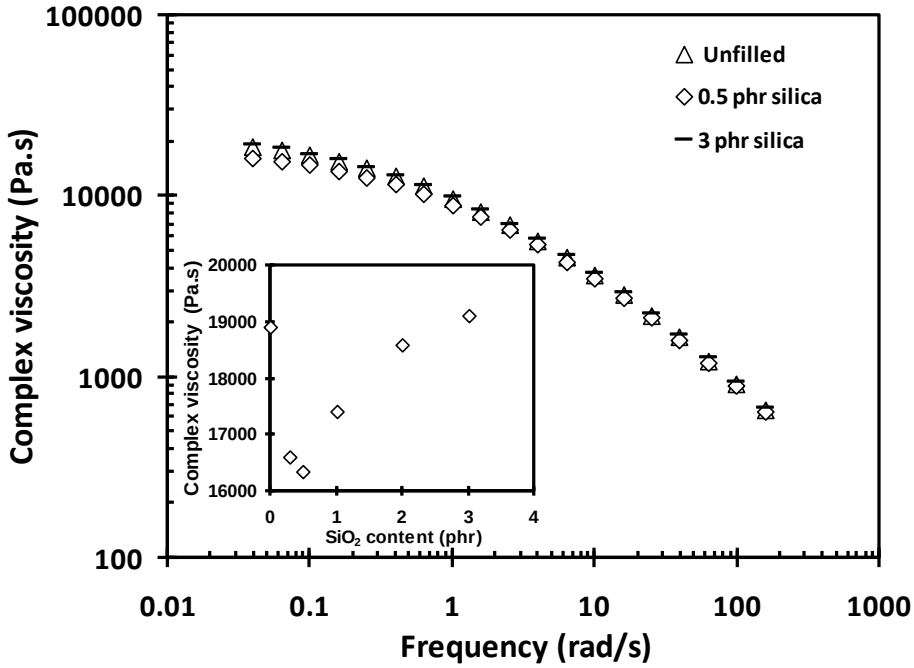

Figure 6.8 Complex viscosity of the PP/SiO_2 nanocomposites, containing 5 phr PP-g-MA and various SiO_2 loadings as a function of frequency at 190 °C. Inset summarizes complex viscosity at 0.04 rad/s as a function of SiO_2 content.

6.3.3 Batch Foaming Visualization of PP/nanosilica Composites

Effect of Silica Content

Optical microscope images obtained during the batch foaming experiments of the PP/nanosilica composites containing different SiO_2 contents are shown in **Figure 6.9**. It is clear that the nucleation process occurred earlier as compared to the unfilled polymer when low amounts of the filler (up to 1 phr) were used. The enhanced ability of the nanosilica particles to act as nucleating agents can also be seen in **Figure 6.10 (a)**, which depicts the cell density, calculated from equations (1-3), as a function of time. As shown in **Figure 6.10 (a)** and **(b)** respectively, the cell density and cell growth rate were higher compared to the unfilled polymer at loadings up to 1 phr.

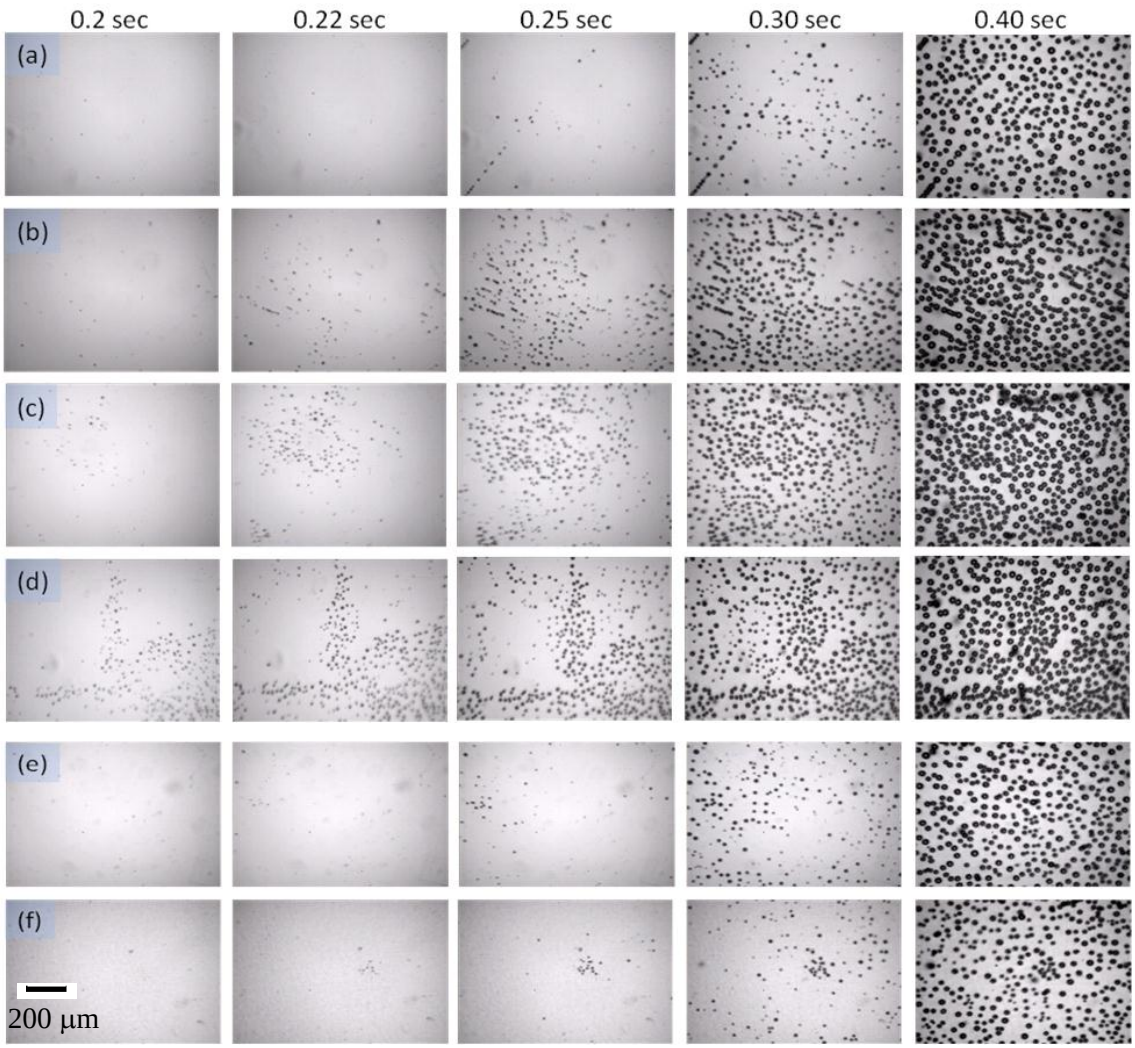

Figure 6.9 Cell nucleation images of PP/silica composites, containing 5 phr PP-g-MA at various SiO_2 contents **(a)** unfilled; **(b)** 0.3 phr; **(c)** 0.5 phr; **(d)** 1.0 phr; **(e)** 2.0 phr; **(f)** 3.0 phr. The temperature was 180°C.

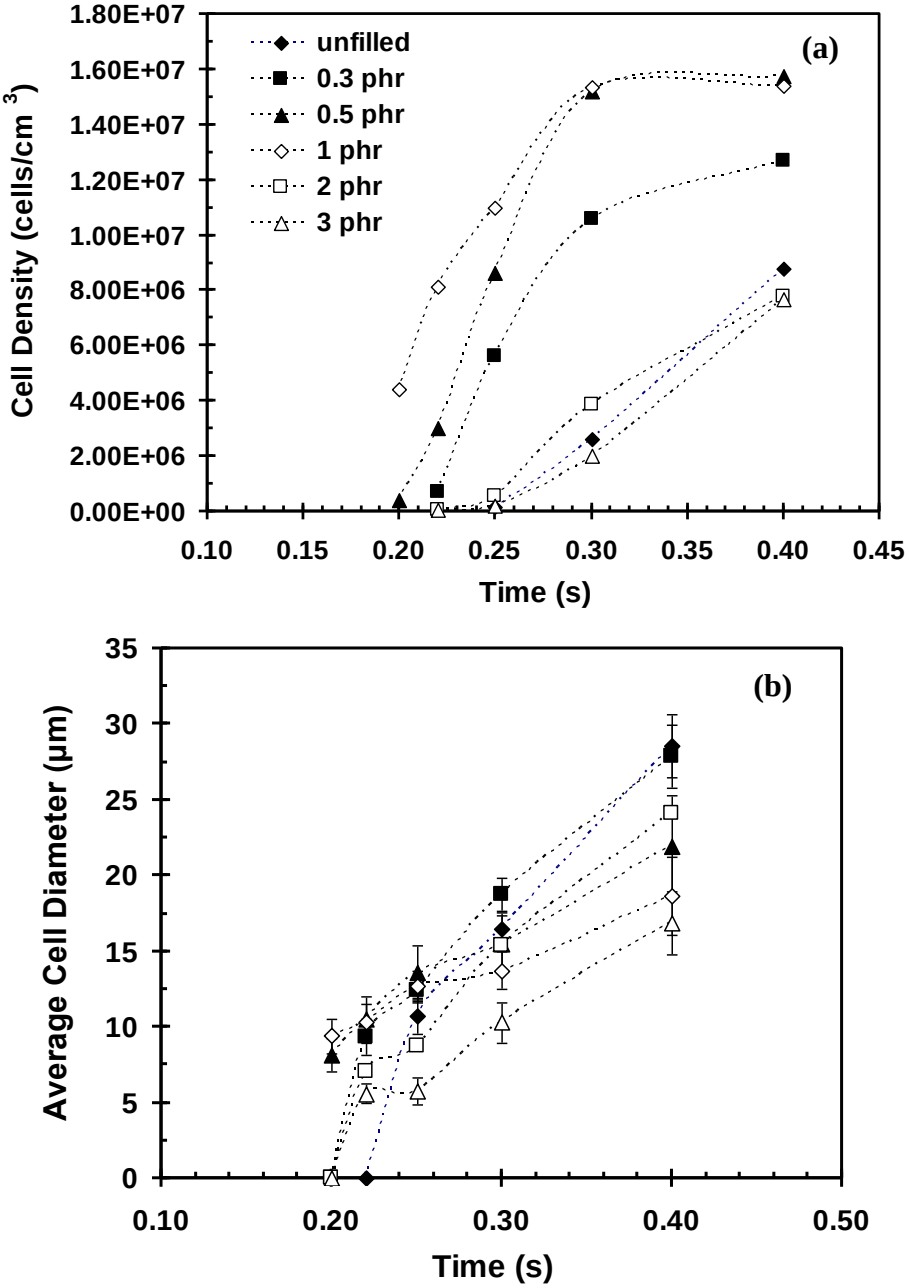

Figure 6.10 Cell nucleation of PP/nanosilica composites containing different silica contents; **(a)** cell density versus time; **(b)** cell diameter versus time. Lines are drawn to guide the eye. The error bars represent 95% confidence intervals.

It is interesting to note however that the enhancement seen in the cell nucleation behaviour in **Figure 6.9** and **6.10** was reversed at higher filler loadings. This is also seen in **Figure 6.11**, which summarizes the final cell density as a function of nanosilica composition.

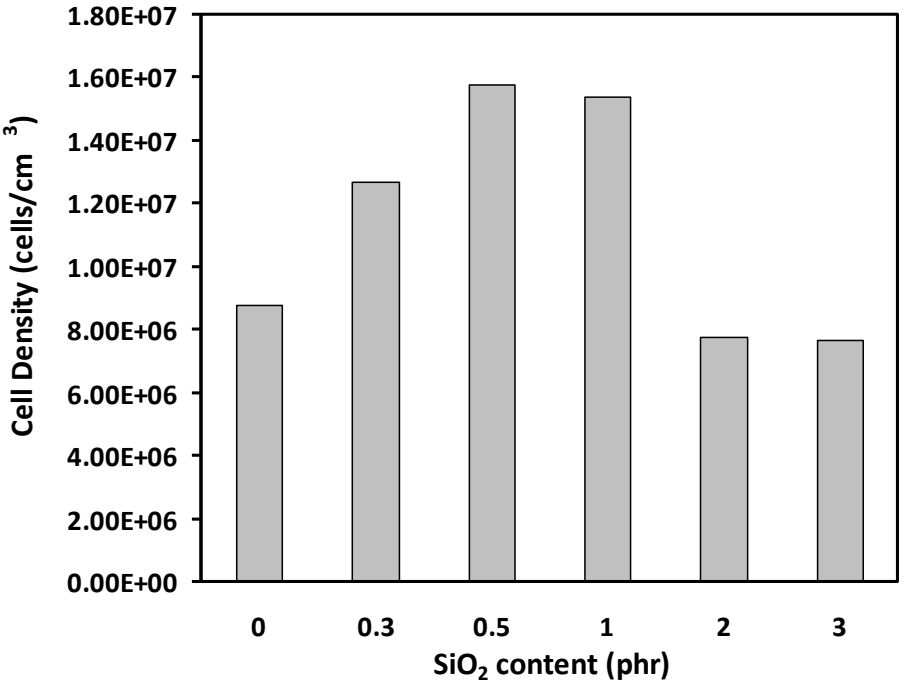

Figure 6.11 Average cell density vs. silica content

The dramatic drop in cell density seen at contents above 1 phr correlates well with the appearance of larger and more irregular filler aggregates at these contents (**Figure 6.5** and **6.6**). This finding suggests that the governing factor in the foaming process is the appearance of aggregates, which acts to reduce the interfacial contact between polymer and filler, thus reducing the capability of the filler to act as an efficient nucleating agent. This observation is similar to previous reports on polyethylene/clay nanocomposites, where very low loadings of exfoliated clay in a polyethylene matrix resulted in a microcellular foam of very high cell density [75]. This finding was attributed to the increased probability for heterogeneous nucleation in the presence of exfoliated clay with

high polymer/filler interfacial contact area. As clay content increased further, however, the degree of exfoliation decreased, thus reducing the interfacial contact area between polymer/clay, and the effect of clay on cell nucleation disappeared. Moreover, Taki et al. [152] noted in their work on PP/clay nanocomposites that in the presence of increasing amounts of clay, the diffusivity of the physical blowing agent might be reduced, thus depressing the mass transfer of the gas from the polymer to the bubbles, so that the bubble growth rate was decreased. Increases in the viscosity of the composites in the presence of nanoparticles have also been cited as possible reasons for the slower cell growth [153-155]. However this does not seem to be the case here, as the changes in viscosity and elasticity are minimal, as explained previously in **Section 6.3.2**.

Another plausible explanation for the trends observed in **Figure 6.11** is that the larger number of cells formed due to enhanced nucleation results in increased probability of coalescence and thus a lower cell density, in the presence of the low melt strength PP matrix.

It is noted that the enhanced nucleation displayed by nanocomposites containing 0.3 to 1 phr nanosilica during the batch foaming process was also observed for TMPTMA and TAM modified L-PP. The analogy between the two systems suggests that heterogeneous nucleation is the prevailing mechanism in both cases. The delay in cell density growth for compounds without sufficient nucleating effect, such as L-PP and nanocomposites containing poorly dispersed nanosilica was also consistent in Chapter 4 and this chapter.

Effect of Silica Surface Modification

The nucleation effect when low amounts of an unmodified, hydrophilic silica, Aerosil 200® was used was compared with the hydrophobic silica. It is clear from **Figure 6.12** that the hydrophobic silica/PP foaming system exhibited a higher bubble nucleation rate and a higher nucleated bubble

density than the unmodified hydrophilic silica/PP one. This phenomenon suggested that the modified silica possessed higher nucleation efficiency.

It is well known that the surface properties as well as size of the inert nucleating agents tend to dramatically affect bubble nucleation during polymeric foaming process [156]. In general, fillers with rough surface structure would be more energy favorable for inducing cell nucleation compared to smooth ones. According to the simulation results of Wang et al. [157], rough surfaces with large amounts of cavities could induce local stress variation in the polymer melt surrounding the fillers, which decreases the free energy barrier and therefore the critical radius for heterogeneous bubble nucleation. As a consequence, more bubbles nucleate early and the cell nucleation rate could be higher.

These findings are at first glance contradictory to this work, since the specific surface areas (SSAs) of the modified and unmodified silica are 150 and 200 m^2/g respectively. Therefore, in this sense, the unmodified silica should exhibit higher bubble nucleation efficiency than the modified one. However, the unmodified silica had a higher tendency to aggregate because of the formation of hydrogen bonds between the surface hydroxyl groups, as shown in **Figure 6.13**. Presence of larger aggregates (average Feret diameter 188 nm) would result in a decrease in the actual amount of the heterogeneous nucleating sites available to induce bubble nucleation, in agreement with the findings of the previous section.

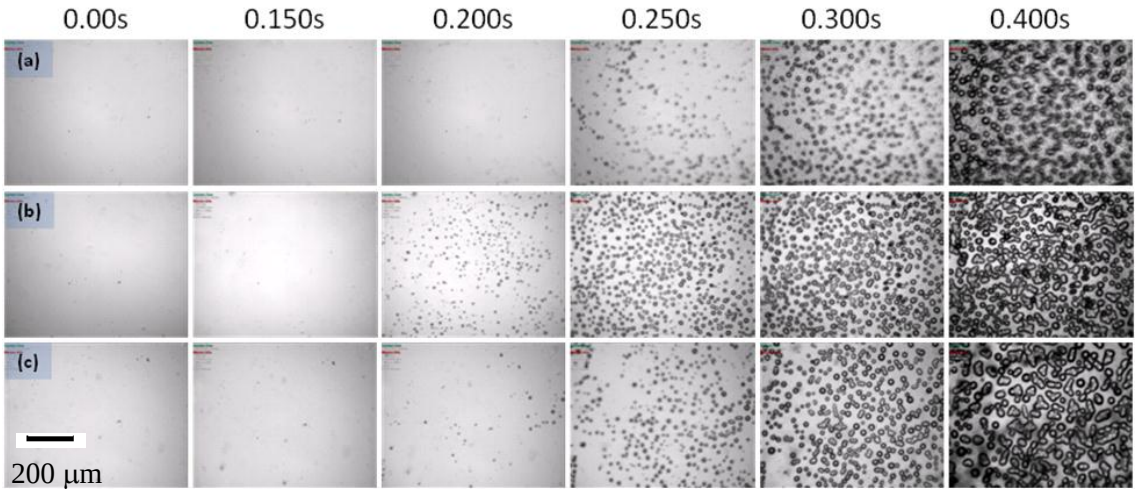

Figure 6.12 Cell nucleation images of PP/silica composites at 180°C **(a)** unfilled PP; **(b)** modified silica 0.3 phr; **(c)** unmodified silica 0.3 phr.

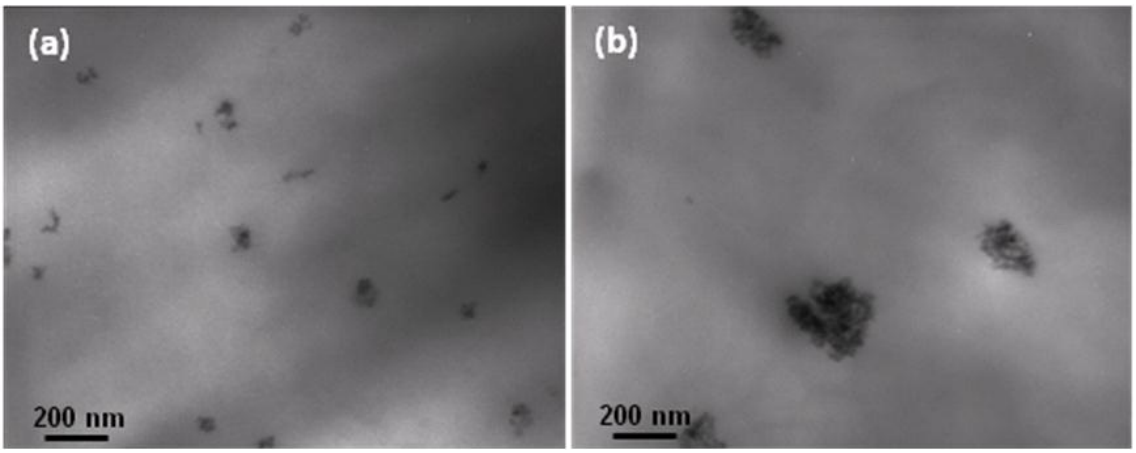

Figure 6.13 Transmission electron photomicrographs for nanocomposites containing 0.3 phr nanosilica prepared using **(a)** modified nanosilica; **(b)** unmodified nanosilica. (Magnification x50,000)

It should also be noted that the composites containing the unmodified silica had a tendency towards increased cell coalescence. This finding suggests that well dispersed surface-modified

nanoparticles may act as physical barriers, inhibiting coalescence – this is discussed more extensively in **Section 6.3.4** below.

6.3.4 Extrusion Foaming of PP/nanosilica Composites

The foaming performance of the composites was further investigated by conducting extrusion foaming experiments, at varying die temperatures. Given that the results from the batch foaming experiments suggested that the maximum cell density was obtained for composites containing 0.5 phr SiO_2, this composition was chosen for the extrusion foaming experiments. To maintain consistency, given that the composite contained maleated PP in the formulation, the foaming behaviour of the composites was compared to an unfilled PP/PP-g-MA compound. The image sequence in **Figure 6.14** compares the foam morphology of the composites containing 0.5 phr SiO_2 to that of the unfilled compounds, at various die temperatures. The unfilled foams exhibited very poor cell morphology, i.e., large cell size, over 500 μm, non-uniform cell structure distribution, and the presence of open cells, resulting from the obvious cell coalescence. With the introduction of nanosilica, however, the cell morphologies of resultant foams improved dramatically; the cell size was smaller, and the cell density was significantly higher, as shown in **Figure 6.15**. These result confirmed that small amounts of nanosilica enhanced the cell nucleation process. Moreover, the addition of nanosilica may widen the processing temperature window, since the minimum attainable temperature in the die in the presence of nanosilica particles was lower (**Figure 6.14 (g)** and **(h)**), although the reason for this needs further investigation.

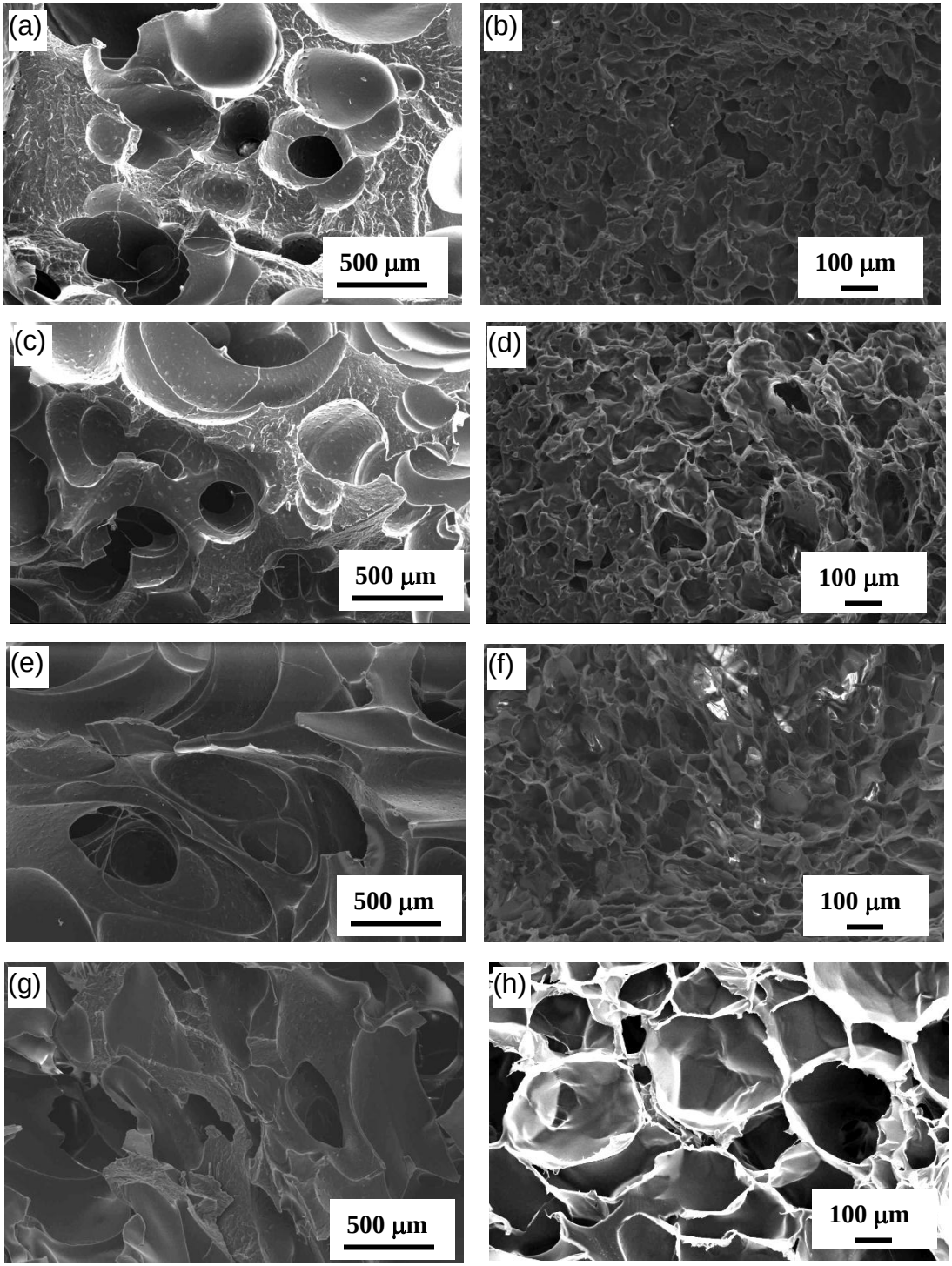

Figure 6.14 SEM images of foamed samples obtained by extrusion foaming at various die temperatures. Images on the left are the unfilled PP/PP-g-MAn compounds, whereas on the right the composites containing 0.5 phr SiO_2. **(a)-(b)** 150°C, **(c)-(d)** 140°C, **(e)-(f)** 145°C, **(g)** 138°C (minimum attainable), **(h)** 132°C (minimum attainable).

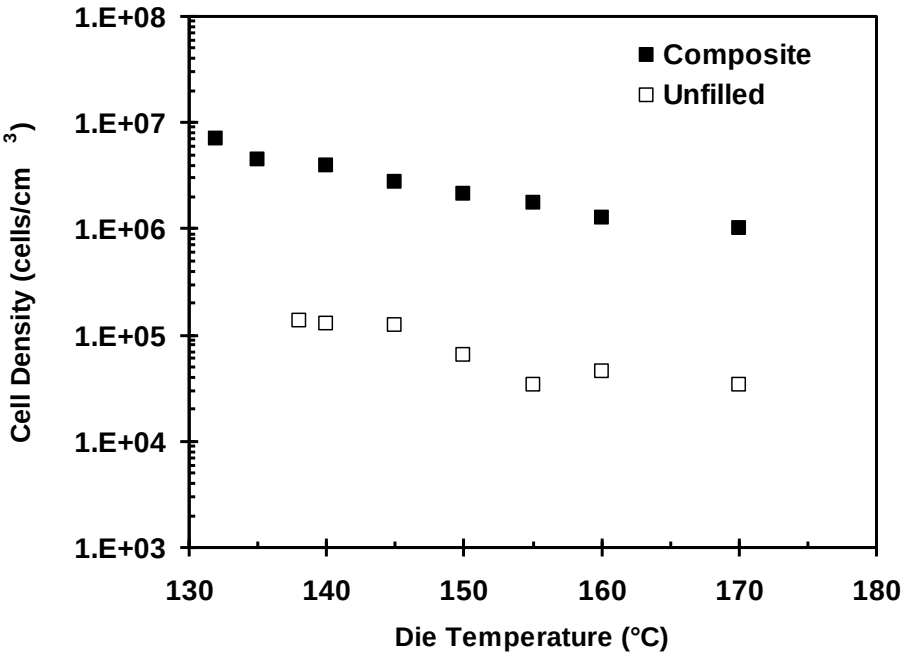

Figure 6.15 The cell densities of the foamed PP/PP-g-MA compounds and composites containing 0.5 phr SiO_2 obtained at various die temperatures.

It should be pointed out that the final cell density of the unfilled polymer and composite foams obtained by extrusion foaming was much lower, at least by an order of magnitude, than that observed in the visualization test. The conditions in extrusion foaming (pressure release rate and temperature) are entirely different from those in batch foaming. Additionally, the cell nucleation mode in the batch process would be quite different from that of the extrusion process. Both the surface of the sapphire window and the additives will govern cell nucleation in the batch process [111] whereas the cell nucleation in the extrusion process is only governed by the additives. Therefore, a direct comparison may not be possible, but generally speaking, despite the higher shear and extensional rates in the extrusion die flow, the cell density of the extruded foams was lower than that of the batch foams. This may be due to active coalescence taking place in the

extrusion die at high shear rates and high melt temperatures, although further study is required to clarify this hypothesis.

It is also noteworthy that, as seen in **Figure 6.14**, a significant number of closed cells are observable in the foams containing nanosilica. This appears contradictory to the cell density measurements, as a higher cell density typically results in thinner cell walls, therefore the cell opening is accelerated [158]. Nanofillers may contribute to the prevention of cell coalescence, through an enhancement in the elasticity of the melt. However as discussed in **Section 6.3.2** the nanosilica only showed a slight effect on the viscoelastic properties of PP melt.

6.4 Discussion

Based on the results outlined above, it is obvious that nanosilica particles can act as nucleating agents for foaming, both in the batch foaming and extrusion foaming setups.

It is well known that heterogeneous nucleation is thermodynamically favoured over homogeneous nucleation in the presence of solid nucleating agents, because of a reduction in the Gibbs free energy necessary for nucleating a stable cell. Zhai et al. [159] estimated that the energy required for cell nucleation at the surface of nanosilica particles is three orders of magnitude lower than that required for homogeneous nucleation. The classical nucleation theory can be evoked to understand the cell nucleation phenomena during foaming in polymers [160]. External particles or surfaces serve as heterogeneous nucleating sites, by providing crevices that trap gas and form preexisting nuclei. The free energy barrier for heterogeneous nucleation, ΔG_{het}, is lower than that for homogeneous nucleation, ΔG_{hom}, by a geometrical factor $S(\theta_c, \beta)$, which is related to the contact angle θ_c of the solid-gas-liquid interface, and the half-angle β which depends on the geometry of the nucleation site [10,160]:

$$\Delta G_{het} = \Delta G_{hom} S(\theta_C, \beta) \tag{6.5}$$

where

$$\Delta G_{hom} = \frac{16\pi\gamma^3}{3\left(P_{bub,Cr} - P_{sys}\right)^2} \quad (6.6)$$

γ is the interfacial energy at the interface between gas and liquid; $P_{bub,cr}$ is the pressure inside a critical bubble and P_{sys} is the system pressure.

ΔG_{het} thus depends on the interfacial properties of the gas-liquid-solid interface and the surface geometry of the heterogeneous nucleating sites. It has been shown that in general heterogeneous nucleation is favoured in conical and spherical cavities that are commonly encountered when irregularly shaped particles, were used as nucleating agents [10]. This is obviously the case for the nanosilica particles, where introduction of small amounts of particles has a positive influence on nucleation rates.

On the other hand, even though the nucleation density increases with silica loading for well dispersed individual silica particles, the actual nucleation density decreases in the presence of larger silica aggregates, because of the reduction in the interfacial area available for heterogeneous nucleation. Aggregated nucleants are less efficient than dispersed ones, since the first nucleant to activate in an aggregate depletes the blowing agent near the others [161]. This is obviously the reason why the formation of larger particles upon increasing the nanosilica content generally resulted in reduced nucleating efficiency.

6.5 Conclusions

Dispersion of nanosilica within a PP matrix is sensitive to extrusion conditions, and to the amount of compatibilizer. The size of the aggregates and their spread increased significantly beyond a SiO_2 content of 1 phr. The degree of dispersion of the SiO_2 particles was associated to their ability to act as nucleating agents, when foaming with N_2 as the blowing agent. Finely dispersed SiO_2 at

loadings less than 1 phr resulted in enhanced nucleation and cell density growth rate. These findings were confirmed by extrusion foaming experiments. The improvement in foam structure was attributed to the enhanced cell nucleation ability in the presence of finely dispersed nanoparticles. Similar effect has been observed for coagent modified PPs containing nanoparticles as a nucleating agent for gas phase. The optimal quantity of 1 phr also agree qualitatively well with the estimation of nanoparticles contained in modified PP matrix.

Chapter 7

Discussion, Conclusions, Significant Contributions and Recommendations for Future Work

7.1 Discussion

Since foaming by a gas expansion process involves the deformation of the polymer melt by a growing gas phase, rheological properties including melt viscosity and strain hardening are inherently the main properties to consider when choosing a polymer grade for foaming. However these properties are also intimately interrelated, with higher viscosity materials generally having more strain hardening for materials with similar structure, therefore their individual effects had not been isolated to date. Chapter 3 has shown that ethylene-α-olefin copolymers with similar viscosity values generated foams with indistinguishable morphology, except from grades displaying poor strain hardening. Specifically it was found that an ethylene-butene copolymer containing short chain branching foamed poorly, due to its lack of strain hardening, compared to its ethylene-octene copolymer counterparts, having long chain branching and similar viscosities. Furthermore it was evident in Chapter 3 that other material properties, such as the crystallization temperature should not be overlooked. Specifically a low density-low crystallization point octene-ethylene copolymer containing the highest amount of octene failed to crystallize during the cooling stage, resulting in foams of poor quality.

This research on ECs has demonstrated unambiguously that when melt viscosity is fixed, extensional viscosity and crystallization temperature are important factors influencing foaming behaviour.

For the purpose of further understanding the effect of material properties on the foaming behaviour of polyolefins, free radical mediated melt state coagent modification of a commercial PP was conducted in Chapters 4 and 5. Through deliberate manipulation of the formulations, the viscosity and chain architecture were controlled separately to give a series of materials with evolving structure and properties. Owning to the distinction in balance between grafting and the coagent oligomeration reactions, TMPTMA resulted in a largely linear PP architecture, while TAM induced LCB; both coagents formed a nanoparticle phase in the modified PP, albeit in different quantities. It was demonstrated that the nanoparticles were effective as nucleating agents for both foaming and crystallization.

The investigation of foaming of controlled rheology PPs established that lower melt viscosity facilitates cell growth, generating larger cell sizes. The presence of nanoparticles into the PP-g-TMPTMA derivative with linear chain architecture resulted in an enhanced nucleation effect, and faster rates of cell density growth. However, the best foams were made from the PP-g-TAM derivatives that possessed a combination of lower viscosity, strain hardening due to LCB, higher crystallization temperature and enhanced nucleation from nanoparticles. Lower viscosity and nucleation favour faster nucleation and higher rates of cell growth, whereas strain hardening and high crystallization temperatures result in improved cell stabilization.

Lastly, Chapter 6 explores further the effect of nucleating agents by using nanosilica as the dispersed particle phase. Processing parameters were optimized to study their effect on nanosilica dispersion. Good dispersion of the nanosilica phase proved to be the key in fully realizing the nucleation potential of these particles.

7.2 Conclusions

Compression foam molding of a series of ethylene-α-olefin copolymers having similar viscosities, revealed that the cell morphology was similar for all the octene-based grades that possessed long chain branching. The performance of a butene-based copolymer, with short chain branching was significantly inferior, due to its lower extensional viscosity, which led to increased propensity for cell coalescence, leading to a coarser morphology.

Coarser morphology was also noted for the octene-based copolymer sample with the lowest density, which did not have a well-defined crystallization point. This presumably led to increased chance of cell coalescence during cooling of the foam.

The mechanical properties of all foams were lower than those of the unfoamed samples, but kept the same trends; the highest density material had increased secant modulus, whereas the elongation at break was essentially unaffected by density.

A series of controlled rheology linear PPs were produced through reaction with dicumyl peroxide as the free radical initiator, to investigate the effect of molecular weight and viscosity on foaming. Foaming experiments, both by compression molding using a chemical blowing agent and by batch foaming using a physical blowing agent revealed that lower viscosity favours higher expansion ratios and larger cells, due to reduced resistance to cell growth.

Furthermore, modification of the linear PP structure through the introduction of LCB using a triallyl trimesate (TAM) coagent, resulted in increased melt strength, with beneficial effects on the volume expansion ratio, and cell stabilization.

Cross-linked nanoparticles generated *in situ* during coagent-modification were detected in the PP formulations. These particles can serve as heterogeneous nucleation sites for crystallization from the melt, and gas phase formation during batch foaming. Therefore, the performance of these materials is dictated not only by the rheological properties brought about by chemical modification, but also through the enhanced nucleation generated by the dispersed solid phase.

Overall the best foams were made from the PP-g-TAM derivatives that possessed a combination of lower viscosity, strain hardening due to LCB, higher crystallization temperature and enhanced nucleation from nanoparticles. Lower viscosity and nucleation favour faster nucleation and higher rates of cell growth, whereas strain hardening and high crystallization temperatures result in improved cell stabilization.

Enhanced nucleation effects were also reported in PP/nanosilica composites containing 0.3 to 1 phr silica prepared by twin-screw extrusion. Dispersion of nanosilica within a PP matrix was sensitive to the extrusion conditions, and the amount of compatibilizer. The size of the aggregates and their size distribution increased significantly beyond a SiO_2 content of 1 phr. The degree of dispersion of the SiO_2 particles was associated to their ability to act as nucleating agents, when foaming with N_2 as the blowing agent. Finely dispersed SiO_2 at loadings less than 1 phr resulted in enhanced nucleation and cell growth rate. These findings were confirmed by extrusion foaming experiments. The improvement in foam structure was attributed to the enhanced cell nucleation ability in the presence of finely dispersed nanoparticles.

7.3 Significant Contributions

This thesis makes several original contributions, summarized below.

First of all a convenient and easy to use compression mold foaming method was developed, to facilitate the fundamental studies of the effects of material properties on foaming. Given its simplicity and reproducibility, this approach offers a means for comparison of the foaming behaviour of different grades of polymer, without dealing with the complications inherently present in extrusion foaming and injection foam molding.

Using the developed compression mold foaming technique, Chapter 3 has presented a rigorous comparison between the fundamental material properties of a series of well characterized ethylene-α-olefin copolymers and their foam properties. Furthermore, this chapter presents for the first time a detailed characterization of the extensional properties of these commercially important polymers. This research on mPEs has demonstrated unambiguously that when melt viscosity is fixed, extensional viscosity and crystallization temperature are important factors influencing foaming behaviour.

The effect of melt viscosity and strain hardening on foaming has been elucidated unambiguously further, by comparing foams based on linear PPs with different viscosities, as well as their coagent modified derivatives containing LCB. This work has developed important guidelines on PP selection, by demonstrating that the best foams are produced from materials having a combination of low viscosity, high strain hardening due to LCB, and high crystallization temperature.

The detection of nanoparticles, formed as a side reaction from the oligomerization of the coagent is a significant finding of this thesis. The thermal properties of the coagent modified PPs are altered significantly in the presence of nanoparticles, including a drastic increase in the

crystallization temperature, and increases in the crystallinity of the final samples. The explanation that the increase in the crystallization temperature is attributed to the formation of nanoparticles within coagent modified PPs constitutes a significant contribution, since this phenomenon has never been explained adequately previously.

Furthermore, the potential of a one-pot simple chemical modification technique, which will provide simultaneously modification on the polymer chain architecture and preparation of a second nanoparticle phase is of considerable significance, since it opens the avenue for novel materials with enhanced processability both in foaming, and other processing applications, such as injection molding .

Finally guidelines have been provided for the synthesis on nanocomposites that can provide enhanced nucleation effects in PPs, resulting in higher quality foams in extrusion foaming.

7.4 Recommendations for Future Work

I. For practical reasons, polyolefin elastomers in their cross-linked form are applied for foaming. However the interplay between the decomposition of the cross-linking agents and the foaming agent has not been studied. A novel contribution would be to study the interplay between cross-linking and cell expansion in cross-linked EC foams, in the hope of identify a technique wherein the cross-linking reaction is achieved while the expansion takes place. A study on new curing systems for the foaming of cross-linked EC will provide more control over the foaming process. A potential approach would be to incorporate persistent nitroxy radicals and their functionalized derivatives into the curing package. The interaction between the curing agent and the nitroxy

radicals will create different time window for EC cross-linking and decomposition of the blowing agent.

II. An accurate measurement of the amount of nanoparticles formed during coagent modification will lay the ground work to more understanding of these particles have on various properties of their matrix polymer. To achieve this, new separation and purification techniques must be developed to retain all the particles while releasing all the polymer chains. A suggestion for this is to build a hot filtering apparatus where all parts of the filtration system are operated at the boiling temperature of the solvent of choice.

III. After achieving an accurate measurement of the particles produced, lots of opportunities present themselves. One of them is to study systematically the effect of these particles on the rheological properties of polymer melts by controlling the amount of particles produced and doping them back into the parent polymer to produce a nanocomposite. The effect of the coagent-rich nanoparticles on the mechanical properties of polymer matrix can be studied to explore if coagent modification aimed at the synthesis of these particles is a viable route to produce nanocomposites.

V. A quantitative comparison of the nucleation effect provided by the nanoparticles to those by conventional nucleating agents such as talc and nanosilica will be possible by having control over how much in-situ particles are added. Nanoparticles formed in-situ during reactive processing, are able to eliminate the extra melt compounding step, while ensuring good dispersion. This prospect opens up significant opportunities in processes such as injection molding, which routinely require the presence of nucleating agents to ensure fast crystallization upon cooling.

REFERENCES

[1] Industry Canada, http://www.ic.gc.ca/eic/site/plastics-plastiques.nsf/eng/h_pl01337.html, accessed August 2102.

[2] G. Burillo and E. Adem, in: Salamone J.C. (Ed.), *Polymeric Materials Encyclopedia,* CRC Press, Boca Raton, (1996).

[3] C.B. Park, "Polyolefin Foams", in: Klempner D., Sendijarevic V. (Eds.), *Handbook of Polymeric Foams and Foam Technology,* Book News, Inc., Portland, United States, Portland, pp. 187-242 (2004).

[4] J.H. Saunders, "Fundamentals of Foam Formation", in: Klempner D., Sendijarevic V. (Eds.), *Handbook of Polymeric Foams and Foam Technology,* Book News, Inc., Portland, United States, Portland, pp. 5-15 (2004).

[5] P. Rachtanapun, S.E.M. Selke, and L.M. Matuana, *J. Appl. Polym. Sci.*, **88**, 2842-2850 (2003).

[6] P. Rachtanapun, S.E.M. Selke, and L.M. Matuana, *J. Appl. Polym. Sci.*, **93**, 364-71 (2004).

[7] F.A. Waldman, MSc Thesis, MIT, (1982).

[8] N.H. Fletcher, *J. Chem. Phys.,* **29**, 572-576 (1958).

[9] J.S. Colton, *Mater. Manuf. Process.*, **4**, 253-262 (1989).

[10] P.M. Wilt, *J. Colloid Interface Sci.*, **112**, 530-538 (1986).

[11] A.L. Yarin, D. Lastochkin, Y. Talmon, and Z. Tadmor, *AICHE J.*, **45**, 2590-2605 (1999).

[12] Shau-Tarng Lee, *Polym. Eng. Sci.*, **33**, p418(5) (1993).

[13] E.J. Barlow and W.E. Langlois, *IBM J. Res. Dev.*, **6**, 329-337 (1962).

[14] M. Amon and C.D. Denson, *Polym. Eng. Sci.,* **24**, 1026-1034 (1984).

[15] M. Amon and C.D. Denson, *Polym. Eng. Sci.,* **26**, 255-267 (1986).

[16] "Encyclopedia of polymer science and engineering", in: Mark H.F., Kroschwitz J.I. (Eds.), Wiley, New York, pp. 3 (1985-1990).

[17] Y. Otsuki and T. Kanai, *Polym. Eng. Sci.*, **45**, 1277-87 (2005).

[18] S.N. Leung, C.B. Park, D. Xu, H. Li, and R.G. Fenton, *Ind. Eng. Chem. Res.*, **45**, 7823-7831 (2006).

[19] K. Taki, T. Nakayama, T. Yatsuzuka, and M. Ohshima, *J. Cell. Plast.*, **39**, 155-169 (2003).

[20] J.E. Martini-vvedensky, N.P. Suh, and F.A. Waldman, United States Patent, 4473665 (1984).

[21] N.J. Mills, "Polymer Foams Handbook" Butterworth-Heinemann, pp. 1-17 (2007).

[22] C.B. Park, 161-163 (1993).

[23] C. Dae Han and C.A. Villamizar, *Polym. Eng. Sci.*, **18**, 687-698 (1978).

[24] C.A. Villamizar and C. Dae Han, *Polym. Eng. Sci.*, **18**, 699-710 (1978).

[25] Y. Zhang, D. Rodrigue, and A. Ait-Kadi, *J. Appl. Polym. Sci.*, **90**, 2111-19 (2003).

[26] Y. Zhang, D. Rodrigue, and A. Ait-Kadi, *J. Appl. Polym. Sci.*, **90**, 2120-9 (2003).

[27] Y. Zhang, D. Rodrigue, and A. Ait-Kadi, *J. Appl. Polym. Sci.*, **90**, 2130-8 (2003).

[28] H.A. Youssef, M.M. Senna, and H.M. Eyssa, *J. Polym. Res.*, **14**, 351-357 (2007).

[29] E. Adem, G. Burillo, V. Dakin, and M. Vazquez, *Radiat. Phys. Chem.*, **46**, 937-940 (1995).

[30] E.C.L. Cardoso, A.B. Lugão, and L.G. Andrade E. Silva, *Radiat. Phys. Chem.*, **52**, 197-200 (1998).

[31] I. Rezaeian, S.H. Jafari, P. Zahedi, M. Ghaffari, and S. Afradian, *Polym. Adv. Technol.*, **20**, 487-492 (2009).

[32] H. Tai and J.B. Wang, *J. Cell. Plast.*, **33**, 304-317 (1997).

[33] M. Yamaguchi and K. Suzuki, *J. Polym. Sci. B*, **39**, 2159-67 (2001).

[34] S. Abe and M. Yamaguchi, *J. Appl. Polym. Sci.*, **79**, 2146-2155 (2001).

[35] H. Tai, *J. Polym. Res.*, **12**, 457-464 (2005).

[36] Y. Mao and R. Qi, *J. Appl. Polym. Sci.*, **109**, 3249-55 (2008).

[37] Y.S. Kim, C.I. Chung, S.Y. Lai, and K.S. Hyun, *J. Appl. Polym. Sci.*, **59**, 125-137 (1996).

[38] J.F. Vega, A. Santamaria, A. Munoz-Escalona, and P. Lafuente, *Macromolecules*, **31**, 3639-3647 (1998).

[39] P. Wood-Adams and J.M. Dealy, *Macromolecules*, **33**, 7481-7488 (2000).

[40] S. Lai, T.A. Plumley, T.I. Butler, G.W. Knight, and C.I. Kao, Publ. Soc. Plast. Eng., San Francisco, CA, USA 1814-1815 (1994).

[41] A. Nojiri, T. Sawasaki, and T. Koreeda, United States Patent, 4424293 (1984).

[42] Y. Lee and L. Wang, *J. Appl. Polym. Sci.*, **32**, 4639-4647 (1986).

[43] Z. Xu, P. Xue, F. Zhu, and J. He, *J. Cell. Plast.*, **41**, 169-185 (2005).

[44] R. Hingmann and B.L. Marczinke, *J. Rheol.*, **38**, 573-87 (1994).

[45] J. Stange, C. Uhl, and H. Munstedt, *J. Rheol.*, **49**, 1059-79 (2005).

[46] J. Stange and H. Munstedt, *J. Cell. Plast.*, **42**, 445-467 (2006).

[47] J. Stange and H. Munstedt, *J. Rheol.*, **50**, 907-23 (2006).

[48] P. Spitael and C.W. Macosko, *Polym. Eng. Sci.*, **44**, 2090-100 (2004).

[49] C.B. Park and L.K. Cheung, *Polym. Eng. Sci.*, **37**, 1-10 (1997).

[50] E. Passaglia, S. Coiai, and S. Augier, *Prog. Polym. Sci.*, **34**, 911-947 (2009).

[51] B.K. Kim and K.J. Kim, *Adv. Polym. Technol.*, **12**, 263-269 (1993).

[52] X. Wang, C. Tzoganakis, and G.L. Rempel, *J. Appl. Polym. Sci.*, **61**, 1395-1404 (1996).

[53] G.J. Nam, J.H. Yoo, and J.W. Lee, *J. Appl. Polym. Sci.*, **96**, 1793-1800 (2005).

[54] E. Borsig, M. van Duin, A.D. Gotsis, and F. Picchioni, *Euro. Polym. J.*, **44**, 200-212 (2008).

[55] J.S. Parent, A. Bodsworth, S.S. Sengupta, M. Kontopoulou, B.I. Chaudhary, D. Poche, and S. Cousteaux, *Polymer,* **50**, 85-94 (2009).

[56] D. Graebling, *Macromolecules,* **35**, 4602-4610 (2002).

[57] A.D. Gotsis, B.L.F. Zeevenhoven, and A.H. Hogt, *Polym. Eng. Sci.*, **44**, 973-982 (2004).

[58] R. Liao, W. Yu, and C. Zhou, *Polymer,* **51**, 6334-6345 (2010).

[59] J. Kurja and N.A. Mehl, "Nucleating Agents for Semi-crystalline Polymers", in: Zweifel H.H., Maier R.D., Schiller M. (Eds.), *Plastics Additives Handbook,* Hanser, Munich, pp. 967-988 (2009).

[60] C.B. Park, L.K. Cheung, and S. Song, *Cell. Polym.*, **17**, 221-251 (1998).

[61] S. Fairgrieve, *Nucleating agents,* Shawbury, Shropshire, U.K (2006).

[62] K. Hamada and H. Uchiyama,United States Patent, 4016118 (1977).

[63] R.L.J. Mahaffey,United States Patent, 4371645 (1983).

[64] M. Tenma and M. Yamaguchi, *Polym. Eng. Sci.*, **47**, 1441-1446 (2007).

[65] Gu-Su Jang, Won-Jei Cho, and Chang-Sik Ha, *J. Polym. Sci. B.*, **39**, 1001-16 (2001).

[66] Q. Gui, Z. Xin, W. Zhu, and G. Dai, *J. Appl. Polym. Sci.*, **88**, 297-301 (2003).

[67] M. Blomenhofer, S. Ganzleben, D. Hanft, H. Schmidt, M. Kristiansen, P. Smith, K. Stoll, D. Mäder, and K. Hoffmann, *Macromolecules,* **38**, 3688-3695 (2005).

[68] L.J. Lee, C. Zeng, X. Cao, X. Han, J. Shen, and G. Xu, *Compos. Sci. Technol.,* **65**, 2344-2363 (2005).

[69] A. Usuki, N. Hasegawa, and M. Kato, *Adv. Polym. Sci.,* **179**, 135-195 (2005).

[70] F. Hussain, M. Hojjati, M. Okamoto, and R.E. Gorga, *J. Compos. Mater.*, **40**, 1511-1575 (2006).

[71] K. Goren, L. Chen, L.S. Schadler, and R. Ozisik, *J. Supercrit. Fluid.*, **51**, 420-427 (2010).

[72] Jui-Ming Yen, Kung-Chin Chang, Chih-Wei Peng, Sheng-Che Chiou, Shyh-Shin Hwang, Jen-Chang Yang, and Hong-Ru Lin, *J. Nanosci. Nanotechnol.*, **8**, 6297-305 (2008).

[73] V.N. Thi Thanh, J. Duchet-Rumeau, A.K. Whittaker, and J. Gerard, *Polymer*, **51**, 3436-44 (2010).

[74] B. Zhu, W. Zha, J. Yang, C. Zhang, and L.J. Lee, *Polymer*, **51**, 2177-2184 (2010).

[75] Y.H. Lee, K.H. Wang, C.B. Park, and M. Sain, *J. Appl. Polym. Sci.*, **103**, 2129-2134 (2007).

[76] G. Guo, K.H. Wang, C.B. Park, Y.S. Kim, and G. Li, *J. Appl. Polym. Sci.*, **104**, 1058-1063 (2007).

[77] W.G. Zheng, Y.H. Lee, and C.B. Park, *J. Appl. Polym. Sci.*, **117**, 2972-2979 (2010).

[78] D.N. Bikiaris, A. Vassiliou, E. Pavlidou, and G.P. Karayannidis, *Euro. Polym. J.*, **41**, 1965-1978 (2005).

[79] Y. Liu and M. Kontopoulou, *Polymer*, **47**, 7731-7739 (2006).

[80] A. Vassiliou, D. Bikiaris, and E. Pavlidou, *Macromol. React. Eng.*, **1**, 488-501 (2007).

[81] M. Bailly and M. Kontopoulou, *Polymer*, **50**, 2472-2480 (2009).

[82] H. Drögemüller, K. Heiland, and W. Kaminsky, "*Copolymerization of Ethene and a-Olefins with a Chiral Zirconocene/Aluminoxane Catalyst*", in: Kaminsky W., Sinn H. (Eds.), *Transition Metals and Organometallics as Catalysts for Olefin Polymerization*, Springer Verlag, Berlin, pp. 303-308 (1988).

[83] M. Zhang, D. Lynch, and S. Wanke, *J. Appl. Polym. Sci.*, **75**, 960-967 (2000).

[84] R. Gendron and C. Vachon, *J. Cell. Plast.*, **39**, 71-85 (2003).

[85] S. Subramonian, P. Filiccia, and J. Alcott, *J. Cell. Plast.*, **43**, 331-343 (2007).

[86] M.L. Sentmanat,US Patent, 6578413 (2003).

[87] M. Sentmanat, E.B. Muliawan, and S.G. Hatzikiriakos, *Rheol. Acta,* **44**, 1-15 (2004).

[88] S.A. Saltikov, "The determination of the size distribution of particles in an opaque material from a measurement of the size distribution of their sections", in: Elias H. (Ed.), *Stereology: Proceedings of the Second International Congress for Stereology,* Springer, New York, pp. 163-173 (1967).

[89] M.N. Bureau, "The relationship between morphology and mechanical properties in thermoplastic foams", in: Gendron R. (Ed.), *Thermoplastic foam processing : principles and applications,* CRC Press, Boca Raton, pp. 235-281 (2005).

[90] B. Patham and K. Jayaraman, *J. Rheol.*, **49**, 989-999 (2005).

[91] S.G. Hatzikiriakos, *Polym. Eng. Sci.,* **40**, 2279-87 (2000).

[92] R. Sabia, *J. Appl. Polym. Sci.,* **8**, 1651-1657 (1964).

[93] W.W. Graessley, *Macromolecules,* **15**, 1164-1167 (1982).

[94] J.W.S. Lee and C.B. Park, *Macromol. Mater. Eng.,* **291**, 1233-1244 (2006).

[95] X. Xu, C.B. Park, D. Xu, and R. Pop-Iliev, *Polym. Eng. Sci.*, **43**, 1378-1390 (2003).

[96] K. Taki, K. Tabata, S. Kihara, and M. Ohshima, *Polym. Eng. Sci.*, **46**, 680-690 (2006).

[97] C.B. Park and N.P. Suh, *Polym. Eng. Sci.*, **36**, 34-48 (1996).

[98] G. Li, J. Wang, C.B. Park, and R. Simha, *J. Polym. Sci. B.,* **45**, 2497-2508 (2007).

[99] G. Li, F. Gunkel, J. Wang, C.B. Park, and V. Altstadt, *J. Appl. Polym. Sci.,* **103**, 2945-53 (2007).

[100] S.N. Leung, C.B. Park, and H. Li, *Plast., Rub. Compos.*, **35**, 93-100 (2007).

[101] S.N. Leung, A. Wong, Q. Guo, C.B. Park, and J.H. Zong, *Chem. Eng. Sci.*, **64**, 4899-907 (2009).

[102] K. Sehanobish, R.M. Patel, B.A. Croft, S.P. Chum, and C.I. Kao, *J. Appl. Polym. Sci.*, **51**, 887-894 (1994).

[103] J.G. Burt, *J. of Cell. Plast.*, **14**, 341-345 (1978).

[104] H.E. Naguib, C.B. Park, N. Reichelt, and U. Panzer, *Polym. Eng. Sci.*, **42**, 1481-1492 (2002).

[105] H.E. Naguib, C.B. Park, and N. Reichelt, *J. Appl. Polym. Sci.*, **91**, 2661-2668 (2004).

[106] H.E. Naguib, J. Wang, C.B. Park, A. Mukhopadhyay, and N. Reichelt, *Cell. Polym.*, **22**, 1-22 (2003).

[107] A.D. Gotsis, B.L.F. Zeevenhoven, and C. Tsenoglou, *J. Rheol.*, **48**, 895-914 (2004).

[108] J. Tian, W. Yu, and C. Zhou, *J. Macromol. Sci., B.*, **45 B**, 969-985 (2006).

[109] S. Li, M. Xiao, Y. Guan, D. Wei, H. Xiao, and A. Zheng, *Euro. Polym. J.*, **48**, 362-371 (2012).

[110] H. Mavridis and R.N. Shroff, *Polym. Eng. Sci.*, **32**, 1778-91 (1992).

[111] Q. Guo, J. Wang, C.B. Park, and M. Ohshima, *Ind. Eng. Chem. Res.*, **45**, 6153-6161 (2006).

[112] R. Pop-Iliev, G.M. Rizvi, and C.B. Park, *Polym. Eng. Sci.*, **43**, 40-54 (2003).

[113] C. Tzoganakis, J. Vlachopoulos, and A.E. Hamielec, *Polym. Eng. Sci.*, **28**, 170-180 (1988).

[114] K. El Mabrouk, J.S. Parent, B.I. Chaudhary, and R. Cong, *Polymer*, **50**, 5390-7 (2009).

[115] J.S. Parent, S.S. Sengupta, M. Kaufman, and B.I. Chaudhary, *Polymer*, **49**, 3884-3891 (2008).

[116] D. Auhl, J. Stange, H. Münstedt, B. Krause, D. Voigt, A. Lederer, U. Lappan, and K. Lunkwitz, *Macromolecules*, **37**, 9465-9472 (2004).

[117] C.J. Tsenoglou and A.D. Gotsis, *Macromolecules*, **34**, 4685-4687 (2001).

[118] A. Durmus, A. Kasgoz, and C.W. Macosko, *Polymer*, **48**, 4492-4502 (2007).

[119] B.J. Anderson and C.F. Zukoski, *Macromolecules*, **42**, 8370-8384 (2009).

[120] H. Park, C.B. Park, C. Tzoganakis, and P. Chen, *Ind. Eng. Chem. Res.*, **46**, 3849-3851 (2007).

[121] J. Wang, W. Zhu, H. Zhang, and C.B. Park, *Chem. Eng. Sci.,* **75**, 390-399 (2012).

[122] W. Wu, J.S. Parent, S.S. Sengupta, and B.I. Chaudhary, *J. Polym. Sci. A.,* **47**, 6561-6570 (2009).

[123] M. Frounchi, A. Sharif-Pakdaman, S.A. Mousavi, and S. Dadbin, *J. Cell. Plast.,* **43**, 445-458 (2007).

[124] S.A. Mousavi-Saghandikolaei, M. Frounchi, S. Dadbin, S. Augier, E. Passaglia, and F. Ciardelli, *J. Appl. Polym. Sci.,* **104**, 950-958 (2007).

[125] J. Tian, W. Yu, and C. Zhou, *J. Appl. Polym. Sci.,* **104**, 3592-3600 (2007).

[126] I.S. Kolesov, R. Androsch, and H.-. Radusch, *J. Therm. Anal. Calorim.,* **78**, 885-895 (2004).

[127] B. Yang, M. Yang, W. Wang, and S. Zhu, *Polym. Eng. Sci.,* **52**, 21-34 (2012).

[128] K. Hoffmann, G. Huber, and D. Mäder, *Macromol. Symp.,* **176**, 83-92 (2001).

[129] D. Libster, A. Aserin, and N. Garti, *Polym. Adv. Technol.,* **18**, 685-95 (2007).

[130] E. Ferrage, F. Martin, A. Boudet, S. Petit, G. Fourty, F. Jouffret, P. Micoud, P. De Parseval, S. Salvi, C. Bourgerette, J. Ferret, Y. Saint-Gerard, S. Buratto, and J.P. Fortune, *J. Mater. Sci.,* **37**, 1561-1573 (2002).

[131] C. Jo and H.E. Naguib, *Polymer,* **48**, 3349-3360 (2007).

[132] C. Zeng, X. Han, L.J. Lee, K.W. Koelling, and D.L. Tomasko, *Adv. Mater.,* **15**, 1743-1747 (2003).

[133] W. Zheng, Y.H. Lee, and C.B. Park, *J. Cell. Plast.,* **42**, 271-288 (2006).

[134] W. Lertwimolnun and B. Vergnes, *Polym. Eng. Sci.,* **47**, 2100-2109 (2007).

[135] V. Vladimirov, C. Betchev, A. Vassiliou, G. Papageorgiou, and D. Bikiaris, *Composites Sci. Technol.,* **66**, 2935-2944 (2006).

[136] M.Z. Rong, M.Q. Zhang, S.L. Pan, B. Lehmann, and K. Friedrich, *Polym. Int.,* **53**, 176-183 (2004).

[137] F. Zoukrami, N. Haddaoui, C. Vanzeveren, M. Sclavons, and J. Devaux, *Polym. Int.,* **57**, 756-763 (2008).

[138] L. Elias, F. Fenouillot, J.C. Majeste, and P. Cassagnau, *Polymer*, **48**, 6029-40 (2007).

[139] H. Nakajima, K. Yamada, Y. Iseki, S. Hosoda, A. Hanai, Y. Oumi, T. Teranishi, and T. Sano, *J. Polym. Sci. B.*, **41**, 3324-3332 (2003).

[140] S. Jain, J.G.P. Goossens, and M. Van Duin, Macromol. Sym. **233**, 225-234 (2006).

[141] H. Cheng and I. Manas-Zloczower, *Polym. Eng. Sci.*, **37**, 1082-1090 (1997).

[142] A. Lawal and D.M. Kalyon, *Polym. Eng. Sci.*, **35**, 1325-1338 (1995).

[143] A. Lawal and D.M. Kalyon, *J. Appl. Polym. Sci.*, **58**, 1501-1507 (1995).

[144] A. Gonzalez-Montiel, H. Keskkula, and D.R. Paul, *J. Polym. Sci., B.*, **33**, 1751-67 (1995).

[145] Q. Zhang and L.A. Archer, *Langmuir*, **18**, 10435-10442 (2002).

[146] A. Tuteja, M.E. Mackay, C.J. Hawker, and B. Van Horn, *Macromolecules*, **38**, 8000-8011 (2005).

[147] D.M. Kalyon, R. Yazici, C. Jacob, B. Aral, and S.W. Sinton, *Polym. Eng. Sci.*, **31**, 1386-1392 (1991).

[148] B.K. Aral and D.M. Kalyon, *Plast. Rubber Compos. Process. Appl.*, **24**, 201-210 (1995).

[149] E.T. Kopesky, T.S. Haddad, R.E. Cohen, and G.H. McKinley, *Macromolecules*, **37**, 8992-9004 (2004).

[150] K. Lakdawala and R. Salovey, *Polym. Eng. Sci.*, **27**, 1035-1042 (1987).

[151] S.G. Hatzikiriakos, N. Rathod, and E.B. Muliawan, *Polym. Eng. Sci.*, **45**, 1098-1107 (2005).

[152] K. Taki, T. Yanagimoto, E. Funami, M. Okamoto, and M. Ohshima, Poly. Eng. Sci. **44**, 1004-1011 (2004).

[153] J.S. Colton and N.P. Suh, *Polym. Eng. Sci.*, **27**, 485-492 (1987).

[154] J.S. Colton and N.P. Suh, *Polym. Eng. Sci.*, **27**, 493-499 (1987).

[155] J.S. Colton and N.P. Suh, *Polym. Eng. Sci.,* **27**, 500-503 (1987).

[156] R.B. McClurg, *Chem. Eng. Sci.*, **59**, 5779-5786 (2004).

[157] C. Wang, S.N. Leung, M. Bussmann, W.T. Zhai, and C.B. Park, *Ind. Eng. Chem. Res.,* **49**, 12783-12792 (2010).

[158] P.C. Lee, J. Wang, and C.B. Park, *Ind. Eng. Chem. Res.,* **45**, 175-181 (2006).

[159] W. Zhai, J. Yu, L. Wu, W. Ma, and J. He, *Polymer*, **47**, 7580-7589 (2006).

[160] S.N. Leung, C.B. Park, and H. Li, *J. Cell. Plast.,* **46**, 441-460 (2010).

[161] P. Spitael, C.W. Macosko, and R.B. McClurg, *Macromolecules,* **37**, 6874-6882 (2004).

APPENDIX A: Compression Foam Molding Procedure

As exhibited in Chapters 3 and 4, compression foam molding is a versatile technique to evaluate the foaming behaviour of polyolefins with a variety of molecular weights and structures without dealing with the complications inherently present in extrusion foaming and injection foam molding. The detailed procedure to prepare polyolefin foams through compression foam molding is documented step by step below.

1. Preheat the press to a set temperature (based on extensive experimentation, typical range of temperature values for PP and EC containing AZ are 190 to 210 °C).
2. Prepare the mold assembly. A mold assembly usually consists of two metal plates (mold plates – 10”x10” **(Figure A.A.1 (a)**) or 6”x6” (**Figure A.A.1 (b)**)), two pieces of tear-resistant polytetrafluoroethylene (PTFE)-coated fiberglass fabric and a mold with desired cut-outs.

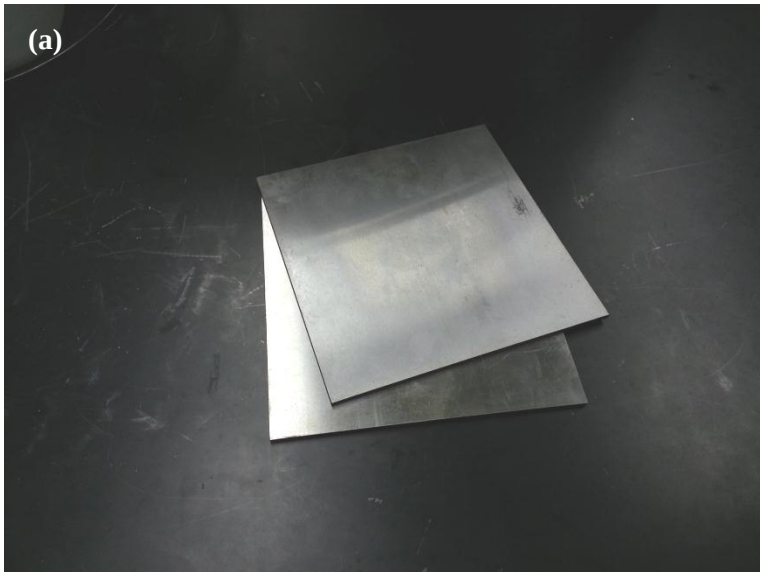

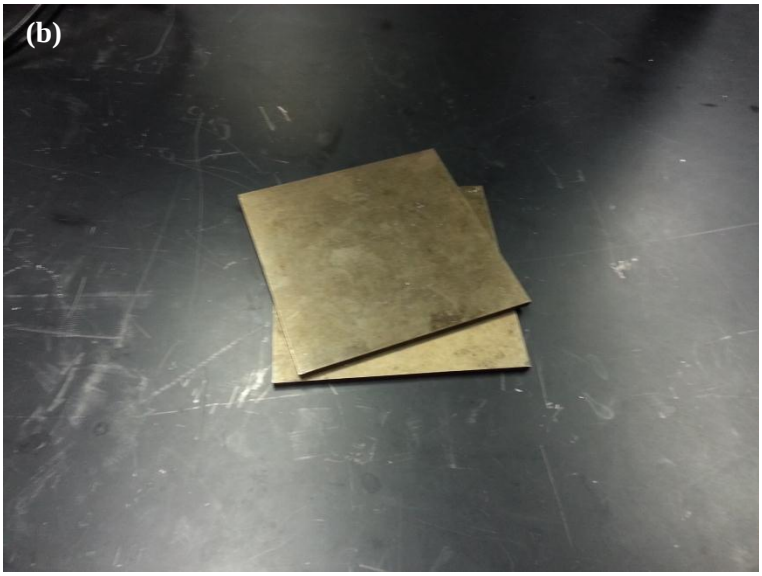

Figure A.A.1 (a) 10”x10” and **(b)** 6”x6” plates for compression foam molding.

3. Preheat the mold assembly. Place the mold assembly onto the Wabash® 12”x12” press surface then elevate the plate so that the mold assembly is clamped between the press plates, but without applying pressure.
4. Load the mold with polyolefin pellets pre-compounded with a chemical blowing agent (CBA). On a preheated mold plate, lay one piece of PTFE fabric, followed by the mold. Then place pre-weighed polymer into the mold cavity. In order to ensure proper sealing of the mold assembly during the heating period, a 20% to 30% over-fill of the mold cavity is recommended. Lay another piece of PTFE fabric on top of the loaded mold, then place a mold plate on top of the fabric. The entire loading step should be performed quickly so that the preheated mold plates remains at high temperature.
5. Heat the mold assembly in the press. Place the loaded mold assembly between the press plates, and apply a sealing pressure. Start timing. Typical heating times when the AZ blowing agent is used is between 3 min (for PP with small mold) and 20 min (for EC with

large mold). A guideline is to ensure total decomposition of the blowing agent and homogeneous diffusion of the resulted gas molecules within the polyolefin melt at the set press temperature.

6. Release the clamping pressure. The expansion of the foam happens during this step, thus several manoeuvers can be applied to control the degree of expansion. Removing the top mold plate together with clamping pressure and then allowing the foamed material to expand freely in the hot press for a controlled amount of time, results in maximum expansion. Caution should be exercised if free expansion is allowed, since it may cause larger cells on the heated side of the mold assembly; in which case the PTFE fabrics containing the mold and the foamed material should be turned over to achieve even heating. After this step, remove the foam from the hot press for cooling.
7. Cool the foam down. Since the thermal properties of polyolefins affect significantly their foaming behaviour, cooling routines are important in controlling the final foam structure. Water with varying controlled temperatures can be used for quenching. Depending on the temperature difference between the hot press and the quenching fluid, result may vary. Another method is natural cooling on a surface of room temperature. Cooling between surfaces at a regulated temperature is another option (for example move to a nearby press with the plates heated at 50°C, to achieve a good surface finish).
8. Remove the solidified foam from the mold.